

**FEDERAL UNIVERSITY OF SANTA MARIA
TECHNOLOGY CENTER
GRADUATE PROGRAM IN ELECTRICAL ENGINEERING**

Olatunji Matthew Adeyanju

**DECENTRALIZED MULTIAREA ECONOMIC DISPATCH CONSIDERING
PARTICIPATION OF LOCAL PRIVATE AGGREGATORS USING META-
HEURISTIC METHOD**

Santa Maria, RS
2022

Olatunji Matthew Adeyanju

**DECENTRALIZED MULTIAREA ECONOMIC DISPATCH CONSIDERING
PARTICIPATION OF LOCAL PRIVATE AGGREGATORS USING META-
HEURISTIC METHOD**

Thesis presented to the Graduate Program in
Electrical Engineering of the Federal
University of Santa Maria (UFSM, RS) as a
requirement for obtaining the title of
Doctorate in Electrical Engineering.

Advisor: Prof.^a Dr.^a Luciane Neves Canha

Santa Maria, RS
2022

The present work has been done with the support from CNPq, the Brazilian National Council for Scientific and Technological Development and TWAS, the academy of sciences for the developing world, process no 148080/2017-0.

Adeyanju, Olatunji Matthew
Decentralized Multiarea Economic Dispatch Considering
Participation of Local Private Aggregators Using Meta
Heuristic Method / Olatunji Matthew Adeyanju.- 2022.
81 p.; 30 cm

Orientadora: Luciane Neves Canha
Tese (doutorado) - Universidade Federal de Santa
Maria, Centro de Tecnologia, Programa de Pós-Graduação em
Engenharia Elétrica, RS, 2022

1. Decentralized Models 2. Multi-Area 3. Power
Systems 4. Private Aggregators 5. Transmission Systems
Operators I. Canha, Luciane Neves II. Título.

Sistema de geração automática de ficha catalográfica da UFSM. Dados fornecidos pelo autor(a). Sob supervisão da Direção da Divisão de Processos Técnicos da Biblioteca Central. Bibliotecária responsável Paula Schoenfeldt Patta CRB 10/1728.

Declaro, OLATUNJI MATTHEW ADEYANJU, para os devidos fins e sob as penas da lei, que a pesquisa constante neste trabalho de conclusão de curso (Tese) foi por mim elaborada e que as informações necessárias objeto de consulta em literatura e outras fontes estão devidamente referenciadas. Declaro, ainda, que este trabalho ou parte dele não foi apresentado anteriormente para obtenção de qualquer outro grau acadêmico, estando ciente de que a inveracidade da presente declaração poderá resultar na anulação da titulação pela Universidade, entre outras consequências legais.

Olatunji Matthew Adeyanju

**DECENTRALIZED MULTIAREA ECONOMIC DISPATCH CONSIDERING
PARTICIPATION OF LOCAL PRIVATE AGGREGATORS USING META-
HEURISTIC METHOD**

Thesis presented to the Graduate Program in
Electrical Engineering of the Federal
University of Santa Maria (UFSM, RS) as a
requirement for obtaining the title of
Doctorate in Electrical Engineering.

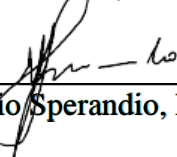
Approved on 20/01/2022



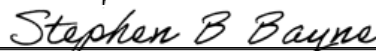
Luciane Neves Canha, Dra. (UFSM) – Video conference
(President/Advisor)



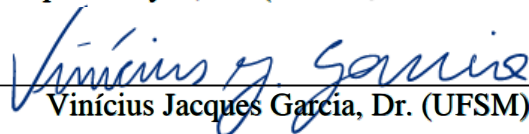
Josué Campos Do Prado, Dr (Washington State University) – Video conference



Mauricio Sperandio, Dr. (UFSM) – Video conference



Stephen Bayne, Dr. (Texas Tech University) – Video conference



Vinicius Jacques Garcia, Dr. (UFSM) – Video conference

Santa Maria, RS
2022

ACKNOWLEDGMENT

To God eternal, immortal, invincible. You indeed dwell in the light that no one can approach unto. Your wisdom is unsearchable. Thank you for the life and knowledge you gave me for prosecuting this PhD program, excellently. To you be all glory!

To my parent, Deaconess Victoria Adeyanju, through whom I metamorphosized into life. I thank you for all your prayers, sacrifices, commitment, and training you gave to me as a growing young man. The morals you instilled in me coupled with the Christian values you exposed me to made my life the worth that it is presently. And I won't stop to get better until I have become what God did purpose for my life through you. Thank you.

To my one big Jesus Family. I thank you all for your support and prayers for breakthroughs during the course of my PhD. Your brotherly love was large and contagious. May the Lord reward you bountifully in many returns. Thank you.

To my God given Family. I specially thank my wife for your maximum support given during the course of this PhD program. You made my life meaningful and beautiful. You are very supportive in everything but your exceptional love is of more colossal values to me. Thank you for making this PhD a successful and memorable one for the entire Olatunji's family.

To my supervisor – Prof. Luciane Neves Canha. You are such an angel brought on my path by God. Your motherly love, care, and support is outstanding to me. Your technical ability and mentorship are very inspiring. The roles you played in my life are countless. You truly made me who I have become today. Thank you so much for everything.

To my teacher and mentor – Prof. Mauricio Sperandio. You are very professional, intelligent, hardworking, loving, and understandable. I was privilege to have gained similar traits from you as my mentor. Your professional advice was very useful for making critical decisions. Thank you for all that you do.

To the School of PPGEE, College of Technology, and entire academic community at UFSM both students and staff. I say thank you all. Specifically, Prof. Daniel Bernardon played a major role in my coming to UFSM, Brazil. You were very accommodating and supportive in every aspect. Thank you so much. Dr. Camilo Alberto Sepulveda Rangel, Dr. Leonardo Da Silva, Engr. Bruno K. Hammer were very brotherly. Thank you all.

RESUMO

DESPACHO ECONÔMICO MULTI ÁREA DESCENTRALIZADO CONSIDERANDO A PARTICIPAÇÃO DE AGREGADORES PRIVADOS LOCAIS USANDO O MÉTODO META-HEURÍSTICO

AUTOR: Olatunji Matthew Adeyanju
ORIENTADORA: Luciane Neves Canha

A operação dos sistemas de energia tem sido majoritariamente baseada em soluções centralizadas. Nos últimos tempos, no entanto, os modelos econômicos do sistema de energia estão mudando devido à inclusão de novos participantes privados no sistema e políticas que apoiam a integração de 100% de energia renovável (ER). Este novo paradigma aumenta a complexidade dos sistemas de energia considerando a autonomia dos participantes individuais. A falta de transparência na troca de dados entre as operadoras também limita a eficácia das soluções centralizadas, tornando a operação centralizada mais desafiadora. Como resultado, a motivação para desenvolver uma solução descentralizada que permita ao operador individual gerenciar efetivamente sua operação enquanto interage com outros operadores torna-se necessária para operações seguras e confiáveis de toda a rede. Além disso, o problema clássico de operação multiárea tem sido estudado por muitos autores usando alguns métodos matemáticos lineares por partes convencionais. Alternativamente, onde há necessidade de abordar funções complexas e não convexas, os métodos metaheurísticos são considerados adequados. No entanto, apesar dessa capacidade, os métodos metaheurísticos existentes limitam-se a usar modelos centralizados ou a não considerar vários participantes autônomos em suas estruturas de tomada de decisão. Conseqüentemente, esta pesquisa desenvolve dois novos modelos de despacho econômico multiárea descentralizado baseado em otimização metaheurística (MO) para gerenciar a operação de alguns operadores de sistemas de transmissão (TSOs) e agregadores privados (PAs) de recursos de ER, incluindo armazenamentos de baterias em um contexto de sistemas de energia multiárea interconectados. O primeiro modelo é um modelo semi-descentralizado (SD) desenvolvido para atrair uma maior inclusão de PAs nos sistemas de transmissão, permitindo-lhes maximizar os lucros. O segundo modelo é um modelo totalmente descentralizado (FD) desenvolvido para coordenar a operação das PAs com os TSOs para preservar suas linhas de base. Os modelos propostos permitem determinar a integração efetiva de PAs autônomos nos sistemas de transmissão (TS) e sua cooperação com os TSOs. O objetivo de ambos os modelos é minimizar o custo total de operação do sistema coordenando efetivamente as operações dos TSOs e PAs. Os TSOs e PAs avaliam suas incertezas operacionais e determinam as reservas de energia considerando os melhores e piores cenários das variáveis incertas, permitindo assim que os modelos resultantes sejam resolvidos em três etapas usando métodos metaheurísticos selecionados (MM). Para preservar a propriedade de TSOs e PAs, o MM utiliza eficientemente conjuntos populacionais separados para resolver as operações das áreas em paralelo em uma abordagem de operação de duas camadas, permitindo que os TSOs e PAs alcancem operações quase ideais, de forma independente. Os estudos de caso são realizados em sistemas de transmissão nigerianos de 330 kV e 39 ônibus modificados, com três TSOs, cada um com três PAs, para demonstrar a eficácia dos modelos propostos. Os resultados de simulação obtidos mostraram a superioridade de desempenho dos novos modelos em relação ao modelo centralizado.

Palavras-chave: Modelos Descentralizados. Multi-Área. Sistemas de Energia. Agregadores Privados. Operadores de Sistemas de Transmissão (TSOs).

ABSTRACT

DECENTRALIZED MULTIAREA ECONOMIC DISPATCH CONSIDERING PARTICIPATION OF LOCAL PRIVATE AGGREGATORS USING META-HEURISTIC METHOD

AUTHOR: Olatunji Matthew Adeyanju
ADVISOR: Luciane Neves Canha

The power systems operation has been mostly based on centralized solutions. In the recent time however, the power system economic models are changing because of the inclusion of new private participants in the system and policies that support 100 percent renewable energy (RE) integration. This new paradigm increases the power systems complexity considering the autonomy of the individual participants. Non transparency in data exchange among operators also limits the effectiveness of the centralized solutions, making centralized operation more challenging. As a result, the motivation to develop decentralized solution that allows individual operator to effectively manage its operation while interacting with other operators becomes necessary for secure and reliable operations of the entire grid. Furthermore, the classical multiarea operation problem has been studied by many authors using some conventional piecewise linearized mathematical methods. Alternatively, where there is need to address complex and non-convex functions, the metaheuristic methods are considered suitable. However, despite this capability, the existing metaheuristic methods have been limited to either using centralized models or not considering multiple autonomous participants in their decision-making frameworks. Consequently, this research develops two novels decentralized multiarea economic dispatch models based on metaheuristic optimization (MO) to manage the operation of some transmission system operators (TSOs) and private aggregators (PAs) of RE resources including battery storages in an interconnected multiarea power systems context. The first model is a semi-decentralized (SD) model developed to attract wider inclusion of PAs in the transmission systems by allowing them to maximize profits. The second model is a fully decentralized (FD) model developed to coordinate the operation the PAs with the TSOs to preserve their baselines. The proposed models allow to determine the effective integration of autonomous PAs in the transmission systems (TS) and their co-operation with the TSOs. The objective of both models is to minimize the total operation cost of the system by effectively coordinating the TSOs and PAs operations. The TSOs and PAs evaluate their operational uncertainties and determine the power reserves considering the best and worst-case scenarios of the uncertain variables, thus enabling the resulting models to be solved in three stages using select metaheuristic methods (MM). To preserve the ownership of TSOs and PAs, the MM efficiently utilizes separate population sets to solve the operations of the areas in parallel in a two-layer operation approach, allowing the TSOs and PAs to achieve near-optimal operations, independently. Case studies are performed on a modified Nigerian 330 kV 39-bus transmission systems having three TSOs each with three PAs to demonstrate the effectiveness of the proposed models. The simulation results obtained showed the performance superiority of the novel models over their centralized counterpart model.

Keywords: Decentralized Models. Multi-Area. Power Systems. Private Aggregators. Transmission Systems Operators (TSOs).

LIST OF FIGURES

Figure 3.1 – Diagrammatic framework showing the inter-area interaction between TSO/TSO and intra-area interaction between TSO/local PA.....	27
Figure 3.2 – Decentralized structure of the proposed semi-decentralized (SD) and fully decentralized (FD) models	30
Figure 3.3 – Flowchart of the proposed decentralized models	31
Figure 3.4 – Interconnected power system area i having TSO _i and PA _{k, i} , and area j having TSO _j and PA _{k, j}	32
Figure 3.5 – The RCEGA working process	40
Figure 4.1 – Modified Nigerian 39-Bus Bulk TS	45
Figure 4.2 – Expected TSO total load profile by area.....	47
Figure 4.3 – Expected exchanged power cost of TSOs and PAs	47
Figure 4.4 – Minimum, expected, and maximum power system total solar power	47
Figure 4.5 – Minimum, expected, and maximum power system total wind power	48
Figure 4.6 – Total optimal generation outputs of PAs and power exchanged with TSO in Area ₃ – FC Model.....	48
Figure 4.7 – Total optimal generation outputs of PAs and power exchanged with TSO – SD Model	49
Figure 4.8 – Total optimal generation outputs of PAs and power exchanged with TSO – FD Model	49
Figure 4.9 – Total optimal generation outputs of TSO ₁ and net power exchanged with local PA ₁ , Area ₂ , and Area ₃ – FC Model	50
Figure 4.10 – Total optimal generation outputs of TSO ₁ and net power exchanged with Area ₂ , Area ₃ and local PA ₁ – SD Model	51
Figure 4.11 – Total optimal generation outputs of TSO ₁ and net power exchanged with TSO, Area ₃ and local PA ₁ – FD Model	51
Figure 4.12 – Impact of the uncertainty on the SD, FD, and FC models.....	54
Figure 4.13 – Performance comparison of SD, FD, and FC models under varying RCEGA parameters (G = number of generations, X = number of chromosomes).....	55
Figure 4.14 – The expected case total operation cost and execution time using the RCEGA.....	57
Figure 4.15 – The expected case total operation cost and execution time using the PSO.....	58
Figure 4.16 – The expected case total operation cost and execution time using the DE.....	59
Figure 4.17 – Battery Power Injection and Total TSO’s Hourly Load.....	62
Figure 4.18 – Battery Depth of Discharge and Hourly Capacity.....	62
Figure 4.19 – Battery Power Injection and Total TSO’s Hourly Load.....	63
Figure 4.20 – Battery Depth of Discharge and Hourly Capacity.....	63
Figure C.1 – Battery Depth of Discharge and Hourly Capacity of PAs in Area 1: FC Model.....	77
Figure C.2 – Battery Power Injection and Total PAs’ Hourly Load in Area 1: FC Model	77
Figure C.3 – Battery Depth of Discharge and Hourly Capacity of PAs in Area 2: FC Model.....	77
Figure C.4 – Battery Power Injection and Total PAs’ Hourly Load in Area 2: FC Model	77
Figure C.5 – Battery Depth of Discharge and Hourly Capacity of PAs in Area 3: FC Model.....	78
Figure C.6 – Battery Power Injection and Total PAs’ Hourly Load in Area 3: FC Model	78
Figure C.7 – Battery Depth of Discharge and Hourly Capacity of PAs in Area 1: FD Model:	78
Figure C.8 – Battery Power Injection and Total PAs’ Hourly Load in Area 1: FD Model:	78
Figure C.9 – Battery Depth of Discharge and Hourly Capacity of PAs in Area 2: FD Model:	79
Figure C.10 – Battery Power Injection and Total PAs’ Hourly Load in Area 2: FD Model	79

Figure C.11 – Battery Depth of Discharge and Hourly Capacity of PAs in Area 3: FD Model79

Figure C.12 – Battery Power Injection and Total PAs’ Hourly Load in Area 3: FD Model ...79

Figure C.13 – Battery Depth of Discharge and Hourly Capacity of TSO in Area 2: FC Model80

Figure C.14 – Battery Power Injection and Total TSO’s Hourly Load in Area 2: FC Model.80

Figure C.15 – Battery Depth of Discharge and Hourly Capacity of TSO in Area 3: FC Model80

Figure C.16 – Battery Power Injection and Total TSO’s Hourly Load in Area 3: FC Model.80

Figure C.17 – Battery Depth of Discharge and Hourly Capacity of TSO in Area 1: FD Model81

Figure C.18 – Battery Power Injection and Total TSO’s Hourly Load in Area 1: FD Model.81

Figure C.19 – Battery Power Injection and Total TSO’s Hourly Load in Area 2: FD Model.81

Figure C.20 – Battery Power Injection and Total TSO’s Hourly Load in Area 2: FD Model.81

LIST OF TABLES

Table 4.1 – Expected operation cost of TSOs and PAs for FD, SD, and FC Models.....	53
Table 4.2 – Power sold and net-operation costs considering FD, SD, and FC Models	53
Table 4.3 – The select MO parameters for the FD Model	56
Table 4.4 – Operation cost, reserve cost and execution time of the centralized models	57
Table 4.5 – Operation cost (OC), reserve cost (RC) and %change of the total operation cost (TC) of the FD model and its centralized counterpart models for the worst-case (minimum and maximum) scenarios.....	60
Table 4.6 – total operation cost of the grid is for the FD and FC models.....	64
Table A.1 – Thermal unit name, output power limit, cost coefficients, and ramp rates limits for TSOs	75
Table A.2 – Thermal unit name, output power limit, cost coefficients, and ramp rates limits for PAs.....	75
Table B.1 – Reservoir storage capacity limits, plant discharge limits, reservoir end conditions and plant generation limits (MW) for TSO by area.	75
Table B.2 – Hydropower plants coefficients.....	76
Table B.3 – Hydraulic system network.....	76
Table B.4 – Reservoir inflows rates (10^4m^3).	76

LIST OF ABBREVIATION AND ACRONYMS

AEMO	Australian Energy Market Operator
ELIA	Belgian Transmission System Operator
EV	Electric vehicle
FC	Fully centralized
FD	Fully decentralized
MAED	Multi-area economic dispatch
MO	Meta-heuristic optimization
MP	Mathematical programming
OPF	Optimal power flow
PA	Private aggregators
PDF	Probability distributed function
PHS	Pumped-hydro storage
RCEGA	Real-coded elitism genetic algorithm
SD	Semi-decentralized
TS	Transmission system
TSO	Transmission systems operator
VPP	Virtual power plant

LIST OF VARIABLES

Indices and sets

$t.$	Index of time
$i, j.$	Index of area
k	Index of local PA
d, l	Index of load/active power loss
r/res	Index of reserve/reservoir
z	Index of thermal unit operating zone
ij/ik	Index of exchanged power between TSO-TSO/ TSO-PA
h, g, w, pv	Index of hydro, thermal, wind and solar units, respectively
gh/ph	Index of pumped hydro storage in generating/pumping modes
TG_i/TG_k	Set of TSO and PA thermal units
H_i	Set of hydro power plants of TSO
WG_i/WG_k	Set of TSO/PA wind units
PV_i/PV_k	Set of TSO/PA solar units
PH_i/PH_k	Set of TSO/PA pumped hydro storage units
$R_{k,i}$	Set of reserve of PA in area i
$R_i.$	Set of reserve of TSO in area i
N_i	Set of PA in area i
$A.$	Set of area
$T.$	Set of time

Parameters:

$f_c(P_{(t)}^g)$	Cost function of thermal units
a_g, b_g, c_g, e_g, f_g	Coefficients of thermal units
P_{min}^g / P_{max}^g	Minimum/maximum power of thermal units
$C_{1h}, C_{2h}, C_{3h}, C_{4h}, C_{5h}, C_{6h}$	Coefficients of hydropower plants
$V_{min}^{h,i} / V_{max}^{h,i}$	Minimum/maximum reservoir volumes
Q_{min}^h / Q_{max}^h	Minimum/maximum water discharge
$I_{(t)}^h / I_{(t)}^{hl}$	Water flow rate of the reservoir/flow rate of the upper reservoir
R_u^h	Number of upper reservoirs
τ_{hl}	Time delay of the upper reservoir
V_0^h / V_T^h	Initial/final volume of reservoir
$P_{min}^{gh} / P_{max}^{gh}$	Minimum/maximum generating power of PHS
$P_{min}^{ph} / P_{max}^{ph}$	Minimum/maximum pumping power of PHS
P_{min}^h / P_{max}^h	Minimum/maximum pumping power of hydropower plants
P_{min}^w / P_{max}^w	Minimum/maximum pumping power of wind units
$P_{min}^{pv} / P_{max}^{pv}$	Minimum/maximum pumping power of solar units
V_{res}^0 / V_{res}^T	Initial/final volume of reservoir of PHS unit
$V_{res}^{start} / V_{res}^{end}$	Initial/final volume of reservoir of PHS unit

$-P_{max}^{ij} / P_{max}^{ij}$	Minimum/maximum exchanged power between TSOs
$-P_{max}^{ik} / P_{max}^{ik}$	Minimum/maximum exchanged power between TSO and PA
$RU_{g,(t)} / RD_{g,(t)}$	Up/down ramping rate limits of thermal units
$k_{w,pv}$	Cost coefficient of overestimating wind and solar power
k_{ex}	Cost coefficients of exchanged power
$P_{(t)}^{eW} / P_{(t)}^{ePV}$	Scheduled wind and solar power
$C_{(t)}^e$	Scheduled exchanged power cost
$P_{(u,1),NZ}^g / P_{(l,1),z}^g$	Lower/upper limits of thermal operating zones
NZ_g	Total number of thermal operating zones

Variables:

$C_{(t)}^{ex}$	Budget associated with underestimating exchanged power cost
$C_{(t)}^a$	Actual exchanged power cost
$P_{(t)}^{ij} / P_{(t)}^{ik}$	Exchanged power between TSO and TSO/TSO and PA
OP_{TSO} / OP_{PAGR}	Operation cost of TSO and PA
$P_{(t)}^h / P_{(t)}^g$	Hydro and thermal generated power
$V_{(t)}^h$	Water volume of the hydropower reservoir
$Q_{(t)}^h / Q_{(t)}^{hl}$	Water discharge of the hydropower reservoir/upper reservoir
$S_{(t)}^h / S_{(t)}^{hl}$	Water spillage of the hydropower reservoir/upper reservoir
$P_{(t)}^{gh} / P_{(t)}^{ph}$	Generating and pumping power of PHS
$Q_{(t)}^{gh} (P_{(t)}^{gh})$	Discharging rate of PHS
$Q_{(t)}^{ph} (P_{(t)}^{ph})$	Pumping rate of PHS
$V_{(t)}^{res}$	Volume of reservoir of PHS
$P_{(t)}^w / P_{(t)}^{pv}$	Wind and solar power generated
$P_{(t)}^d / P_{(t)}^l$	Total load demand/ active power loss
$K_{(t)}$	Total reserve cost
$\Delta P_{(t)}^R$	Total reserve required
$P_{(t)}^{aW} / P_{(t)}^{aPV}$	Actual or available wind/solar power

SUMMARY

1	INTRODUCTION.....	15
1.1	OPPORTUNITIES FOR PRIVATE AGGREGATORS IN THE POWER SYSTEMS	15
1.2	MULTI-AREA ECONOMIC DISPATCH (MAED) SOLUTIONS	17
1.3	MOTIVATION OF RESEARCH	18
1.4	JUSTIFICATION OF RESEARCH.....	18
1.5	RESEARCH OBJECTIVES	19
1.5.1	General Objective.....	19
1.5.2	Specific Objectives:	19
1.6	INNOVATIVE CONTRIBUTIONS.....	19
1.7	ORGANIZATION OF THE CHAPTERS	20
2	LITERATURE REVIEW.....	21
2.1	AGGREGATORS OF DISTRIBUTED ENERGY RESOURCES	21
2.2	MULTI-AREA ECONOMIC DISPATCH.....	23
2.3	SECTION SUMMARY II.....	26
3	PROPOSED METHODOLOGY.....	27
3.1	SEMI-DECENTRALIZED MODEL (SD)	28
3.2	FULLY DECENTRALIZED MODEL (FD)	29
3.3	MATHEMATICAL FORMULATION OF THE DECENTRALIZED MODELS	31
3.3.1	Operating Cost of TSO	32
3.3.2	Operating Cost of PA.....	37
3.4	UNCERTAINTY CONSIDERATION AND HANDLING	37
3.4.1	Quantifying power reserves need and associated costs.	38
3.5	THE REAL-CODED ELITISM GENETIC ALGORITHM (RCEGA)	39
3.5.1	Initial Population Sets.....	41
3.5.2	Handling Area Coupling and Other Systems Constraints	41
3.5.3	Decentralized Solution Implementation Procedures	42
3.6	SECTION SUMMARY III	43
4	CASE STUDIES	44
4.1	CASE 1 – IMPLEMENTING REAL-CODED GENETIC ALGORITHM	44
4.1.1	Parameter Settings – Case 1.....	44
4.1.2	Simulation Results Using Real-Coded Genetic Algorithm.....	48
4.2	CASE 2 - PERFORMANCE COMPARISON OF SELECT METAHEURISTIC ALGORITHMS	55
4.2.1	Parameter Settings – Case 2.....	55

4.2.2	Simulation Results of the Select Metaheuristic Algorithms.....	56
4.3	CASE 3 - CONSIDERATION FOR BATTERY ENERGY STORAGE SYSTEMS.	61
4.3.1	Parameter Settings – Case 3.....	61
4.3.2	Simulation Results Considering Battery Energy Storage System (BESS).....	61
4.4	SECTION SUMMARY IV	64
5	CONCLUSION.....	66
5.1	FUTURE STUDIES.....	67
5.2	PUBLICATIONS	68
5.2.1	Journal Publications	68
5.2.2	Conference Papers	68
	REFERENCES	69
	APPENDICES	75
	APPENDIX A – PARAMETERS OF TSOS AND PAS	75
	APPENDIX B – HYDRO GENERATOR PARAMETERS.....	75
	APPENDIX C – BESS PERFORMANCE.....	77

1 INTRODUCTION

The recent changes in the traditional power systems operation imposed by the integration of variable energy resources have necessitated new changes in the system's operation and economic models. Currently, the operation of many systems worldwide includes high renewable energy while many conventional generators in the system are declining substantially (MAKAROV, et al., 2017). This trend is envisaged to persist in the electricity market considering the economic and environmental benefits that renewable energy presents (KABOURIS and KANELLOS, 2010). However, these benefits come with a price. As renewable energy grows in the system, the system operation becomes more complex and the system operator faces the challenge of maintaining the system's reliable and security, considering the variability and uncertainty of renewable resources (KUMAR, et al., 2016), especially, where the dispatch of renewable energy is prioritized over the conventional generators.

Traditionally, the system operator would rely on power sharing with other areas or operators to manage its power imbalances (JI and TONG, 2018; MADADI, et al., 2019). However, over-reliance on inter-area power sharing during instances of inadequate reserve provision can lead to unimaginable price surges in the market and could make the system operation less cost-effective (HIRTH and ZIEGENHAGEN, 2015). This cost becomes increasingly important to system operators as the share of variable renewable resources increases in the system. Furthermore, the increase in the renewable energy resources permits the participation of new technologies in the system. As such, the transmission systems operator (TSO) must meet the challenge of keeping its existing infrastructure effectively open to new services to enhance the operation and cost-effectiveness of the system. Consequently, the need to make the integration of variable renewable energy in the power systems less complex, more effective, and economical becomes necessary.

1.1 OPPORTUNITIES FOR PRIVATE AGGREGATORS IN THE POWER SYSTEMS

The research on the inclusion of aggregators of distributed energy resources has been considered very promising in an electricity market environment with increasing variable renewable generation (HIRTH and ZIEGENHAGEN, 2015). Power balancing is required mostly during imminent emergency or power imbalance situations (MAZZI, et al., 2018). The power balancing or regulation provisioning have been majorly considered from conventional

generators in literatures with little attention on reserves from aggregated renewable sources (LUCÍA and JIM, 2018; MAZZI, et al., 2018). However, a number of available balancing providers is expected to decline in some systems, envisaged due to the retirement of more conventional generators in some systems. This situation indicates a foreseeable state of inadequate power balance provision and unimaginable price surges in the market during certain instances (DIVÉNYI, et al., 2019; MAKAROV, et al., 2017; RAMTEEN SIOSHANSI, 2010).

In this sense, including aggregators in the system operation can benefit the system in some major ways. One, the strategic coordination and control of the aggregators resources can help respond quickly to power imbalances in the system, especially while considering the ramping rate limitations of the conventional generators (MAZZI, et al., 2018; OLSEN, et al., 2012). Two, aggregators can support the system operator in deferring the built-out of new transmission delivery, and as more conventional generators declines in the system, they can help increase flexibility by providing both negative and positive balancing power to maintain the system operation (HELLMERS, et al., 2016; OLSEN, et al., 2012; REZA, et al., 2020). Also, beyond serving the function of balancing, the optimal allocation (location and sizing) of the aggregators can benefit the system in terms of active power loss and congestion relieves, steady-state voltage stability, and reduction in cost of operation (KARDAKOS, et al., 2016; MAZZI, et al., 2018).

Enabling robust investment recovery process can attract wider participation of aggregators in the transmission systems to meet some of the current power systems operational needs. However, preserving the baselines of the existing operators is also needful as: One, the new aggregators may seek to maximize their profits and consequently, their optimal operation could jeopardize the operation of the existing system operators, especially if the aggregators are autonomous, having their own customers and existing operation strategies (MOHITI, et al., 2019). Two, the operational uncertainties and power reserves in the area could increase drastically as the number of aggregators increases (MAKAROV, et al., 2017; MOHITI, et al., 2019), more so if the aggregators' operation include high intermittent renewable energy resources. From this perspective, the effective planning and operation of the entire power systems will rely on robust decentralized model that can coordinate the operation of multiple agents and energy resources, allowing each participant to manage its operation more effectively.

1.2 MULTI-AREA ECONOMIC DISPATCH (MAED) SOLUTIONS

In the deregulated systems, the focus of power pool is to ensure an effectiveness of the system operation while satisfying the power demand and system constraints. This is facilitated through transmitting power from an area with cheaper costs of generation to another area with high generation costs. Usually, power pool is made up of several areas that are interconnected via the tie-lines with the aim to facilitate reliability, power sharing, and security for cost-effective operation of the overall system (BASU, 2019a; BASU, 2019b; DOOSTIZADEH, et al., 2016; KHANABADI, et al., 2018). Each of the area has its own generation cost, load pattern and spinning reserves. Hence the main aim of the multi-area economic dispatch (MAED) is to determine optimal scheduling of the online generators and power exchange among the areas to minimize the overall system operation cost while satisfying the system operational constraints

The common methods in the literatures used for solving the MAED problems are the mathematical programming (MP) methods and meta-heuristic optimization (MO) methods. The usual practice in MP methods is to decouple the optimal power flow (OPF) problems around tie-lines or by manipulating the voltage angles of some buses in the boundary areas or considering both to coordinate the operation of the entire system (DOOSTIZADEH, et al., 2016; GUO, et al., 2017; LI, et al., 2016; MHANNA and VERBI, 2019; WANG and FU, 2016; WU, 2019). On the other hand, the MO methods decouple the areas via the tie-lines (GHASEMI, et al., 2016; LIN and WANG, 2019). The choice of methods used is a trade-off between pros and cons. For example, the MP methods may be computationally cheaper than the MO methods but suffers from linearization and complexity issues. Furthermore, while some MP methods have achieved decentralized solution for MAED (DOOSTIZADEH, et al., 2016; KHANABADI, et al., 2018; WU, 2019; ZHANG, et al., 2020), the existing MO methods (GHASEMI, et al., 2016; LIN and WANG, 2019) are usually conducted using centralized approaches.

Generally, the MO methods are developed to mitigate the linearization and complexity issues associated with the MP methods, since they are relatively easy to implement and can handle large scale non-linear and non-convex optimization problems and constraints (BASU, 2014; JEBARAJA, et al., 2017). However, their implementation for decentralized solution is still necessary considering that centralized models are relatively computationally expensive, complex to manage, disrespect privacy, and do not fully support regional integration (DIVÉNYI, et al., 2019; WU, 2019). As a result, the future power system operation models

may rely less on centralized approaches. From this background, this study develops two specific decentralized solution frameworks considering metaheuristics methods and thus, enabling them to meet the challenges of future power system operation involving multiple autonomous entities.

1.3 MOTIVATION OF RESEARCH

The classical multi-area economic dispatch has been studied by many authors. However, in the recent time, the power system economic models are changing because of the inclusion of new participants in the system. This new paradigm makes the operation of the power system to be more complex, considering large number of objectives and constraints to fulfill. Obviously, the previously developed models for power systems solution need to be reviewed to ensure the effective operation of the power systems, now considering the participation of numerous independent entities. Consequently, the motivation of this work is to develop practical MO-based decentralized models that permit the effective co-operation of multiple independent agents including the TSOs and PAs to enhance the overall operation of the power systems.

1.4 JUSTIFICATION OF RESEARCH

Some MP methods have achieved decentralized solution for MAED (DOOSTIZADEH, et al., 2016; KHANABADI, et al., 2018; WU, 2019; ZHANG, et al., 2020), however, they are indicated to suffer from linearization and complexity issues. Reference (ROSTAMPOUR, et al., 2019) indicated that the linearized model may not achieve optimal solution in real systems especially for weak or highly stressed systems. Therefore, the MO-based decentralized solution is necessary to address the linearization problems of the MP-based methods. Although the MO methods may not guarantee optimal solutions, still their solutions represent the actual behaviour of the power system as they do not need any form of linearization and could as well handle large number of linear and non-linear constraints.

Furthermore, the power system operation which now includes multiple TSOs and PAs becomes more complicated. This new complexity weakens the use of most centralized models considering the shortcomings already mentioned (JEAN-MICHEL and JAVIER RODRÍGUEZ-GARCÍA, 2020; NARIMANI, et al., 2018; ROSTAMPOUR, et al., 2019). In contrast, the existing MO-based MAED models (GHASEMI, et al., 2016; LIN and WANG, 2019) and even the decentralized MP-based MAED studies in the literature (KHANABADI,

et al., 2018; LU, et al., 2018; MHANNA and VERBI, 2019; ZHANG, et al., 2020;) did not include multiple local PAs in their decision-making framework. Therefore, developing effective practical decentralized models for the operation of PAs while preserving the baselines of the TSOs becomes evident and justifiable.

1.5 RESEARCH OBJECTIVES

1.5.1 General Objective

This research implements a semi-decentralized (SD) and a fully decentralized (FD) multiarea economic dispatch (MAED) model based on meta-heuristic optimization (MO) to minimize the total operation cost of transmission system operators (TSOs) and private aggregators (PAs), effectively coordinating their operations. The research specific objectives are as follow:

1.5.2 Specific Objectives:

- Modelling of the hydropower generators with cascaded reservoir, thermal generators with valve-point effects, pumped-hydro and battery energy storage units.
- Modelling the worst-case scenarios of load, wind and solar power uncertainties including the uncertainty of the exchanged power of the TSO and PAs using specific probabilistic modelling methods.
- Evaluation of the power systems optimal operation costs and net-operation costs under varying tie-line power restrictions of the TSOs and PAs, respectively.
- Analysis of the combined uncertainty impacts on the developed decentralized models.
- Performance comparison of the proposed decentralized models and their centralized counterpart model in terms of operation cost and net-operation cost.
- Validation of the developed decentralized models on a real modified interconnected multi-area power system.

1.6 INNOVATIVE CONTRIBUTIONS

The main contributions of the research are summarized as follow:

- It presents novel methodologies for conducting MO-based decentralized solutions

for MAED problems including multiple autonomous entities.

- The development of novel decentralized MAED models based on MO method for operating multi-area power systems including multiple autonomous entities.
- The proposed novel decentralized solution is developed into two distinct models namely, Semi-decentralized (SD) and fully decentralized (FD) models. The SD model is developed to attract wider inclusion of PAs in the transmission systems by allowing them to maximize profits. On the other hand, considering that optimal operation of the new PAs can jeopardize the operation of the TSOs, the FD model is developed to coordinate the operation of the PAs with the TSOs' to preserve their baselines.
- Preservation of privacy and ownership of entities considering their operation independency considering MO frameworks.
- Performance of several case studies on a modified real transmission system to demonstrate the effectiveness of the proposed models.

1.7 ORGANIZATION OF THE CHAPTERS

The rest of the research is organized as follow:

Chapter 2: Presents the literature review relating to the research. The need and roles of aggregator of distributed energy resources including the various methods used to address the multi-area economic dispatch are discussed.

Chapter 3: Presents the proposed SD and FD models and the mathematical formulations including the operation cost of the TSO and PA, uncertainty consideration and handling, reserve quantification and its associated cost, including the description of the RCEGA, the handling of area coupling and other system constraints, and implementation procedures of the proposed models.

Chapter 4: Presents several case studies constructed with the proposed SD and FD models and their fully centralized (FC) counterpart. Also, the parameter settings of the RCEGA algorithm and relevant simulation results are presented.

Chapter 5: Presents relevant states of the research including possible future studies.

2 LITERATURE REVIEW

In the following sections, the review of the new participants here-in referred as aggregators including their relevant roles in the power systems, and the common methods used for addressing multi-area economic dispatch problems are presented.

2.1 AGGREGATORS OF DISTRIBUTED ENERGY RESOURCES

The research on the inclusion of aggregators of distributed energy resources has been considered very promising in an electricity market environment with increasing intermittent renewable generation (HIRTH and ZIEGENHAGEN, 2015). Mostly, aggregators are teased to influence both the energy and balancing reserve market. In any case, the inclusion of the aggregators in the power systems provides different options for the system operator to mitigate the overall system cost of operation.

In Kardakos, et al., (2016), the optimal bidding strategy problem of a commercial virtual power plant (CVPP), which comprises of distributed energy resources (DERs), battery storage systems (BSS), and electricity consumers, and participates in the day-ahead (DA) electricity market was addressed. The CVPP model maximized the DA profit by minimizing the anticipated real-time production and the consumption of imbalance charges by formulating a three-stage stochastic bi-level optimization model while considering the uncertainty in the DA CVPP DER production and load consumption, as well as in the rivals' offer curves and real-time balancing prices.

Mueller, et al., (2017) introduced a generic and scalable approach for flexible energy systems to quantitatively describe and price their flexibility based on zonotopic sets. The description proposed allowed the aggregators to efficiently pool the flexibility of large numbers of systems and make control and market decisions on the aggregate level. In addition, an algorithm was presented that distributes aggregate-level control decisions among the individual systems of the pool in an economically fair and computationally efficient way. It was shown how the zonotopic description of flexibility could enable an efficient computation of aggregate regulation power bid-curves.

In Faria, et al., (2018), a methodology capable of managing resources through the activities of an aggregator as in the case of a Virtual Power Player, providing different choices of aggregation and remuneration strategies. The methodology was validated in a case study regarding a 21-bus network composed of 20 consumers and 26 producers with relevant results.

Mazzi, et al., (2018) proposed an innovative market framework where the participant (virtual power plant, VPP) in the balancing market was allowed to act as an active agent (i.e., a provider of regulating energy) in some trading intervals and as a passive agent (i.e., a user of regulating energy) in some others. Computational experiments showed that the VPP expected revenues could increase substantially compared to an active-only or passive-only participation.

Jiang, et al., (2019) proposed a bi-level optimization model for developing optimal bidding strategies of independent power producer in the monthly sequential contract and balancing markets based on an existing implemented monthly pre-listing balancing mechanism. The simulation results showed that the presented model could assist independent power producers in adjusting their monthly bidding strategies with relevant factors, such as the minimum output level of each producer, risk preference, and forecast information including system energy imbalance status and bidding strategies of rivals.

Tavakoli, et al., (2019) investigated an energy exchange strategy between a generating company (GenCO) and an electric vehicle load aggregator (EVLA) in the energy and ancillary services markets by proposing an optimal self-scheduling problem for a GenCO together with an EVLA and renewable generation units under an energy exchange strategy, considering the offer prices and EV tariffs under a price-maker approach and uncertainties in a two-levels operation approach. The results showed that the energy exchange strategy under flexible EV tariffs resulted in an increase of the renewable energy penetration and the profitability of the GenCO.

Alshehri, et al., (2020) focused on the aggregation of distributed energy resources (DERs) through a profit-maximizing intermediary that enables participation of DERs in wholesale electricity markets. Particularly, they studied the market efficiency brought in by the large-scale deployment of DERs and explore the extent the benefits could offset by the profit-maximizing nature of the aggregator. Their numerical experiments illustrated the impact of uncertainty and amount of DER integration on the overall market efficiency.

In Guzman, et al., (2020), a linear programming model for the aggregator's coordination strategy to maximize its profit through the management of DERs and the participation in the day-ahead reserve market was proposed. The model used EV charging control provided up/down reserves to reduce operation cost by taking advantage of the DG. The proposed mathematical model was a representation of the daily EDS operation (hourly resolution) that enforced voltage and current magnitude constraints. A case study carried out in an unbalanced 34-bus EDS with 660 EVs demonstrated that the application of the proposed method could enhance the DER aggregator's strategy with better outcomes in both profits and

EDS operation.

2.2 MULTI-AREA ECONOMIC DISPATCH

Doostizadeh, et al., (2016) developed a parallel decentralized methodology for multi-area energy and reserve clearance under wind power uncertainty. It considered preserving the independency of regional markets while fully taking the advantages of interconnection as a salient feature of the new model. Additionally, the parallel procedure simultaneously clears regional markets for the sake of acceleration particularly in large-scale systems. To achieve the optimal solution in a distributed fashion, the augmented Lagrangian relaxation along with alternative direction method of multipliers were applied. The effectiveness and robustness of the proposed method were evaluated through several case studies on a two-area 6-bus and the modified three-area IEEE 118-bus test systems.

In Madadi, et al., (2019), a decentralized methodology was proposed for optimal scheduling of generation units taking into consideration environmental constraint, dynamic line rating, wind power generations, compressed air energy storage and power pool market. A ε -constraint approach was applied to solve the proposed dynamic economic/environmental dispatch of multi-area model. In addition, a fuzzy satisfying technique was used to select the best compromise solution. An interconnected, multi-area power system with cross-border trading in the presence of wind power uncertainty and the storage unit was considered for evaluating the proposed method.

In Ding, et al., (2019), a novel distributed continuation power flow (CPF) algorithm based on block matrix computations was presented for realizing the decomposition and coordination calculation of multiple regional subsystems. This distributed algorithm could preserve the precision and convergence of integrated CPF algorithms and has an advantage in terms of the calculation speed. The performance of the proposed CPF model and distributed algorithm was demonstrated via case studies and comparative analyses.

Similar to the MP methods described above, an augmented Lagrangian method is proposed in (FU, et al., 2016), alternating direction method of multipliers (ADMM) in (MHANNA and VERBI, 2019), stochastic optimization in (WANG and FU, 2016), quadratic programming in (GUO, et al., 2017), linear programming in (LI, et al., 2016), mixed integer programming (MIP) in (KHANABADI, et al., 2018) and distributed interior point method in (LU, et al., 2018). Although the MP studies were conducted in remarkably interesting manner, however, they are indicated to suffer from linearization issues which makes them less suitable

for very complex non-linear and non-convex optimization problems.

Consequently, in Basu (2014), teaching learning-based optimization algorithm was proposed for solving MAED problem with tie line constraints considering transmission losses, multiple fuels, valve-point loading and prohibited operating zones. The effectiveness of the proposed algorithm was verified on three different test systems, both small and large, involving varying degree of complexity.

In Jadoun, et al. (2015), improved PSO was proposed to solve multi area economic dispatch (MAED) problem. The objective of the MAED problem determined the optimal value of power generation and interchange of power through tie-lines interconnecting areas to minimize the total fuel cost of thermal generating units of all areas while satisfying system non-linear operational constraints. To obtain more accurate solution, the control equation of the proposed PSO was modified by suggesting improved cognitive component of the particle's velocity by suggesting preceding experience. The effectiveness of the proposed method was tested on four areas, 40 generators test system. The application results showed the robustness of the proposed model to solve large-dimensional MAED problem effectively.

In Secui (2015), a chaotic optimizing method based on the global best artificial bee colony algorithm, where the random sequences used in updating the solutions of this algorithm are replaced with chaotic sequences generated by chaotic maps was proposed. The algorithm chaotic global best artificial bee colony algorithm was used to solve the multi-area economic/emission dispatch problem taking into consideration the valve-point effects, the transmission line losses, multi-fuel sources, prohibited operating zones, tie line capacity and power transfer cost between different areas of the system. Experimental results were used to verify the robustness of the model.

Basu (2016) presented a quasi-oppositional group search optimization for solving multi-area dynamic economic dispatch problem with multiple fuels and valve-point loading. The proposed model employed quasi-oppositional based learning (QOBL) for population initialization and also for generation jumping. The model was tested on two multi-area test systems having valve point loading and multi-fuel option. It was found that the proposed model provided attractive solution for the MAED.

In Ghasemi, et al., (2016), an efficient and powerful heuristic-hybrid algorithm using hybrid DE (differential evolution) and PSO (particle swarm optimization) techniques DEPSO (differential evolution particle swarm optimization) was proposed to solve several optimization problems including the MAED (multi-area economic dispatch), RCMAED (reserve constrained MAED) and RCMAEED (reserve constrained multi area environmental/economic

dispatch) problems with reserve sharing in power system operations. The effectiveness and efficiency of the proposed algorithm was affirmed by the experimental results presented.

In First and Jinbei (2018), an efficient and powerful crisscross optimization algorithm (CSO) combining Pareto multi-objective processing strategy (MOCSO) was proposed. The proposed MOCSO approach addressed the different types of complex multi-objective MAED problem by applying two interacting search operators, namely horizontal crossover and vertical crossover. The former was used to enhance the MOCSO's global search ability in complex solution space by introducing a distinctive cross-border crossover mechanism while the latter prevented the premature convergence by a unique dimensional crossover approach. The effectiveness and efficiency of the MOCSO algorithm was demonstrated with relevant results.

Olang, et al. (2018) presented a multi objective, multi area hydrothermal environmental economic dispatch (MOMAHEED) problem to determine the optimal generating level of all the hydro and thermal generating units to adequately supply the demand, such that the total fuel cost of thermal plants in all areas and emissions are simultaneously curtailed while satisfying all physical and operational constraints. MOMAHEED was solved using Bat Algorithm (BA) which is inspired by echolocation behavior of micro bats. The multi objective function is converted to a single objective one using weighted sum method and cardinal priority ranking is used to select the optimal solutions. The algorithm when tested on a four-area system considering three test cases resulted in cost-effectiveness of the system.

Basu (2019a), presented a squirrel search algorithm (SSA) for solving intricate multi-region combined heat and power economic dispatch problem with integration of renewable energy sources. The valve point effect and proscribed workable area of thermal generators and solar and wind power uncertainty was addressed. SSA is a swarm-based intelligence algorithm which emulates the dynamic scavenging activities of squirrels. The efficiency of the suggested method was revealed on a three-region test system with capability to bestow with better-quality solution.

In Lin and Wang (2019), an improved stochastic fractal search (ISFS) was proposed to solve the MAED problem considering the area load demands, the tie-line limits and various operating constraints. To balance exploration and exploitation, the ISFS introduced an opposition-based learning method for population initialization as well as for generation jumping. By combining with the differential evolution strategy, a hybrid diffusion process was then developed and used as the local search technique to enhance the exploitation ability. Furthermore, a novel repair-based penalty approach was presented and incorporated into the ISFS to find feasible solutions more efficiently. The effectiveness of the ISFS was

demonstrated on a real test system.

Basu (2019b), presented nondominated genetic algorithm–II (NSGA-II) for solving multi-area dynamic economic emission dispatch (MADEED) of hydro-wind-thermal power system where power generations are allocated among the on-line units in such a manner that total cost and emission level are optimized simultaneously while fulfilling all operational constraints. Test results of a four-area system acquired from the suggested technique were fit to that acquired from strength pareto evolutionary algorithm 2 (SPEA 2).

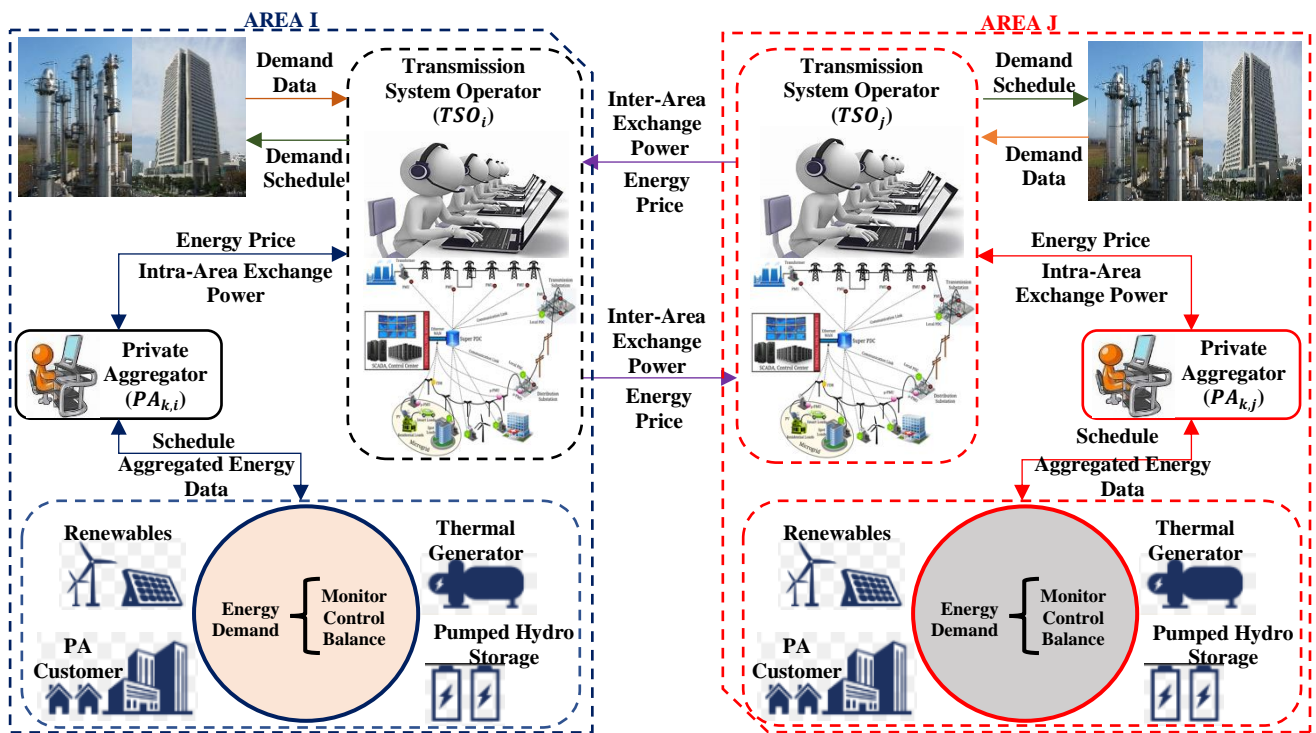
2.3 SECTION SUMMARY II

These previous studies have presented interesting results in terms of cost-effectiveness of the system operation; however, they did not include uncertainties in their decision-making frameworks. And where uncertainties were considered, the solution methods for the participation of the aggregators in the power systems were limited to mathematical programming (MP) methods which do suffer from the linearization issues. In systems where there is need to address complex and multiple non-convex functions, the metaheuristic methods are considered suitable. Even with this capability, the existing metaheuristic methods are still limited to either not considering multiple autonomous participants in their decision-making frameworks or using centralized approaches. Considering that centralized models are relatively computationally expensive, complex to manage, disrespect privacy, and do not fully support regional integration, the future power system operation models may rely less on centralized approaches. Therefore, implementing the metaheuristic methods for decentralized solutions becomes very necessary.

3 PROPOSED METHODOLOGY

This research develops two decentralized MAED models based on MO method to solve the MAED problem consisting of multiple transmission system operators (TSOs) and private aggregators (PAs) with minimal cost. The diagrammatic framework showing the inter-area interaction between TSO/TSO and intra-area interaction of TSO/PAs is presented in Figure 3.1.

Figure 3.1 – Diagrammatic framework showing the inter-area interaction between TSO/TSO and intra-area interaction between TSO/local PA



Source: Authors.

Note the term “private” is used to connote the “independency” of the PAs. The proposed decentralized models allow to determine the effective integration of autonomous PAs in the transmission systems (TS) and their co-operation with the TSOs. The objective of both models is to minimize the total operation cost of the system by effectively coordinating the TSOs and PAs operations.

The first model is a SD model developed to attract wider inclusion of PAs in the transmission systems by allowing them to maximize profits. The second model is a FD model developed to coordinate the operation the PAs with the TSO to preserve their baselines. Unlike

the previous MO-based MAED studies, both models use multiple input-output population sets to achieve decentralization for the entire system.

The developed models manage the ownership of TSOs and PAs, and consider the combined uncertainties of wind, solar, and load, including the uncertainties of the intra- and inter-area exchanged power costs of TSOs and PAs. Both models are solved using a Real-Coded Elitism Genetic Algorithm (RCEGA). To preserve the operation independence of TSOs and PAs, the RCEGA efficiently utilizes separate population sets to solve the operations of the areas in parallel in a two-layer operation approach, allowing the TSOs and PAs to achieve optimal operations, independently.

Considering that optimality is strictly based on accurate probability distribution function (PDF) (KHANABADI, et al., 2018; BASU, 2019), this study assumes that TSOs and PAs evaluate their degree of conservatism using the expected values along with the minimum and maximum deviations of the uncertain variables and account for their impacts on the power system operation in terms of power reserves requirement and associated costs (MELODI, et al., 2016; MOHITI, et al., 2019). This way, the inherent risks are still preserved, and the total execution time is reduced.

To reduce the problem complexity, the operation of the PAs is differentiated from the existing transmission participants in each area assuming that the TSO of the area owns all the existing generating units in the area. Although, the generators may be owned by different owners in the actual sense, the idea is to be able to properly account for the impact of operation of the new PAs in the system. Therefore, the TSO and PAs in each area are treated as separate entities with their operations coupled via the tie-lines. The proposed day-head semi and fully decentralized economic dispatch models are described in section 3.1 and 3.2, respectively.

3.1 SEMI-DECENTRALIZED MODEL (SD)

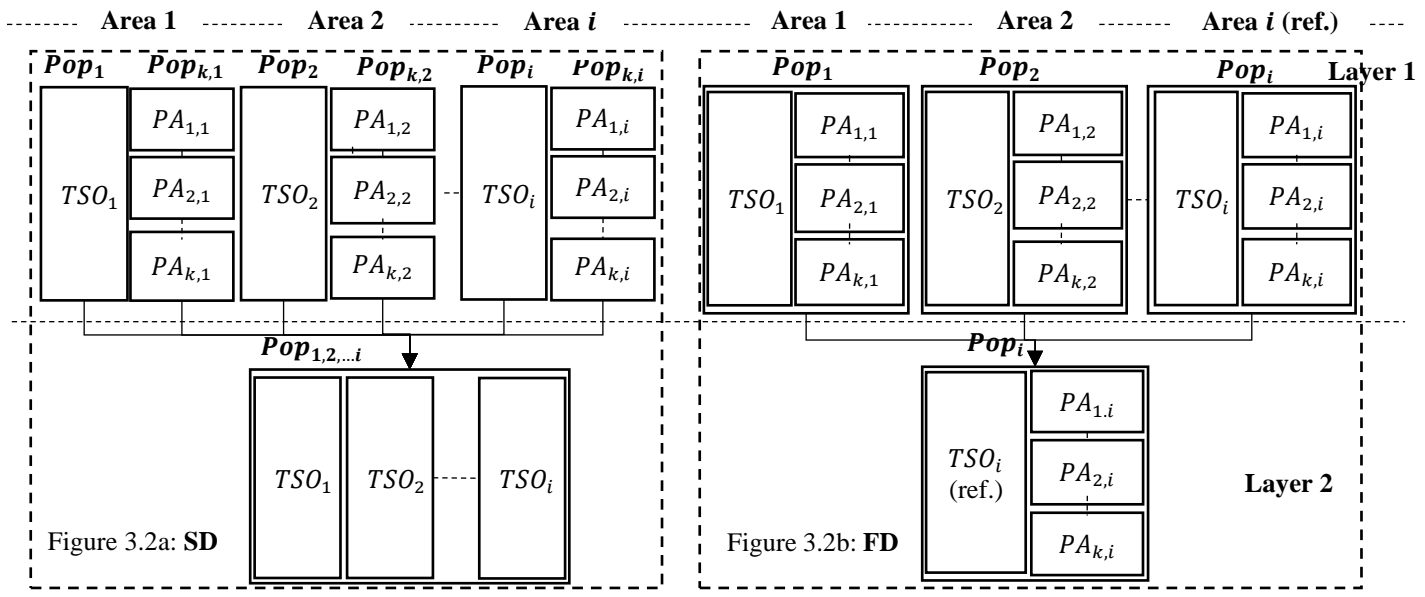
The decentralized structure of the SD model is presented in Figure 3.2a. Still recall that the SD model is particularly developed to attract wider inclusion of PAs in the transmission systems by allowing them to maximize profits. Note that individual participants (i.e., TSO and PAs) are organized into separate input-output population sets for the RCEGA implementation, giving complete operation autonomy to each party. Furthermore, the SD model is divided into two independent layers. A layer refers to an operational level where the operation of the respective areas takes place. In the first layer, the scheduling of PAs is prioritized together with the TSOs' hydropower, pumped-hydro storage (PHS), wind, and solar units in a decentralized

manner. However, to mitigate the increased power system uncertainties, an inter-area power exchange is facilitated using a centralized strategy to re-coordinate and reschedule all TSOs' thermal units in the second layer. It should be mentioned that the SD model only preserves the privacy of the local PAs as they interact with the responsible TSO via the TSO-PA tie-lines in the area but ultimately destroys the privacy preservation of the responsible TSO as it interacts with the neighbouring TSOs via the TSO-TSO tie-lines. As a result, the SD model is termed a semi-decentralized model.

3.2 FULLY DECENTRALIZED MODEL (FD)

The decentralized structure of the FD model is presented in Figure 3.2b. The FD model is developed to investigate the power system operation assuming that the operation of the PAs is coordinated with the TSOs' to preserve their baselines. Unlike the SD model which uses independent population sets for the TSO and PAs across the entire power system, the FD model only organizes the areas into separate input-output population sets for RCEGA implementation, allowing the TSO in each area to coordinate the PAs operations in the area. The FD solution is further divided into two independent layers. The first layer is concerned with the decision making of each power system area with their decentralized operations. The individual area's dispatch is coordinated using the thermal operation cost, the exchanged power with neighbouring areas and the associated hourly prices for a day-ahead operation. However, the independent approach may violate some operational constraints, especially the power output constraints of the reference generator and could compromise the solution optimality. To address this issue, the reference area in which the reference generator is located is assigned to coordinate the overall power system operation in the second layer. To realize this, other areas send their optimal operational data to the reference TSO who readjusts the operations of participants in the reference area accordingly.

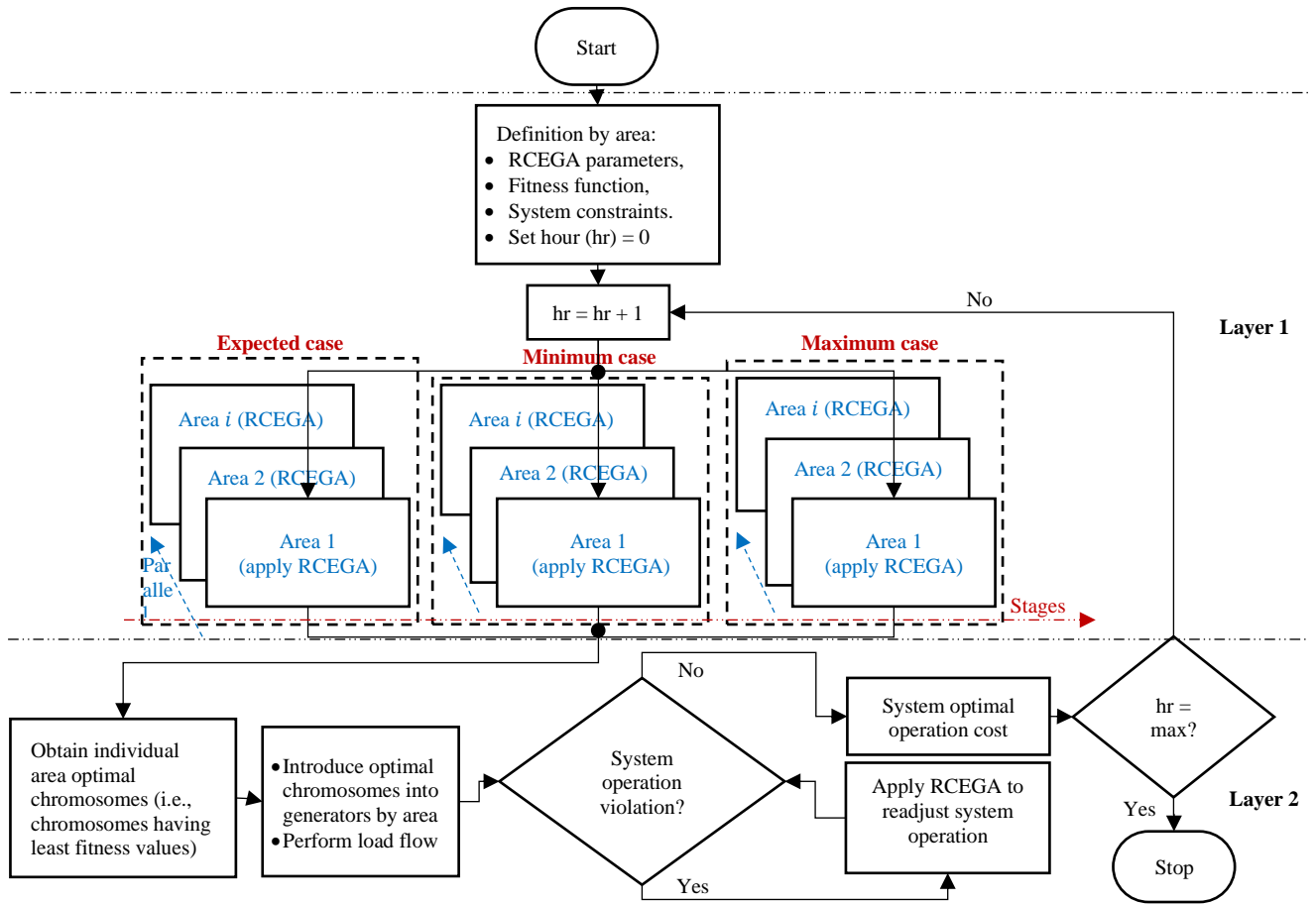
Figure 3.2 – Decentralized structure of the proposed semi-decentralized (SD) and fully decentralized (FD) models



Source: Authors.

Considering that the TSOs and PAs evaluate their operations using the expected variables and their worst-case deviations, a three-stage optimization approach is employed to coordinate the TSOs and PAs operations. In the first stage, the expected variables (load, wind, solar, and exchanged power cost) are considered for evaluating the power system objective function. In the second and third stages, the uncertainties (modelled as the minimum and maximum deviations of the expected variables) are evaluated in the objective function to validate the effectiveness of the models. The flowchart describing the parallel operations of the areas and multi-stage solutions for the base case and scenario cases is shown in Figure 3.3.

Figure 3.3 – Flowchart of the proposed decentralized models



Source: Authors.

3.3 MATHEMATICAL FORMULATION OF THE DECENTRALIZED MODELS

Assuming area i as the reference, the objective function is to minimize the total system operation cost PS_{oc} , comprising the $TSOs$ and PAs total operation costs, given in Equation (1) and (2) for the SD and FD models, respectively.

$$PS_{oc}^{SD} = \min \begin{cases} \sum_{\substack{t \in T, \\ i \in A}} OP_{TSO_i(t)} + \sum_{\substack{t \in T, \\ k \in N_i}} OP_{PA_{k,i}(t)}, & \text{layer} = 1 \\ A_c + \sum_{\substack{t \in T, \\ i \in A}} OP_{TSO_i(t)}, & \text{layer} = 2 \end{cases} \quad (1)$$

$$PS_{oc}^{FD} = \min \begin{cases} \sum_{\substack{t \in T, \\ i \in A, \\ k \in N_i}} (OP_{TSO_i(t)} + OP_{PA_{k,i}(t)}), & \text{layer} = 1 \\ B_c + \sum_{\substack{t \in T, \\ i=1, \\ k \in N_i}} (OP_{TSO_i(t)} + OP_{PA_{k,i}(t)}), & \text{layer} = 2 \end{cases} \quad (2)$$

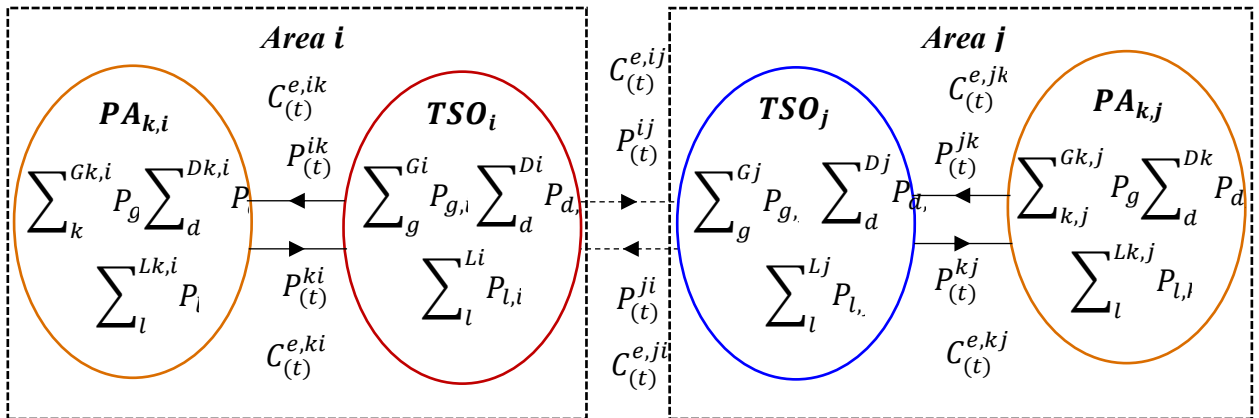
Equation (1) represents the total system operation cost with the SD model. Note that A_c

is a constant representing the optimal operation cost in layer 1 excluding the operation cost of the *TSOs*' thermal units in all areas, Equation (2) represents the total system operation cost with the FD model. Note that B_c is a constant representing the optimal operation cost in layer 1 excluding the reference area. In addition, t is the time index in hours, T is the total number of hours, i is the area index, A is the total number of power system areas, k is the *PA* index, N_i is the total number of *PA*s in area i , and $OP_{TSO_i(t)}$ and $OP_{PA_{k,i}(t)}$ are the operation costs of the TSO_i and $PA_{k,i}$, respectively. It should be mentioned that the SD and FD models are two distinct models and therefore, their performance simulation are performed separately.

3.3.1 Operating Cost of TSO

A multiarea power system is shown in Figure 3.4, consisting of areas i and j . The notations " ij " and " ik " denote the power flowing from area i to area j and from TSO_i to $PA_{k,i}$, respectively. The TSO_i exchanges power $P_{(t1)}^{ij}$ with TSO_j at cost $C_{(t1)}^{e,ij}$, while TSO_j exchanges power $P_{(t2,t2 \neq t1)}^{ji}$ with TSO_i at cost $C_{(t2,t2 \neq t1)}^{e,ji}$.

Figure 3.4 – Interconnected power system *area i* having TSO_i and $PA_{k,i}$, and *area j* having TSO_j and $PA_{k,j}$



Source: Authors.

When the TSO_i and TSO_j relate to more than one tie-lines, the TSO with net power exchange deficit pays the cost of the net power exchanged. A similar principle exists between TSO_i and local $PA_{k,i}$. Considering that TSO_i owns all the existing generating units in its area, the penalty cost of underestimating wind and solar power, and load are neglected. Hence, the operation cost of the TSO_i is obtained using Equation (3).

$$OP_{TSO_i} = \sum_{t \in T} \left\{ \sum_{g \in TG_i} \sum_{i \in A} f_c(P_{(t)}^{g,i}) + \sum_{\substack{j \in A \\ j \neq i}} C_{(t)}^{e,ji} P_{(t)}^{ji} + \sum_{k \in N_i} C_{(t)}^{e,ki} P_{(t)}^{ki} \right\} \quad (3)$$

where $f_c(P_{(t)}^{g,i})$ is the fuel cost function of thermal unit g , TG_i is total number of thermal units, $P_{(t)}^{ji}$ and $P_{(t)}^{ki}$ are the expected power purchases from TSO_j and $PA_{k,i}$, and $C_{(t)}^{e,ji}$ and $C_{(t)}^{e,ki}$ are the associated costs, in area i . The fuel cost function of thermal unit g in area i considering valve-point effect is obtained using Equation (4) (BASU, 2019; LIN and WANG, 2019).

$$f_c(P_{(t)}^{g,i}) = a_{g,i}(P_{(t)}^{g,i})^2 + b_{g,i}P_{(t)}^{g,i} + c_{g,i} + \left| e_{g,i} \sin \left(f_{g,i} \left(P_{min}^{g,i} - P_{(t)}^{g,i} \right) \right) \right| \quad (4)$$

where $f_c(P_{(t)}^{g,i})$ is the fuel cost function, $P_{(t)}^{g,i}$ is the active power generated, and $a_{g,i}$, $b_{g,i}$, $c_{g,i}$, $e_{g,i}$, and $f_{g,i}$ are the fuel cost coefficients of thermal unit g in area i . Since the real forecast data of wind and solar power are used for this study, their modelling is not presented. However, more details about their modelling can be found in (BASU, 2019a; BASU, 2019b).

3.3.1.1 Modelling of the hydropower generator

The hydropower plant generation output modelling is based on (BASU, 2019a; BASU, 2019b; DUBEY, et al., 2016), given in Equation (5).

$$P_{(t)}^{h,i} = C_{1h,i}(V_{(t)}^{h,i})^2 + C_{2h,i}(Q_{(t)}^{h,i})^2 + C_{3h,i}V_{(t)}^{h,i}Q_{(t)}^{h,i} + C_{4h,i}V_{(t)}^{h,i} + C_{5h,i}Q_{(t)}^{h,i} + C_{6h,i} \quad (5)$$

where $V_{(t)}^{h,i}$ is the reservoir storage volume, $Q_{(t)}^{h,i}$ is the discharge rate, and $C_{1h,i}$, $C_{2h,i}$, $C_{3h,i}$, $C_{4h,i}$, $C_{5h,i}$, and $C_{6h,i}$ are the hydropower plant coefficients in area i .

3.3.1.2 Hydraulic network constraints:

The hydraulic constraints are presented in (6)-(9) (BASU, 2019a; BASU, 2019b; DUBEY, et al., 2016; LIAO, et al., 2013). The physical limitations on reservoir storage volumes and discharge rates are given by (6) as follows:

$$\begin{cases} V_{min}^{h,i} \leq V_{(t)}^{h,i} \leq V_{max}^{h,i} \\ Q_{min}^{h,i} \leq Q_{(t)}^{h,i} \leq Q_{max}^{h,i} \end{cases} \quad (6)$$

where V_{min}^h, V_{max}^h are the min./max. storage volume of hydro-plant reservoir h , Q_{min}^h, Q_{max}^h are the min./max. water discharge of hydro-plant reservoir h .

The continuity equation for the hydro reservoir network is.

$$V_{(t+1)}^{h,i} = V_{(t)}^{h,i} + I_{(t)}^{h,i} - Q_{(t)}^{h,i} - S_{(t)}^{h,i} + \sum_{l=1}^{R_u^{h,i}} \left(Q_{(t-\tau hl,i)}^{hl,i} + S_{(t-\tau hl,i)}^{hl,i} \right) \quad (7)$$

where $I_{(t)}^h$ is the water inflow rate of hydro-plant reservoir h , $I_{(t)}^{hl}$ is the water inflow rate of upper reservoir l to h , R_u^h is the number of upstream units directly above hydro plant reservoir h , τ_{hl} is the water transport delay from reservoir l .

Assuming the spillage to be zero for simplicity, the hydraulic continuity constraints are:

$$V_0^{h,i} - V_T^{h,i} = \sum_{t=1}^T Q_{(t)}^{h,i} - \sum_{t=1}^T \sum_{l=1}^{R_u^h} Q_{(t-\tau_{hl,i})}^{hl,i} - \sum_{t=1}^T I_{(t)}^{h,i} \quad (8)$$

where V_0^h/V_T^h are the initial/final storage volume of hydro-plant reservoir h .

In order to meet exactly the restrictions on the initial and final reservoir storage levels, the water discharge rate of the h hydro plant $Q_d^{h,i}$ in the dependent interval d is then calculated by:

$$Q_d^{h,i} = V_0^{h,i} - V_T^{h,i} + \sum_{t=1}^T I_{(t)}^{h,i} + \sum_{t=1}^T \sum_{l=1}^{R_u^h} Q_{(t-\tau_{hl,i})}^{hl,i} - \sum_{\substack{t=1, \\ t \neq d}}^T Q_{(t)}^{h,i} \quad (9)$$

The dependent water discharge rate must satisfy the above constraints on the physical limitations of the reservoir storage volumes and discharge rates.

3.3.1.3 Modelling pumped storage hydropower (PSH)

The PSH model considering its generating and pumping modes is modelled according to (BASU, 2019) as given in (10) and (11), respectively.

$$\begin{cases} P_{min}^{gh,i} \leq P_{(t)}^{gh,i} \leq P_{max}^{gh,i} & MW; \\ P_{min}^{gh,i} = 0; P_{max}^{gh,i} > 0 & MW; \\ Q_{(t)}^{gh,i} (P_{(t)}^{gh,i}) = \rho_i + 2P_{(t)}^{gh,i} & acre - ft/hr; \end{cases} \quad (10)$$

$$\begin{cases} P_{min}^{ph,i} \leq P_{(t)}^{ph,i} \leq P_{max}^{ph,i} & MW; \\ P_{min}^{ph,i} < 0; P_{max}^{ph,i} = 0 & MW; \\ Q_{(t)}^{ph,i} (P_{(t)}^{ph,i}) = -\mu_i & acre - ft/hr; \end{cases} \quad (11)$$

where $P_{(t)}^{gh,i}$, $P_{(t)}^{ph,i}$ are the generating and pumping power, respectively, $Q_{(t)}^{gh,i} (P_{(t)}^{gh,i})$ is the discharging rate, $Q_{(t)}^{ph,i} (P_{(t)}^{ph,i})$ is the pumping rate, and ρ_i and μ_i are real positive values. It should be mentioned that $P_{(t)}^{gh,i} \geq 0$ and $P_{(t)}^{ph,i} = 0$ when the PHS is in generating mode, $P_{(t)}^{gh,i} = 0$ and $P_{(t)}^{ph,i} < 0$ when the PHS is in pumping mode. For each time the PHS performs a changeover function, it enters a temporary state of rest for a period due to its physical limitation. At these instances, $P_{(t)}^{gh,i} = P_{(t)}^{ph,i} = 0$.

3.3.1.4 Modelling battery energy storage system (BESS)

First, a major consideration for BESS is its charging and discharging capacities. Both State of Charge (SoC) and Depth of Discharge (DoD) are usually used for limiting the ESS power injection. The SOC is calculated by (FARROKHIFAR, 2016; LUO, et al, 2015):

$$SoC_{(t)}^i = \frac{C_{(t)}^{bess,i}}{C_{max}^{bess}} \quad (12)$$

$$DoD_{(t)}^i = 1 - SoC_{(t)}^i \quad (13)$$

$$0 \leq |P_{(t)}^{bess,i}| \leq P_{max}^{ess} \quad (14)$$

$$C_{min}^{bess} \leq C_{(t)}^{bess,i} \leq C_{max}^{bess} \quad (15)$$

$$C_{(t)}^{bess,i} = C_{(t-1)}^{bess,i} + (P_{(t)}^{bess,i} * \rho^{bess,i})\Delta t \quad (16)$$

$SoC_{(t)}^i$ is the State of Charge, $DoD_{(t)}^i$ is the Depth of Discharge, C_{max}^{ess} is the rated energy capacity in MWh, $C_{(t)}^{ess,i}$ is the energy capacity, $P_{(t)}^{ess,i}$ is the BESS power injected/consumed, P_{max}^{ess} is the rated power capacity of the BESS in MW, $C_{min}^{bess}/C_{max}^{bess}$ are the minimum and maximum energy allowed in each state of time t of the i -th BESS unit, $\rho^{bess,i}$ is the efficiency of charging or discharging of the BESS, and Δt is the operation time-step of the BESS in hours.

3.3.1.5 Power balance constraints

The power balance for the power system considering the operating modes of the PHS is given in (12)-(14) (BASU, 2019):

- When PHS in the generation mode ($t \in T_{gen}$) and BESS is discharging:

$$\begin{aligned} & \sum_{\substack{g \in TG_i \\ i \in A}} P_{(t)}^{g,i} + \sum_{\substack{h \in H_i \\ i \in A}} P_{(t)}^{h,i} + \sum_{\substack{w \in WG_i \\ i \in A}} P_{(t)}^{w,i} + \sum_{\substack{pv \in PV_i \\ i \in A}} P_{(t)}^{pv,i} + P_{(t)}^{gh,i} + P_{(t)}^{bess,i} + \sum_{k \in N_i} P_{(t)}^{n,ik} + \sum_{\substack{j \in A \\ j \neq i}} P_{(t)}^{n,ij} \\ & = P_{(t)}^{d,i} + P_{(t)}^{l,i} \end{aligned} \quad (12)$$

- When PHS is in pumping mode ($t \in T_{pump}$) and the BESS is charging:

$$\begin{aligned} & \sum_{\substack{g \in TG_i \\ i \in A}} P_{(t)}^{g,i} + \sum_{\substack{h \in H_i \\ i \in A}} P_{(t)}^{h,i} + \sum_{\substack{w \in WG_i \\ i \in A}} P_{(t)}^{w,i} + \sum_{\substack{pv \in PV_i \\ i \in A}} P_{(t)}^{pv,i} + \sum_{k \in N_i} P_{(t)}^{n,ik} + \sum_{\substack{j \in A \\ j \neq i}} P_{(t)}^{n,ij} \\ & = P_{(t)}^{d,i} + P_{(t)}^{ph,i} + P_{(t)}^{bess,i} + P_{(t)}^{l,i} \end{aligned} \quad (13)$$

- When PHS is in changeover mode ($t \in T_{changeover}$) and BESS is resting:

$$\begin{aligned}
& \sum_{\substack{g \in TG_i \\ i \in A}} P_{(t)}^{g,i} + \sum_{\substack{h \in H_i \\ i \in A}} P_{(t)}^{h,i} + \sum_{\substack{w \in WG_i \\ i \in A}} P_{(t)}^{w,i} + \sum_{\substack{pv \in PV_i \\ i \in A}} P_{(t)}^{pv,i} + \sum_{k \in N_i} P_{(t)}^{n,ik} + \sum_{\substack{j \in A \\ j \neq i}} P_{(t)}^{n,ij} \\
& = P_{(t)}^{d,i} + P_{(t)}^{l,i}
\end{aligned} \tag{14}$$

where $P_{(t)}^{w,i}$ and $P_{(t)}^{pv,i}$ are the wind and solar power realizations, respectively, H_i , WG_i and PV_i are the total number of hydro, wind and solar power units, respectively, $P_{(t)}^{d,i}$ and $P_{(t)}^{l,i}$ are the total load and active power loss in area i , $P_{(t)}^{n,ik}$ is the net-power exchange between TSO_i and $PA_{k,i}$, $P_{(t)}^{n,ij}$ is net-power exchange between TSO_i and TSO_j , and T_{gen} , T_{pump} , $T_{changeover}$ are the times when the PHS is in the generating, pumping and changeover modes respectively. Recall that the PHS power is zero when it changes from the generating to pumping mode and vice versa. Observe the active power loss $P_{(t)}^{l,i}$ is duly represented in the respective power balance constraints.

3.3.1.6 Generation limits

All generating units must operate within their minimum and maximum generating capacities as given in (16) (BASU, 2019a; BASU, 2019b).

$$\begin{cases} P_{min}^{h,i} \leq P_{(t)}^{h,i} \leq P_{max}^{h,i} \\ P_{min}^{g,i} \leq P_{(t)}^{g,i} \leq P_{max}^{g,i} \\ P_{min}^{w,i} \leq P_{(t)}^{w,i} \leq P_{max}^{w,i} \\ P_{min}^{pv,i} \leq P_{(t)}^{pv,i} \leq P_{max}^{pv,i} \end{cases} \tag{16}$$

where $P_{min}^{h,i}$, $P_{max}^{h,i}$, $P_{min}^{w,i}$, $P_{max}^{w,i}$, $P_{min}^{pv,i}$, $P_{max}^{pv,i}$ are the minimum and maximum generating power of hydro, wind, and solar power plants in area i , respectively.

3.3.1.7 Thermal generator ramp rate limits constraints

The ramp up/down rates limitations $RU_{g,i}$ and $RD_{g,i}$, respectively, of thermal unit g are defined in (17) (BASU, 2019; ROSTAMPOUR, et al., 2019):

$$\begin{cases} P_{(t)}^{g,i} - P_{(t-1)}^{g,i} \leq RU_{g,i,t} \\ P_{(t-1)}^{g,i} - P_{(t)}^{g,i} \leq RD_{g,i,t} \end{cases} \tag{17}$$

3.3.1.8 Tie line capacity and security constraints

The tie-line power transfer $P_{(t)}^{ij}$, $P_{(t)}^{ji}$ and $P_{(t)}^{ik}$, $P_{(t)}^{ki}$ should be less or equal to the tie-line maximum transfer capacity, as expressed in (18) (JI and TONG, 2018; BASU, 2019).

$$\begin{cases} (-P_{max}^{ij} = P_{max}^{ji}) \leq P_{(t)}^{ij} \leq (P_{max}^{ij} = -P_{max}^{ji}) \\ (-P_{max}^{ik} = P_{max}^{ki}) \leq P_{(t)}^{ik} \leq (P_{max}^{ik} = -P_{max}^{ki}) \end{cases} \quad (18)$$

3.3.2 Operating Cost of PA

The operating cost of PAs, neglecting the maintenance cost and the penalty cost associated with the wind and solar power imbalances, is given in Equation (19).

$$OP_{PA_{k,i}} = \sum_{k \in N_i} \sum_{i \in A} f_c(P_{(t)}^{g,k}) + \sum_{k \in N_i} C_{(t)}^{e,ik} P_{(t)}^{e,ik} \quad (19)$$

where $f_c(P_{(t)}^{g,k})$ is the fuel cost function of thermal unit g of $PA_{k,i}$ and $P_{(t)}^{e,ik}$, and $C_{(t)}^{e,ik}$ are the expected purchased power and the associated cost from TSO_i , respectively. The fuel cost function of thermal unit g of $PA_{k,i}$ in area i is obtained using Equation (20) (BASU, 2019A; BASU, 2019B; SHIWEI, et al., 2020).

$$f_c(P_{(t)}^{g,k}) = a_{g,k}(P_{(t)}^{g,k})^2 + b_{g,k}P_{(t)}^{g,k} + c_{g,k} \quad (20)$$

where $f_c(P_{(t)}^{g,k})$ is the fuel cost function, $P_{(t)}^{g,k}$ is the active power generated, and $a_{g,k}$, $b_{g,k}$, and $c_{g,i}$, are the fuel cost coefficients of thermal unit g of $PA_{k,i}$ in area i .

For the $PA_{k,i}$ in area i , the mathematical modeling of the pumped storage hydropower unit is obtained as in Equation (10)-(11). The power balance constraints and generators power limits are obtained as in (10)-(15) but without hydropower unit. The generator ramp rates limits, line capacity and security constraints are obtained as in (16)-(18).

3.4 UNCERTAINTY CONSIDERATION AND HANDLING

Without regard to ownership of wind and solar units, the decentralized planning model must account for the operational uncertainties if the available load, wind, and solar power are less than their expected values. This is modeled in terms of the power reserves needed. The actual values of wind and solar power and load are modelled in terms of their expected value using probabilistic modelling methods (GUAN and WANG, 2014; MELODI, et al., 2016; SHAHIRINIA, et al., 2016; MOHITI, et al., 2019). The worst-case scenarios are the minimum and maximum deviations of the expected values given by (21).

$$\begin{cases} P_{(t)}^{aW} = (P_{(t)}^W + \Delta P_{(t)}^W), & \begin{cases} \Delta P_{(t),min}^W, & P_{(t)}^{aW} < P_{(t)}^W \\ \Delta P_{(t),max}^W, & P_{(t)}^{aW} > P_{(t)}^W \end{cases} \\ P_{(t)}^{aPV} = (P_{(t)}^{PV} + \Delta P_{(t)}^{PV}), & \begin{cases} \Delta P_{(t),min}^{PV}, & P_{(t)}^{aPV} < P_{(t)}^{PV} \\ \Delta P_{(t),max}^{PV}, & P_{(t)}^{aPV} > P_{(t)}^{PV} \end{cases} \\ P_{(t)}^{ad} = (P_{(t)}^d + \Delta P_{(t)}^d), & \begin{cases} \Delta P_{(t),min}^d, & P_{(t)}^{ad} < P_{(t)}^d \\ \Delta P_{(t),max}^d, & P_{(t)}^{ad} > P_{(t)}^d \end{cases} \end{cases} \quad (21)$$

where $P_{(t)}^W$, $P_{(t)}^{PV}$, $P_{(t)}^d$ / $P_{(t)}^{aW}$, $P_{(t)}^{aPV}$, $P_{(t)}^{ad}$ / $\Delta P_{(t)}^W$, $\Delta P_{(t)}^{PV}$, $\Delta P_{(t)}^d$ are the expected values, actual, and deviations of wind and solar power, and load, respectively.

3.4.1 Quantifying power reserves need and associated costs.

The required power reserve is computed using the net-deviation concept (i.e., the combined wind and solar power and load forecast deviations) instead of treating the deviations separately, as in Equation (22) (MAKAROV, et al., 2017).

$$\Delta P_{(t)}^R = \sum_{t \in T} \begin{cases} (P_{(t)}^W - P_{(t)}^{aW}), \\ (P_{(t)}^{PV} - P_{(t)}^{aPV}), \\ (P_{(t)}^d - P_{(t)}^{ad}), \end{cases} \quad (22)$$

where $\Delta P_{(t)}^R$ is the total reserve power required due to the uncertainties of load and wind and solar power. For the TSO_i , the associated cost of the reserves consists of three major components, given in Equation (23).

$$K_{(t)}^i = \sum_{i \in A} k_{Ri} C_{(t)}^{R,i} \Delta P_{(t)}^{R,i} + \sum_{k \in i} C_{(t)}^{exbgt,ki} + \sum_{\substack{j \in A, \\ j \neq i}} C_{(t)}^{exbgt,ji} \quad (23)$$

where $C_{(t)}^{R,i}$ is the cost of $\Delta P_{(t)}^{R,i}$ in \$/MWh, k_{Ri} is the coefficient of $C_{(t)}^{R,i}$, and $C_{(t)}^{exbgt,ki}$ and $C_{(t)}^{exbgt,ji}$ are the extra cost budgets to account for the market price uncertainties of $PA_{k,i}$ and TSO_j during which TSO_i purchases power from $PA_{k,i}$ and TSO_j in \$, defined in Equation (24) and (25), respectively.

$$C_{(t)}^{exbgt,ki} = k_{ki} (C_{(t)}^{a,ki} - C_{(t)}^{e,ki}) P_{(t)}^{ki} \quad (24)$$

$$C_{(t)}^{exbgt,ji} = k_{ji} (C_{(t)}^{a,ji} - C_{(t)}^{e,ji}) P_{(t)}^{ji} \quad (25)$$

The $PA_{k,i}$ reserve cost is obtained using a similar approach of that in (21)-(25), and is given as:

$$K_{(t)}^k = \sum_{\substack{k \in i, \\ i=1}} k_{Rk} C_{(t)}^{R,k,i} \Delta P_{(t)}^{R,k,i} + \sum_{\substack{k \in i, \\ i=1}} C_{(t)}^{exbgt,ik} \quad (26)$$

where $C_{(t)}^{R,k,i}$ is the cost of $\Delta P_{(t)}^{R,k,i}$ in \$/MWh, k_{Rk} is the coefficient of $C_{(t)}^{R,k,i}$, and $C_{(t)}^{exbgt,ik}$ is the extra cost budget to account for the market price uncertainty of TSO_i during which $PA_{k,i}$ purchases power from TSO_i in \$, as in Equation (27).

$$C_{(t)}^{exbgt,ik} = k_{ik} (C_{(t)}^{a,ik} - C_{(t)}^{e,ik}) P_{(t)}^{ik} \quad (27)$$

It should be mentioned that $C_{(t)}^{exbgt}$ equals to zero when the available exchanged power cost is less than the expected cost. Assuming that the exchanged power costs is proportional to the cost of energy in the area, $C_{(t)}^{R,i}$ and $C_{(t)}^{R,k,i}$ are determined in terms of the expected exchanged power costs, given in (28) and (29), respectively.

$$C_{(t)}^{R,i} = \begin{cases} \max(C_{(t)}^{e,j}, C_{(t)}^{e,k,i}) & P_{(t)}^{ij} + P_{(t)}^{ji} + P_{(t)}^{ik} + P_{(t)}^{ki} < 0 \\ C_{(t)}^{e,i} & P_{(t)}^{ij} + P_{(t)}^{ji} + P_{(t)}^{ik} + P_{(t)}^{ki} > 0 \\ 0 & \Delta P_{(t)}^{R,i} < 0 \end{cases} \quad (28)$$

$$C_{(t)}^{R,k,i} = \begin{cases} C_{(t)}^{e,i} & P_{(t)}^{ki} + P_{(t)}^{ik} < 0 \\ C_{(t)}^{e,k,i} & P_{(t)}^{ki} + P_{(t)}^{ik} > 0 \\ 0 & \Delta P_{(t)}^{R,k,i} < 0 \end{cases} \quad (29)$$

where $C_{(t)}^{e,i}$ and $C_{(t)}^{e,j}$ are the expected power selling prices in area i and area j , respectively, and $C_{(t)}^{e,k,i}$ is the expected power-selling price of $PA_{k,i}$ in area i . By considering Equations (23) and (26), the total operation cost, including reserves cost of the TSO_i and $PA_{k,i}$, is re-written as Equation (30) and (31), respectively.

$$OP_{TSO_i} = \sum_{t \in T} \left(\sum_{g \in TG_i} \sum_{i \in A} f_c(P_{(t)}^{g,i}) + \sum_{\substack{j \in A \\ j \neq i}} C_{(t)}^{e,ji} P_{(t)}^{ji} + \sum_{k \in N_i} C_{(t)}^{e,ki} P_{(t)}^{ki} + K_{(t)}^i \right) \quad (30)$$

$$OP_{PA_{k,i}} = \sum_{t \in T} \left(\sum_{k \in N_i} \sum_{g \in TG_k} f_c(P_{(t)}^{g,k}) + \sum_{k \in N_i} C_{(t)}^{e,ik} P_{(t)}^{ik} + K_{(t)}^k \right) \quad (31)$$

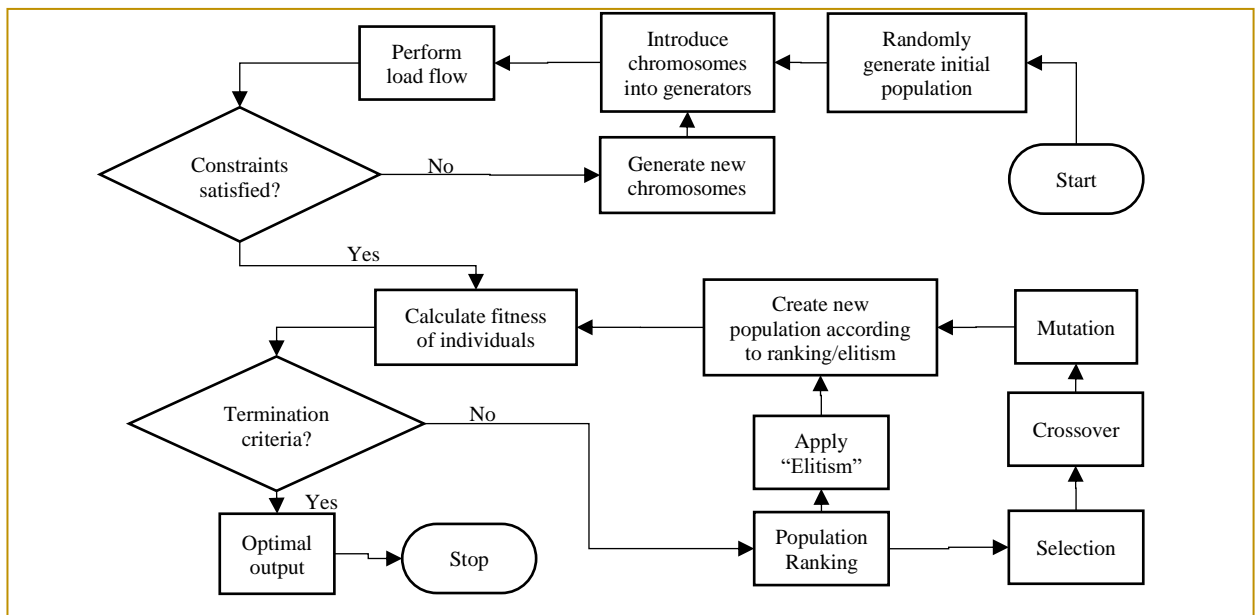
It should be mentioned that the resulting Equations (30) and (31) are non-linear and non-convex problems, although it includes some linear and convex functions.

3.5 THE REAL-CODED ELITISM GENETIC ALGORITHM (RCEGA)

The RCEGA evolves populations based on the principle of natural selection (THAKUR and KUMAR, 2016). First, an individual is represented as a chromosome structure which is

made up of several genes. During the creation of an individual, chromosomes traits are randomly chosen from the pool of possible values generated between the minimum and maximum values of the decision variables and introduced into the generators. For each chromosome introduced into generator, load flow is conducted to check if the power systems constraints are satisfied. The chromosomes which do not satisfy the predefined constraints are considered as invalid and therefore rejected. For every invalid chromosome, a new chromosome is generated and re-introduced into the population. After a population of solutions is created, ranking is performed according to fitness values and genetic operators (e.g., elitism, selection, crossover, and mutation) are applied to evolve and generate new solutions. In each generation, the fitness function evaluates the individual survival likelihood in the new generation. The RCEGA flowchart is summarized in Figure 3.5.

Figure 3.5 – The RCEGA working process



Source: Authors.

The consideration for the RCEGA algorithm for the current work is its suitable to handle the non-convexity and non-linearity functions and constraints (KUMAR and NARESH, 2007). Note that different MO algorithms have performance comparative advantage over another. However, with the proposed decentralized models, the economic dispatch solution should improve when compared to the centralized counterpart model for any given MO algorithm.

3.5.1 Initial Population Sets

To achieve both FD and SD models, separate set of population is created for the TSO and PAs in each area as described in Chapter 2. The control variables of the individual TSO and PA over the entire time frame can be expressed as in Equation (32) and (33), respectively.

$$X_p^0 = \begin{bmatrix} Q_1^{h,i} & P_1^{g,i} & P_1^{w,i} & P_1^{pv,i} & P_1^{gh,i} & P_1^{ph,i} \\ Q_2^{h,i} & P_2^{g,i} & P_2^{w,i} & P_2^{pv,i} & P_2^{gh,i} & P_2^{ph,i} \\ \vdots & \vdots & \vdots & \vdots & \vdots & \vdots \\ Q_T^{h,i} & P_T^{g,i} & P_T^{w,i} & P_T^{pv,i} & P_T^{gh,i} & P_T^{ph,i} \end{bmatrix} \quad (32)$$

$$X_u^0 = \begin{bmatrix} P_1^{g,k} & P_1^{w,k} & P_1^{pv,k} & P_1^{gh,k} & P_1^{ph,k} \\ P_2^{g,k} & P_2^{w,k} & P_2^{pv,k} & P_2^{gh,k} & P_2^{ph,k} \\ \vdots & \vdots & \vdots & \vdots & \vdots \\ P_T^{g,k} & P_T^{w,k} & P_T^{pv,k} & P_T^{gh,k} & P_T^{ph,k} \end{bmatrix} \quad (33)$$

The initial populace (X_p^0/X_u^0) of the control variables are selected at random based on uniform probability distribution for all variables to cover the entire search space uniformly as in Equation (34) and (35) for the TSO and PA, respectively.

$$x_{p,q}^0 \sim U(x_q^{min}, x_q^{max}), \quad q \in n_i, p \in N_{i,p} \quad (34)$$

$$x_{u,v}^0 \sim U(x_v^{min}, x_v^{max}), \quad v \in n_k, u \in N_{k,p} \quad (35)$$

where n_i and n_k are the number of decision variables in an individual, $N_{i,p}$ and $N_{k,p}$ are the populace sizes; $x_{p,q}^0$ and $x_{u,v}^0$ signify the initial q th and v th variables of the p th and u th populaces; x_q^{min}/x_v^{min} and x_q^{max}/x_v^{max} are the lower and upper bounds of the q th and v th decision variables, respectively; $U(x_q^{min}, x_q^{max})/U(x_v^{min}, x_v^{max})$ indicates a uniform random variables ranging over $[x_q^{min}, x_q^{max}]/[x_v^{min}, x_v^{max}]$, where $N_{i,p} = N_{k,p}$. Subsequently, the individual fitness is calculated and passed to the RCEGA algorithm as described in Chapter 2 to obtain the optimal solutions for TSO and PA, respectively.

3.5.2 Handling Area Coupling and Other Systems Constraints

Recall that the decentralized operations of the power system areas are decoupled around the tie-lines while the operations of the areas are solved in parallel to achieve decentralization. However, to ensure the consistency of coupling constraints of the areas, first, the tie-line limits between the areas are predefined in the solution algorithm, and both the base case and scenario cases must satisfy the specified tie-lines limits and other system's constraints. Secondly, initial population of chromosome is randomly generated in each area. Each chromosome generated is introduced into the generator units in the area and load flow is initiated to obtain the area's

information including tie-line power, line flows and losses, bus voltages, and generator power. The RCEGA algorithm is then implemented for each area taking the area's information from the load flow simulation results. Because the objective function does not include a penalty function, the RCEGA operation is conducted such that every chromosome that violates the predefined constraints are considered as invalid and therefore rejected. During this process, the boundary mismatches including the tie-line power constraints are managed and satisfied. For every invalid chromosome, a new chromosome is generated and re-introduced into the population to complete the RCEGA process for the system optimal solution.

3.5.3 Decentralized Solution Implementation Procedures

Note that the base case and scenario cases are solved in different stages. For each case, the RCEGA solves the operations of the areas in parallel in a two-layer operation approach as detailed in Section 2. The parallel steps for the implementation of the SD and FD models shown in Figure 1 and 2 are summarized as follows:

- Step 1:** Define all constraints: tie-lines, generators, ramp rates, and set RCEGA parameters: chromosome number, population size, fitness function by area/entity, and set the hour = 0.
- Step 2:** Randomly generate initial parent population between the min. and max. decision variables.
- Step 3:** Introduce chromosomes into the generators and perform load flow.
- Step 4:** Check if the power system constraints are satisfied. if so, go to Step 5; if no, go to Step 2.
- Step 5:** Set $hr = hr + 1$, solve the layer 1 problems for each area in parallel using Equation (1a/2a).
- Step 6:** Solve the layer 2 problems considering information from layer 1 using Equation (1b/2b).
- Step 7:** Check if the reference generator output constraints are violated. If so, go to Step 6; if not, go to Step 8.
- Step 8:** Repeat Steps 2-7 for the minimum case and then go to Step 9.
- Step 9:** Repeat Steps 2-7 for the maximum case and then go to Step 10.
- Step 10:** Check if $hr = 24$. if so, go to Step 11; if no, go to Step 5.
- Step 11:** Stop.

3.6 SECTION SUMMARY III

This research develops two novel decentralized multiarea economic dispatch (MAED) models based on metaheuristic optimization (MO) to manage the operation of some transmission system operators (TSOs) and private aggregators (PAs) of distributed energy resources in an interconnected multiarea bulk-power systems context. The first model is a semi-decentralized (SD) model developed to attract wider inclusion of PAs in the transmission systems by allowing them to maximize profits. The second model is a fully decentralized (FD) model developed to coordinate the operation the PAs with the TSOs to preserve their baselines. The proposed models allow to determine the effective integration of autonomous PAs in the transmission systems (TS) and their co-operation with the TSOs. The objective of both models is to minimize the total operation cost of the system by effectively coordinating the TSOs and PAs operations. The TSOs and PAs evaluate their operational uncertainties and determine the power reserves considering the best and worst-case scenarios of the uncertain variables, thus enabling the resulting models to be solved in three stages using a robust Real-Coded Elitism Genetic Algorithm (RCEGA). To preserve the ownership of TSOs and PAs, the RCEGA efficiently utilizes separate population sets to solve the operations of the areas in parallel in a two-layer operation approach, allowing the TSOs and PAs to achieve near-optimal operations, independently.

4 CASE STUDIES

For this study, three case studies are performed. The first case implements real-coded genetic algorithm to solve the proposed models. In the second case, select metaheuristic algorithms are implemented. The performance of the select algorithms are then compared in terms of overall operation cost of the grid and simulation time. On the other hand, the third case include the battery energy storage systems (BESS) in the operation of the independent entities in all area. In this case, the BESS is used for peak load leveling for each entity. In all cases, the results obtained are compared with the centralized counterpart models.

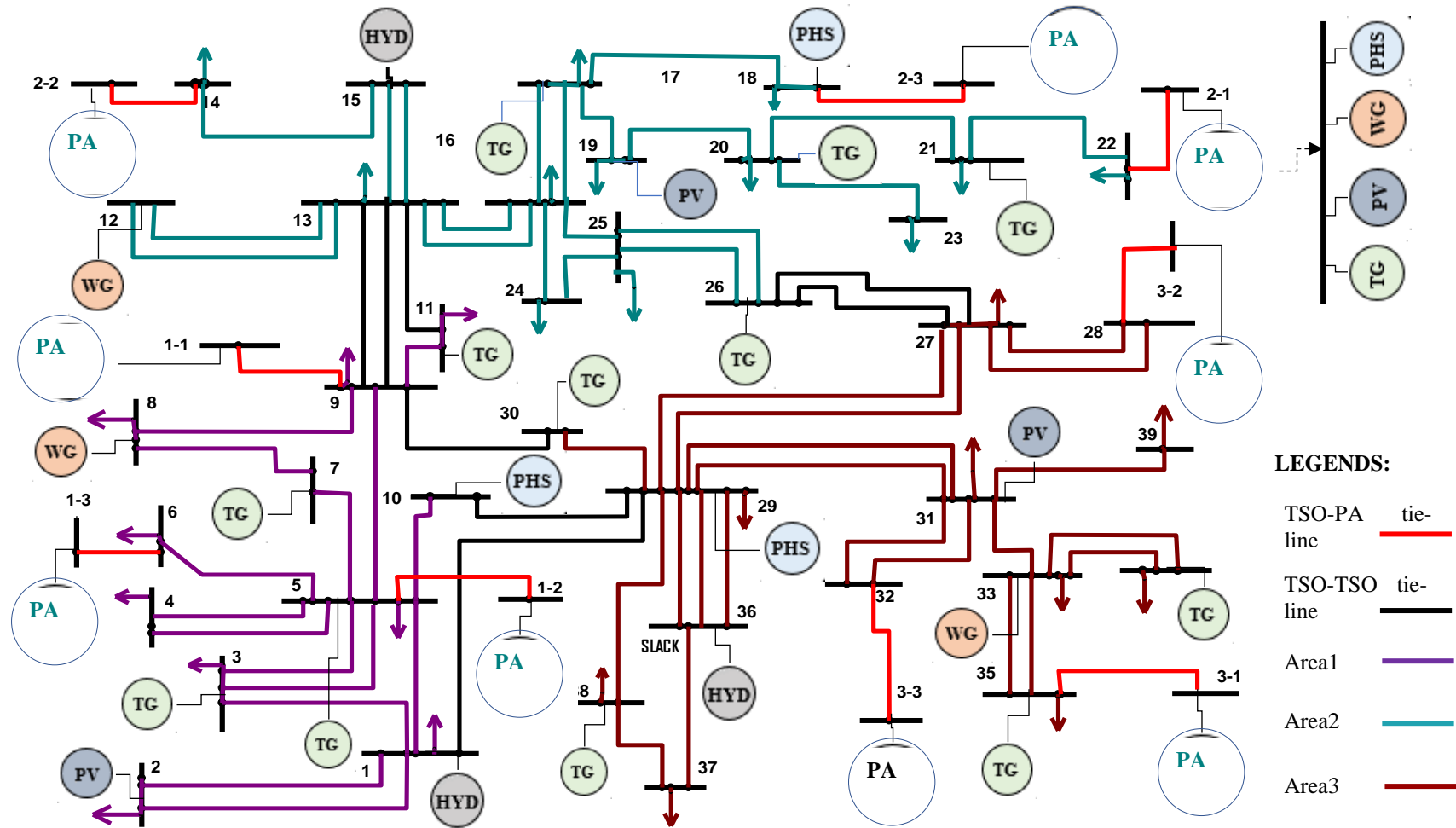
4.1 CASE 1 – IMPLEMENTING REAL-CODED GENETIC ALGORITHM

For the case 1, three simulation considering only real-coded genetic algorithm are performed. The first and second simulations are performed for the SD and FD models described above. The third simulation is performed for a fully centralized (FC) model where operations of all entities are solved in a centralized way. Each simulation is further divided into two sub-simulations considering: “with and without restrictions” on the maximum capacity of tie-lines concerning the exchanged power between TSO-TSO and TSO-PAs. The results of the three simulation and sub-simulations are thereafter compared.

4.1.1 Parameter Settings – Case 1

The performance of the proposed methodology is tested on the modified Nigerian 39-bus 330 kV transmission system as shown in Figure 4.1, consisting of three areas, each with multi-chain cascade of four reservoir hydropower plants, four thermal generators with non-smooth fuel cost function, one PHS unit, and one wind and solar power unit. Also, each area has three PAs each with a wind, solar, thermal, and PHS unit. All notations are as presented in the formulation.

Figure 4.1 – Modified Nigerian 39-Bus Bulk TS



Source: Authors.

The expected load and energy price data used in evaluating the day-ahead operation of TSOs are the scaled-down aggregated load and energy price data of April 10, 2020 recorded at the Australian Energy Market Operator (AEMO) for QLD, NSW, and VIC regional operators, while all PAs are constructed from TAS regional network to foster consistent prices among PAs. Similarly, the expected wind and solar power for all TSOs and PAs are the day-ahead scaled-down wind and solar power data of April 10, 2020 recorded at the ELIA power system in Belgium.

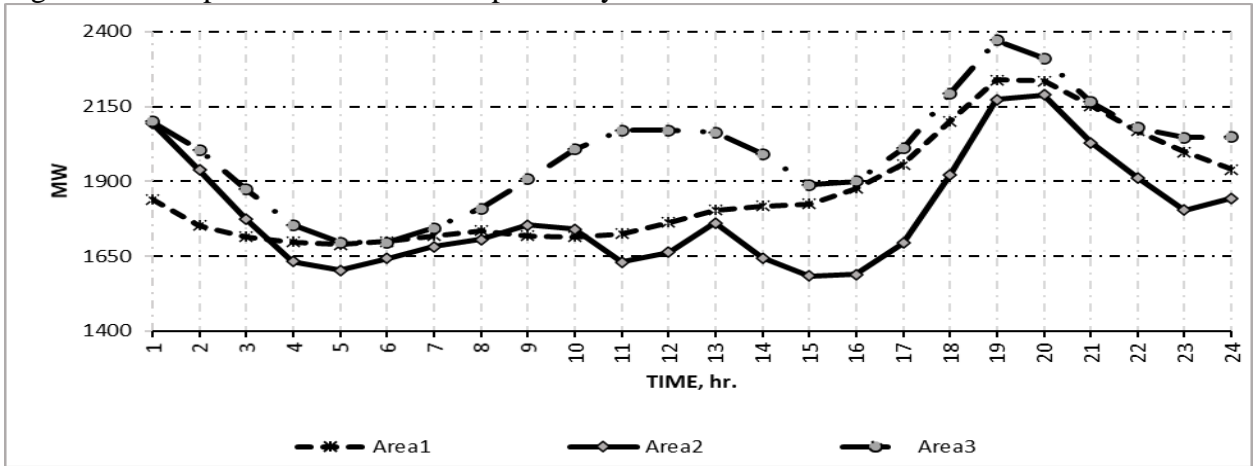
It should be mentioned that all TSOs' thermal units have the same capacity but different fuel cost coefficients. It is also assumed that all the installed wind and solar power units of PAs have unity power factors but are of different capacities. The technical parameters of the hydropower plants, PHS units and cost coefficients of thermal units of TSOs and PAs are obtained from (BASU, 2019; DUBEY, et al., 2016; LIAO, et al., 2013). The maximum generating power of the TSOs thermal generators are 550 MW while that of the PAs are 250 MW. However, considering that the wind and solar power dispatches are prioritized over the conventional units, the minimum thermal generated power for the TSOs and PAs is 0 MW and ramp up/down rates are modified as 300/300 MW/hr and 100/100 MW/hr, to better accommodate wind and solar fluctuations, as shown in Table A.1 and A.2, respectively.

The PHS parameters for TSOs include, $\rho = 70 \text{ acre} - \text{ft}/\text{h}$, $\mu = 200 \text{ acre} - \text{ft}/\text{h}$ while PHS pumping power is fixed at -100 MW and it generates power within $0 - 100 \text{ MW}$. The reservoir starts at 3000 acre-ft and must be at 3000 acre-ft at the end of the 24 h. Similarly, for PAs, $\rho = 7 \text{ acre} - \text{ft}/\text{h}$, $\mu = 20 \text{ acre} - \text{ft}/\text{h}$ while PHS pumping power is fixed at -10 MW and it generates power within $0 - 10 \text{ MW}$. The reservoir starts at 300 acre-ft and must be at 300 acre-ft at the end of the 24 h. The water inflow rate and spillage is not considered.

The standard deviations of the wind and solar power are assumed to be 10% of their expected values and the exchanged power cost is 5% of their expected values (MOHITI, et al., 2019; GUAN and WANG, 2014). To construct the uncertainty sets, a 95% prediction confidence interval is considered (MOHITI, et al., 2019). The interval predictions of wind and solar power are computed as 120% and 80% of their expected values, respectively, while the load and the exchanged power costs are computed as 110% and 90% of their expected values, respectively (GUAN and WANG, 2014). All uncertainty coefficients of net-deviation and exchanged power cost budget are equal to 1. The total TSOs' load and costs of exchanged power are presented in Figure 4.2 and 4.3, respectively, while the prediction intervals of the

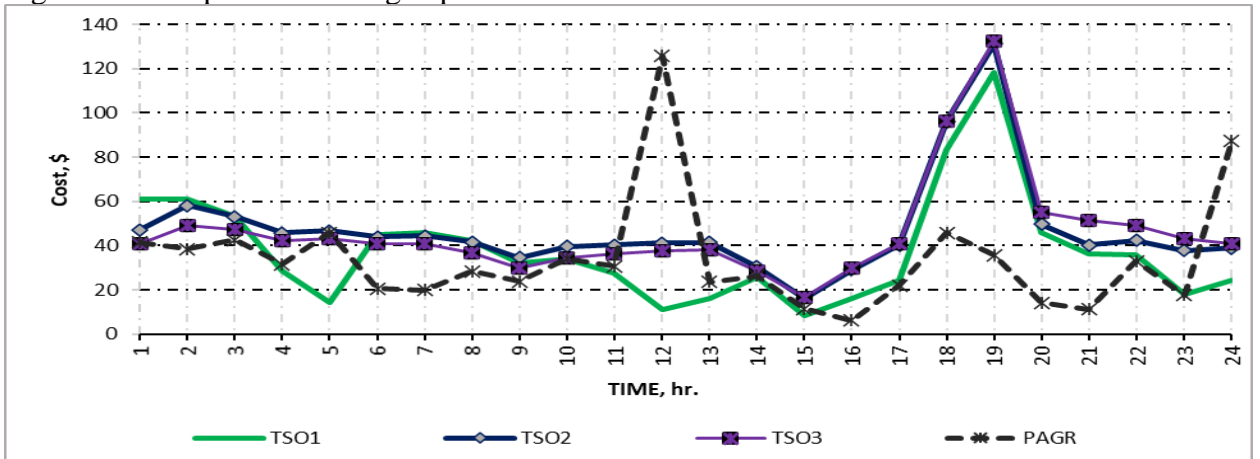
power system total wind and solar power are presented in Figure 4.4 and 4.5, respectively.

Figure 4.2 – Expected TSO total load profile by area



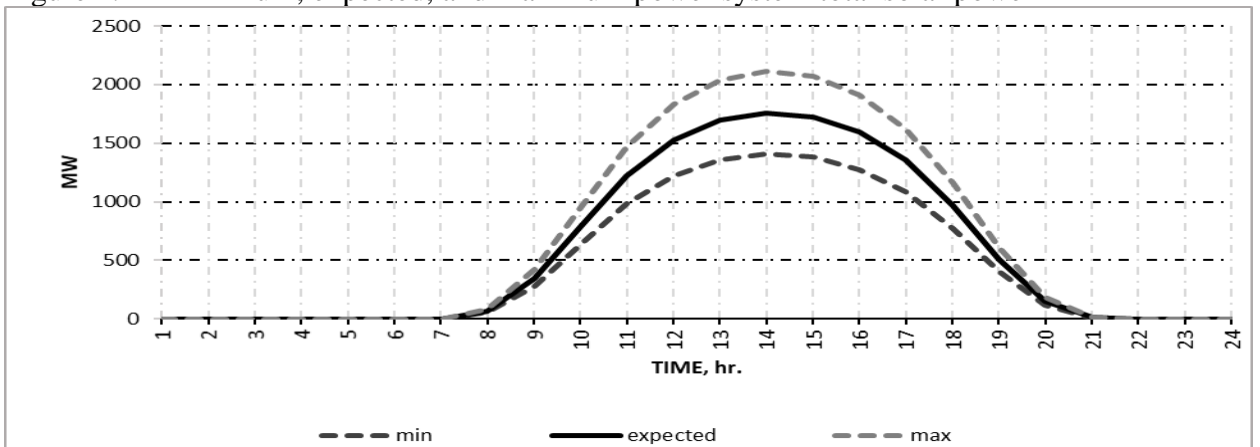
Source: Authors.

Figure 4.3 – Expected exchanged power cost of TSOs and PAs



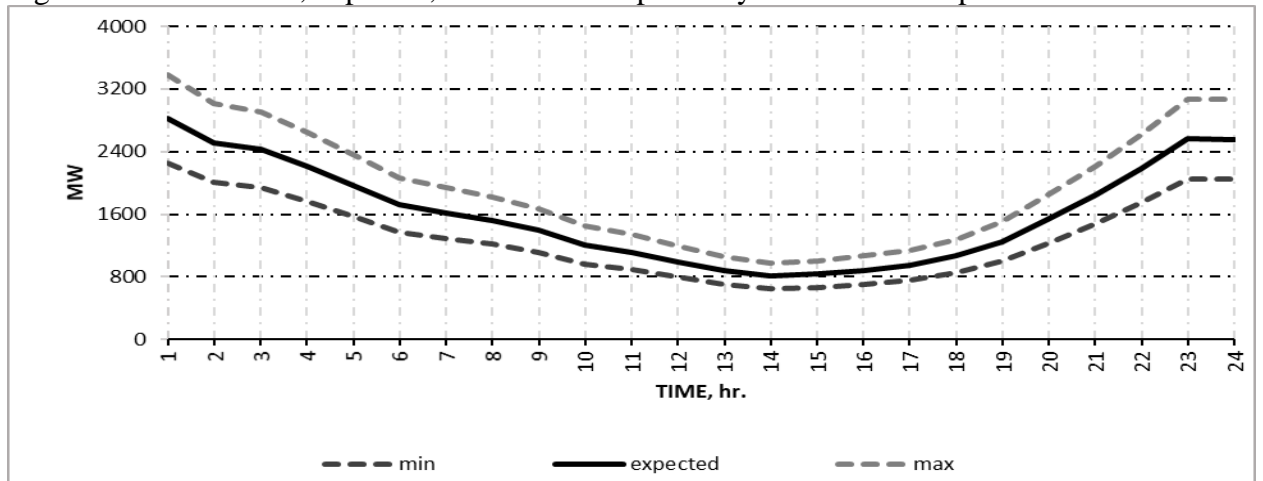
Source: Authors.

Figure 4.4 – Minimum, expected, and maximum power system total solar power



Source: Authors.

Figure 4.5 – Minimum, expected, and maximum power system total wind power



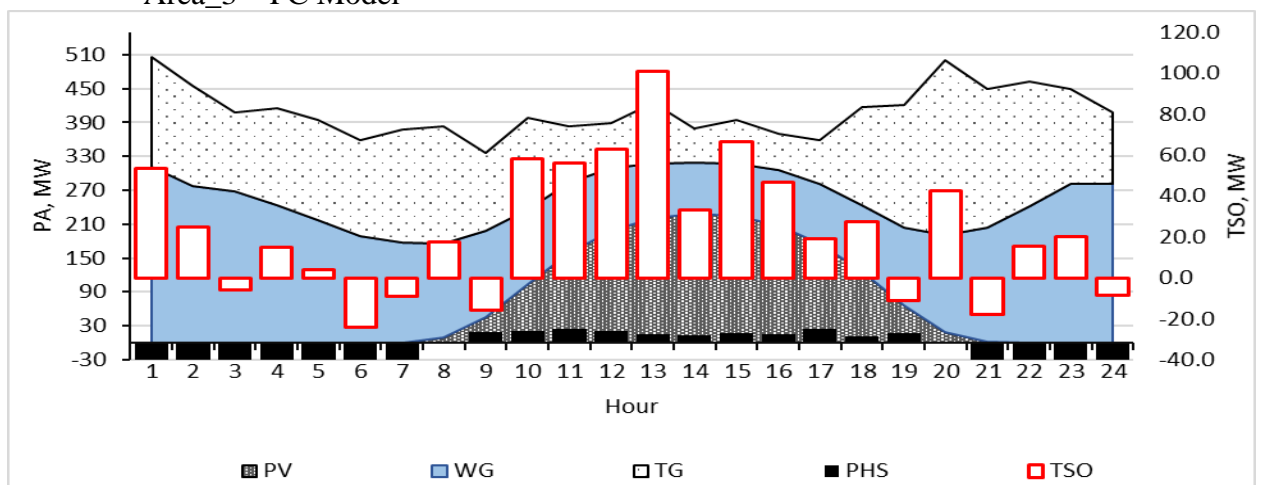
Source: Authors.

The maximum exchanged power between TSO-TSO and TSO-PA is set to 500 MW and 200 MW, respectively. The RCEGA parameters include 25 generations, 20 chromosomes, 0.75 cross-over probability and 0.15 mutation probability for all cases. The entire scheduling period is 1 day and is divided into 24-hour intervals. All cases (including the RCEGA coding) are entirely conducted in the PowerFactory 2019 SP4 environment using the DIgSILENT Programming Language (DPL) on a 2.50-GHz intel Core i3 CPU computer with 4 GB of RAM.

4.1.2 Simulation Results Using Real-Coded Genetic Algorithm

From the perspective of PAs, the total optimal generation outputs of the PAs and the power exchanged with the TSO in Area_3 considering the FC model is presented in Figure 4.6.

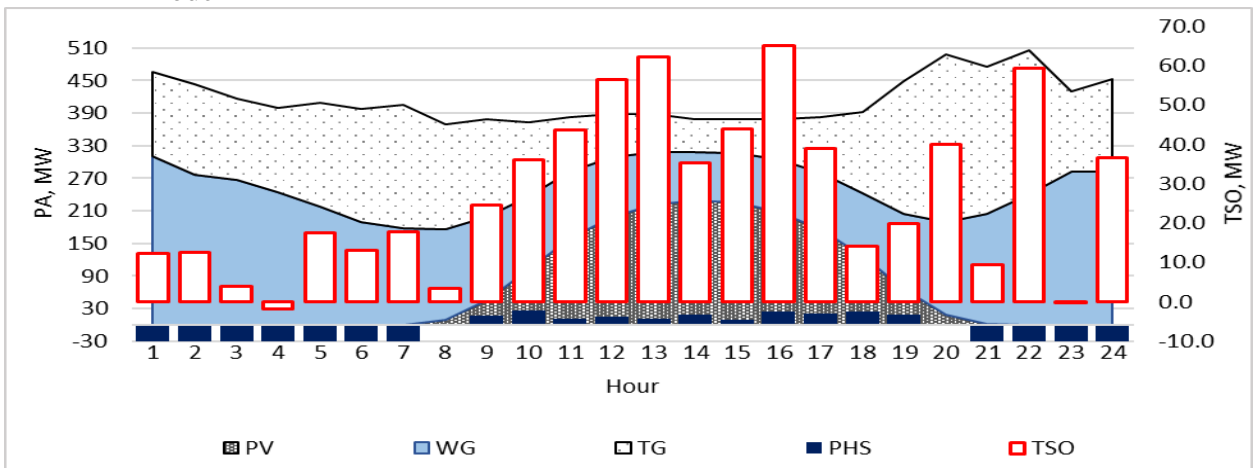
Figure 4.6 – Total optimal generation outputs of PAs and power exchanged with TSO in Area_3 – FC Model



Source: Authors.

As shown in Figure 4.6, the PAs exported 663.9 MW into the transmission system and imported 92.7 MW from the TSO for their optimal operations. The optimal thermal generation is 3768.4 MW and the power generated from PHS units is 198.5 MW for the entire scheduling period. The total optimal generation outputs of PAs and the power exchanged with the TSO in Area_3 considering the SD model is presented in Figure 4.7.

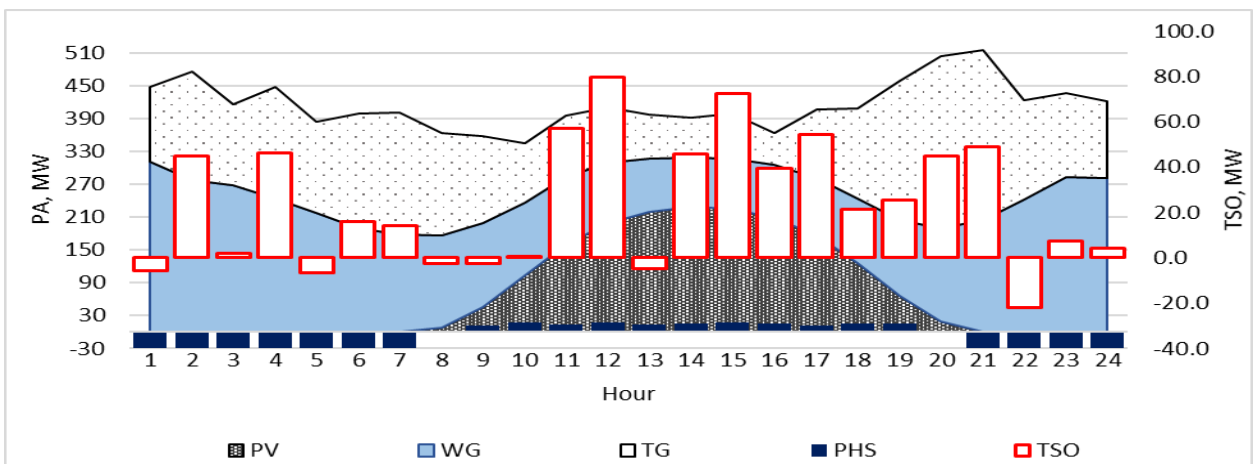
Figure 4.7 – Total optimal generation outputs of PAs and power exchanged with TSO – SD Model



Source: Authors.

In Figure 4.7, the PAs exported 665.6 MW into the system and imported just 1.7 MW from TSO for their operations. The total thermal output is 3862.1 MW while the PHS power generated is 197.4 MW for the entire scheduling period. The total optimal generation outputs of PAs in Area_3 and the power exchanged with the TSO with the FD model are presented in Figure 4.8.

Figure 4.8 – Total optimal generation outputs of PAs and power exchanged with TSO – FD Model



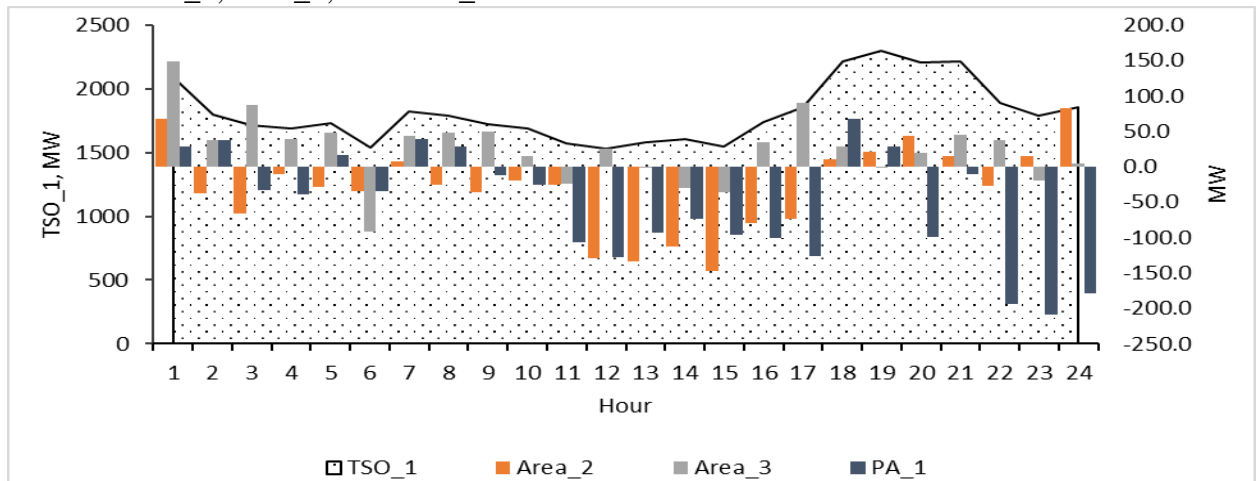
Source: Authors.

As shown in Figure 4.8, the total power exported by the PAs into the power system is 622.9 MW while a total of 45.1 MW is imported from the TSO. In this case, the total power generated from thermal units amounts to 3891.5 MW and the total power generated from PHS units is 161.6 MW for the entire scheduling period.

Comparing Figure 4.6, 4.7, and 4.8, it turned out that the PAs imported more power from the transmission system with the FC model in comparison with the SD and FD models. This contradicts the objective of the PAs to sell more power in the transmission system. Following the objective to enable incentive-based participation for the PAs, the PAs exported most power into the transmission system with the SD model. On the other hand, to preserve the existing participants and enable equal operation opportunity for all entities, the exported and imported power of the PAs with the FD model is more effectively coordinated with the TSOs compared to the FC model.

From the perspective of the TSO in Area_1, the total optimal generation outputs of the TSO_1 and its net power exchanged with the local PAs, Area_2 and Area_3 considering the FC model are presented in Figure 4.9.

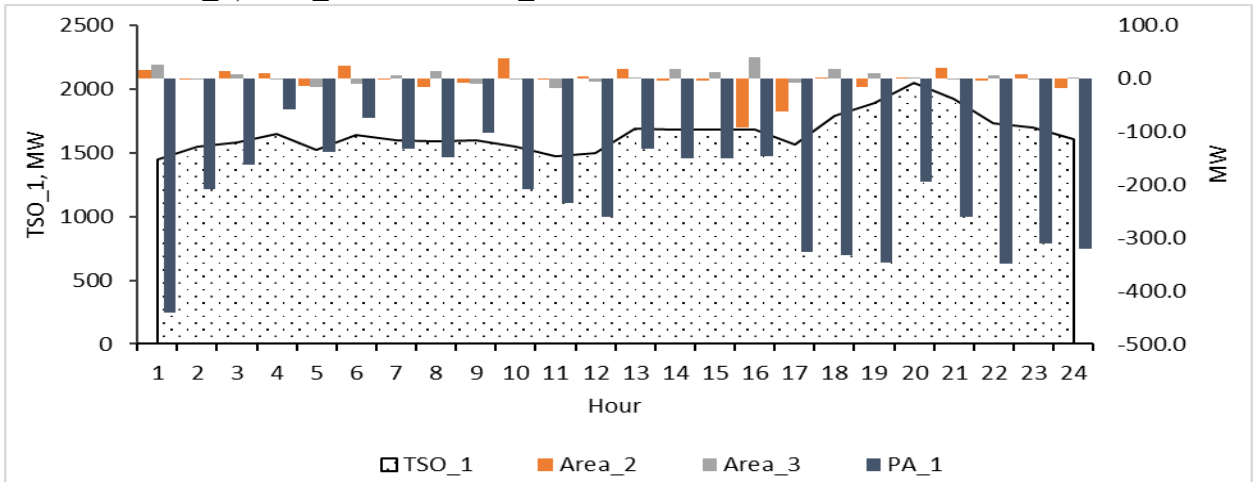
Figure 4.9 – Total optimal generation outputs of TSO_1 and net power exchanged with local PA_1, Area_2, and Area_3 – FC Model



Source: Authors.

As shown in Figure 4.9, the net power imports of TSO_1 from Area_2, Area_3 and local PA_1 are 722.9, 0.0, and 1314.8 MW, respectively. On the other hand, the TSO_1 exported a net total of 0.0 MW to Area_2 and local PA_1, and 600 MW to Area_3. The TSO_1 total power generated is 43511.5 MW. The total optimal generation outputs of TSO_1 and the net power exchanged with the Area_2 and Area_3 and local PA_1 considering the SD model are presented in Figure 4.10.

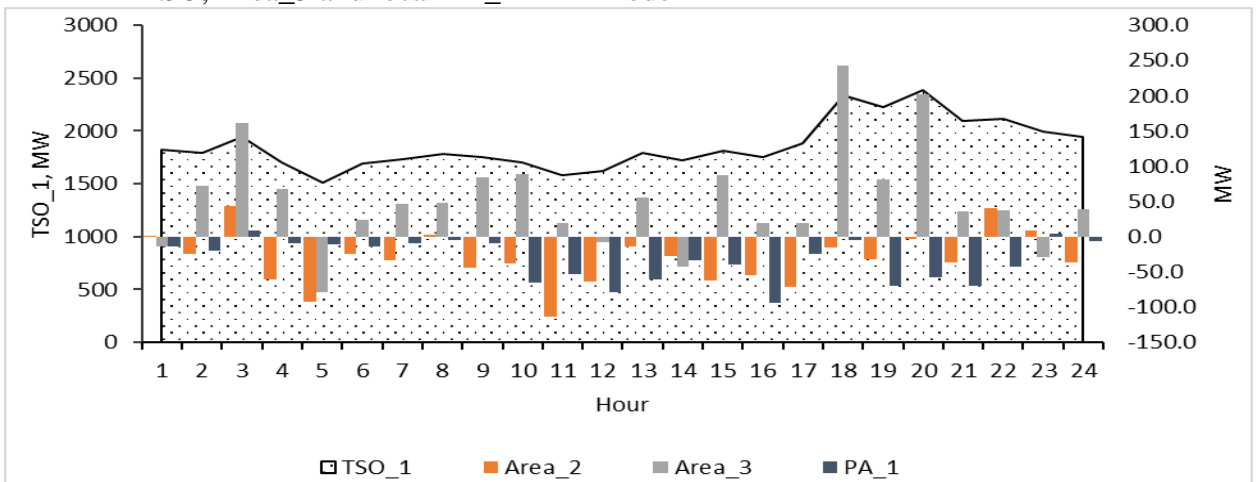
Figure 4.10 – Total optimal generation outputs of TSO_1 and net power exchanged with Area_2, Area_3 and local PA_1 – SD Model



Source: Authors.

As shown in Figure 4.10, the net power imports of TSO_1 from Area_2, Area_3, and local PA_1 are 98.5, 0.0, and 5198.1 MW, respectively. On the other hand, the TSO_1 exported a net total of 0.0 MW to Area_2 and PA_1, and 77.3 MW to Area_3. The TSO_1 total power generated is 39658.7 MW. The total optimal generation outputs of TSO_1 and the net power exchanged with the Area_2 and Area_3 and local PA_1 considering the FD model are presented in Figure 4.11.

Figure 4.11 – Total optimal generation outputs of TSO_1 and net power exchanged with TSO, Area_3 and local PA_1 – FD Model



Source: Authors.

As shown in Figure 4.11, the TSO_1 net power import from Area_2, Area_3, and PA_1 is 749.2, 0.0 and 777.3 MW, respectively. Meanwhile, TSO_1 exported a net total of 0.0 MW to Area_2 and PA_1, and 1258.4 MW to Area_3. The Area_1 total power generated is 44704.5 MW.

Comparing Figure 4.9, 4.10 and 4.11, it turned out that the SD model indicates its effectiveness to incentivize and support regional integration as the PA_1 exported most power into the transmission system. Also, the TSO_1's total power generated was reduced by 8.9% and the total power purchased from its neighbours (i.e., Area_2 and Area_3) was reduced by 86.4% compared to the FC model. On the other hand, the effectiveness of the FD model to coordinate PA_1 operation with the TSO is demonstrated. The FD model reduced the PA_1 exported power by 69.1% and improved the Area_1's selling capacity by 52.3% compared to the FC model, thus ensuring a balance between the TSO_1 and PA_1.

The power system operation costs with the FD, SD and FC models considering sub-cases; with and without power exchange restrictions are presented in Table 4.1. On the other hand, the power system net-operation costs for the SD, FD, and FC models are shown in Table 4.2.

Table 4.1 – Expected operation cost of TSOs and PAs for FD, SD, and FC Models

Model	Entity	Thermal Operation Cost, \$		Power Purchased, \$				Total Operation Cost, \$	
				From TSOs		From PAs			
		WTR	WOR	WTR	WOR	WTR	WOR	WTR	WOR
FD	TSO	827,944	823,633	171,821	200,585	103,743	123,858	1,103,508	1,148,077
	PAs	172,127	177,792	27,352	20,476	-	-	199,479	198,269
	TOTAL							1,302,987	1,346,345
SD	TSO	760,427	748,484	38,114	46,051	315,367	361,757	1,113,908	1,156,292
	PAs	207,882	217,362	3,150	2,322	-	-	211,032	219,684
	TOTAL							1,324,940	1,375,975
FC	TSO	825,431	827,233	111,494	145,762	184,203	210,734	1,121,128	1,183,728
	PAs	178,522	185,850	60,751	48,825	-	-	239,273	234,675
	TOTAL							1,360,401	1,418,403

SUB-CASES: *WTR = With restrictions; *WOR = Without restrictions.

Source: Authors.

Table 4.2 – Power sold and net-operation costs considering FD, SD, and FC Models

Model	Entity	Power Sold, \$				Net Operation Cost (Thermal + Purchased - Sold), \$		Total Net-Operation Cost, \$	
		To TSOs		To PAs		WTR	WOR	WTR	WOR
		WTR	WOR	WTR	WOR				
FD	TSOs	171,821	200,585	27,352	20,476	904,334	927,015	1,000,070	1,001,426
	PAs	103,743	123,858	-	-	95,736	74,411		
SD	TSOs	38,114	46,051	3,150	2,322	1,072,643	1,107,919	968,309	965,845
	PAs	315,367	361,757	-	-	-104,335	-142,074		
FC	TSOs	111,494	145,762	60,751	48,825	948,884	989,142	1,003,954	1,013,083
	PAs	184,203	210,734	-	-	55,069	23,941		

SUB-CASES: *WTR = With restrictions; *WOR = Without restrictions.

Source: Authors.

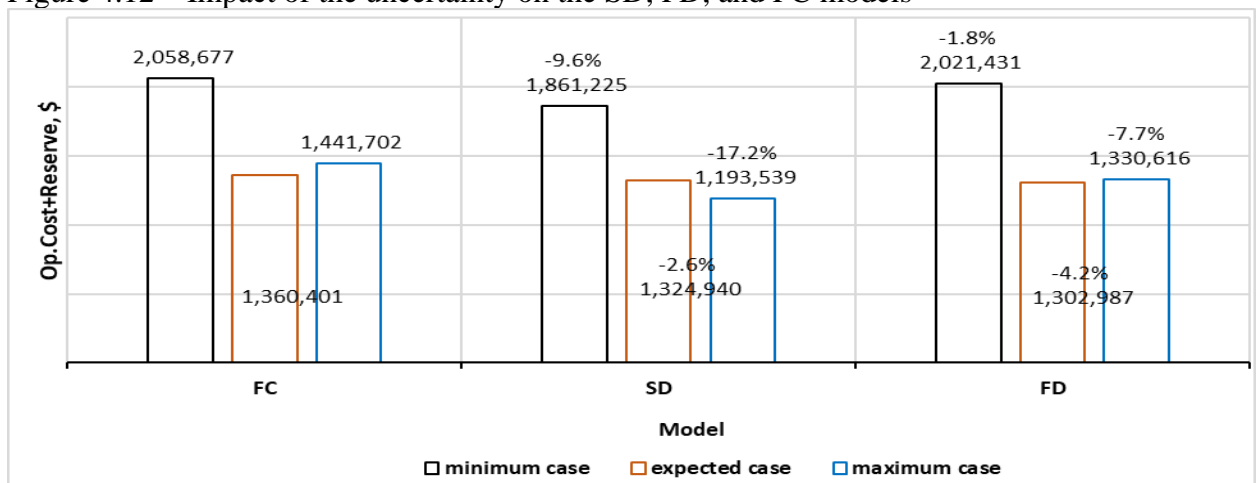
As shown in Table 4.1, the power system operation cost with the SD model was reduced by 2.6 and 3.0% with and without restrictions, respectively, compared to the costs obtained with the FC model. Similarly, the power system operation cost with the FD model was reduced by 4.2 and 5.1% with and without restrictions, respectively, when compared to the cost obtained with the FC model.

As shown in Table 4.2, the SD model provided the power system with least net-operation costs of \$968,309 and \$965,845 with and without restrictions, respectively. Observe that the PAs net-operation costs with and without restrictions is -\$104,335 and -\$142,074, respectively, where the negative sign indicates surplus gain for the PAs. A decrease in the TSOs’ thermal operating cost is also noticed (see Table 4.1). Compared to the FC model, the SD model is more effective to create better investment opportunity for the PAs as it is profit oriented with quick investment recovery potential.

In the case where the operation of PAs is over-prioritized, requiring the power system planner to improve the TSOs’ net-operation cost, the FD model is preferred in terms of net-operation cost as it is 4.7 and 6.3% better than the FC counterpart with and without restrictions, respectively. Also notice that the ratios of the TSOs and PAs net-operation cost of (94.5/5.5) and (97.6/2.4) with the FC model are significantly lopsided in comparison with the ratios of the FD model which are (90.4/9.6) and (92.6/7.4) with and without restrictions, respectively.

The impact of the uncertainty (i.e., the worst-case scenarios) on the proposed SD and FD models, and their FC counterpart model are presented in Figure 4.12.

Figure 4.12 – Impact of the uncertainty on the SD, FD, and FC models



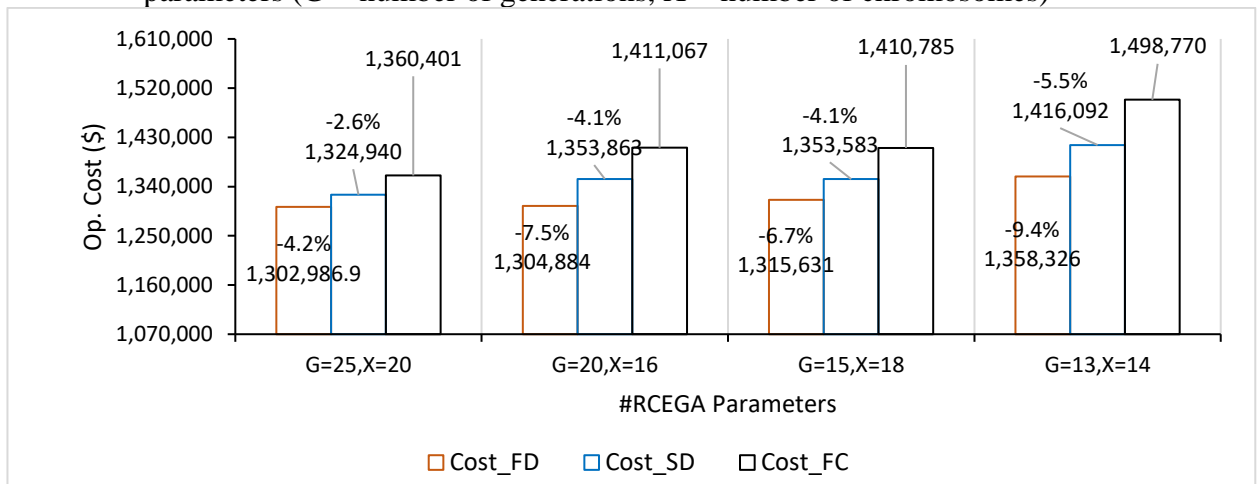
Source: Authors.

As shown in Figure 4.12, the operation cost (including the reserve cost) considering the worst-case (i.e., minimum deviations of the expected variables) scenario with the SD and FD

models are 9.6 and 1.8% less compared with the FC model. Similarly, the operation cost (including the reserve cost) considering the worst-case (i.e., maximum deviations of the expected variables) scenario with the SD and FD models are 17.2 and 7.7% less compared with the FC model.

The RCEGA performance is further verified for varied number of chromosomes and generations. Although the RCEGA solution is indicated to vary according to problem complexity and parameters turning, conducting the solution with the SD and FD models still reduced the total operation cost by up to 5.5 and 9.4% compared to the FC model, as shown in Figure 4.13.

Figure 4.13 – Performance comparison of SD, FD, and FC models under varying RCEGA parameters (G = number of generations, X = number of chromosomes)



Source: Authors.

4.2 CASE 2 - PERFORMANCE COMPARISON OF SELECT METAHEURISTIC ALGORITHMS

The performance of the FD model is verified considering differential evolution and particle swarm optimization methods, and the results obtained for each method are compared with the one obtained for the genetic algorithm in terms of performance and speed.

4.2.1 Parameter Settings – Case 2

The parameters of the select MO algorithms are presented in Table 4.3.

Table 4.3 – The select MO parameters for the FD Model

MO Algorithm	MO Parameters	Iteration No. (max)
RCEGA	Crossover probability, 0.75	No. of chromosomes, X = 40 No. of generation, G = 20
	Mutation probability, 0.15	
PSO	Randomness coefficient, 0.5	No. of particles, X = 20 No. of generation, G = 30
	Personal coefficient, 0.65	
	Global coefficient = 0.85	
DE	Differential factor = 0.5	No. of agents, X = 20 No. of generation, G = 30
	Crossover probability = 0.85	

Source: Authors.

The simulation procedures are summarized as follows:

Step 1: Simulate the centralized model using the select MO algorithms considering maximum number of iterations.

Step 2: Simulate the FD model using the select MO algorithms considering maximum number of iterations.

Step 3: Simulate the FD model using the select MO algorithms by varying X and G, respectively.

The scheduling period is 1-day and is divided into 24-hour intervals. All cases (including DE, PSO and RCEGA coding) are performed in the DIgSILENT PowerFactory 2020 SPA2 environment using DIgSILENT Programming Language (DPL) on a 2.50-GHz intel Core i3 4 GB RAM CPU computer.

4.2.2 Simulation Results of the Select Metaheuristic Algorithms

The total operation cost, reserve cost and execution time of the centralized model for the expected and worst-case (i.e., minimum, and maximum) scenarios using the select MO algorithms are presented in Table 4.4.

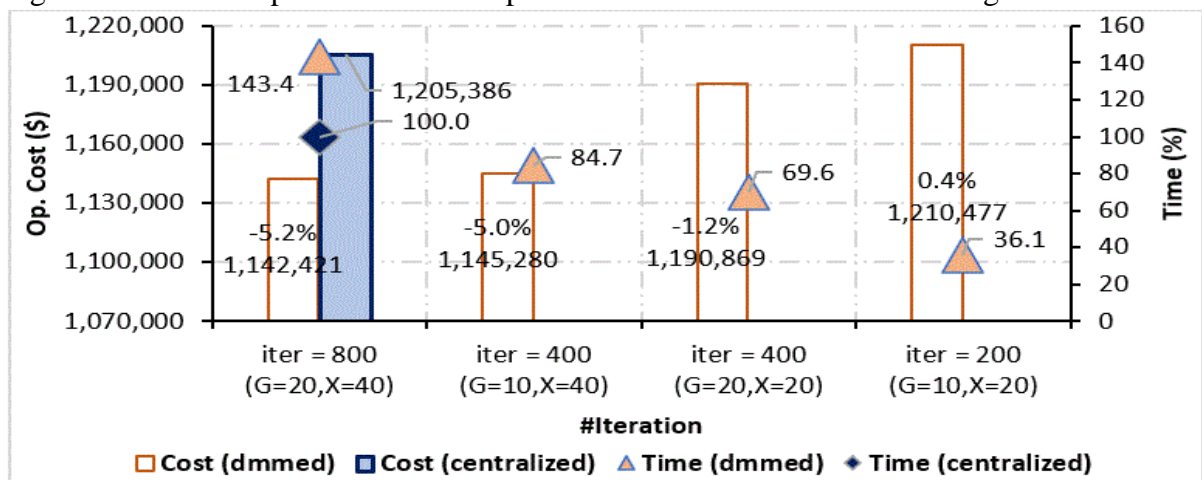
Table 4.4 – Operation cost, reserve cost and execution time of the centralized models

MO	Cost (\$)	CASE			#Iteration (max) (G*X)	Execution Time (mins)
		Expected	Minimum	Maximum		
RCEGA	Operation	1,205,386	1,101,886	1,296,344	G=20, X=40	303.2
	Reserve	-	421,819	7,077		
	Total	1,205,386	1,523,705	1,303,421		
PSO	Operation	1,228,208	1,122,682	1,340,564	G=30, X=20	399.9
	Reserve	-	441,831	8,754		
	Total	1,228,208	1,564,513	1,349,318		
DE	Operation	1,214,056	1,075,232	1,336,920	G=30, X=20	451.2
	Reserve	-	449,509	7,280		
	Total	1,214,056	1,524,741	1,344,200		

Source: Authors.

As shown in Table 4.4, the total operation cost of the centralized model for the expected case are \$1,205,386, \$1,228,208, and \$1,214,056 using the RCEGA, PSO, and DE, respectively. For the worst-case (minimum) scenario, the total operation cost increased by 26.4, 27.4, and 25.6% for the RCEGA, PSO and DE compared to their expected cases, respectively. Similarly, the total operation cost for the worst-case (maximum) scenario increased by 8.1, 9.9, and 10.7% for the RCEGA, PSO and DE compared to their expected cases, respectively. Observed that larger share of the reserve costs is incurred mostly from overestimating (minimum scenario) the renewable generation outputs. Also, the resulting execution time using the RCEGA, PSO and DE algorithms are 303.2, 399.9, and 451.2 mins, respectively. The total operation cost and execution time of the FD model using RCEGA algorithm is compared with its centralized counterpart model for the expected case in Figure 4.14.

Figure 4.14 – The expected case total operation cost and execution time using the RCEGA

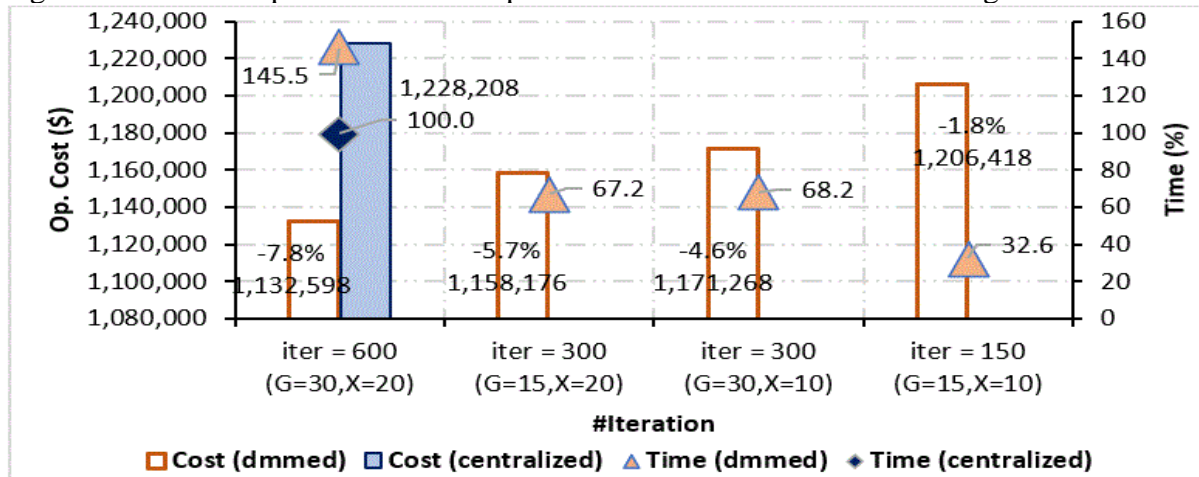


Source: Authors.

As shown in Figure 4.14, when iteration number $I = 800$, the FD model achieved 5.2% reduction in the total operation cost but with 43.4% increase in total execution time compared

to its centralized counterpart model. However, when G was halved such that $I = 400$, the FD model achieved 15.3% reduction in the total execution time and 5.0% reduction in the total operation cost compared to its centralized counterpart model. Similarly, when X was halved such that $I = 400$, the FD model achieved 30.4% decrease in the total execution time and 1.2% reduction in the total operation cost compared to its centralized counterpart model. In 200 iterations when X and G were both halved, the total execution time of the FD model further reduced by 63.9% but the total operation cost increased by just 0.4% compared to its centralized counterpart model. The total operation cost and execution time of the FD model using PSO algorithm is compared with its centralized counterpart model for the expected case in Figure 4.15.

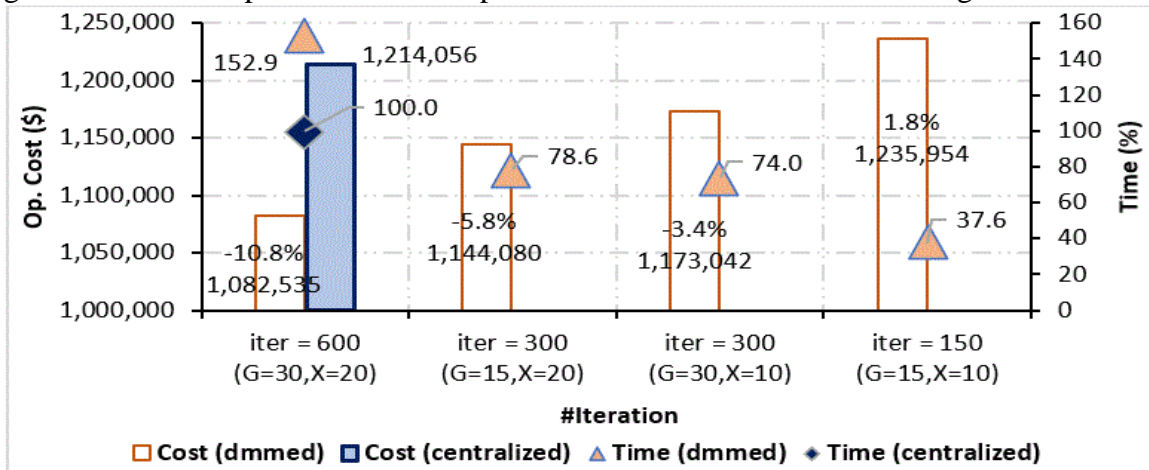
Figure 4.15 – The expected case total operation cost and execution time using the PSO



Source: Authors.

As shown in Figure 4.15, when iteration number $I = 600$, the FD model achieved 7.8% reduction in the total operation cost but with 45.5% increase in total execution time compared to its centralized counterpart model. When G was halved such that $I = 300$, the total execution time and operation cost of the FD model reduced by 32.8% and 5.7% respectively compared to its centralized counterpart model. Similarly, when X was halved such that $I = 300$, the total execution time and operation cost of the FD model reduced by 31.8% and 4.6%, respectively compared to its centralized counterpart model. In just 150 iterations when X and G were both halved, the total execution time and operation cost of the FD model reduced by 67.4% and 1.8%, respectively compared to its centralized counterpart model. The total operation cost and execution time of the FD model using DE algorithm is compared with its centralized counterpart model for the expected case in Figure 4.16.

Figure 4.16 – The expected case total operation cost and execution time using the DE



Source: Authors.

As shown in Figure 4.16, when iteration number $I = 600$, the FD model achieved 10.8% reduction in the total operation cost but with 52.9% increase in total execution time compared to its centralized counterpart model. However, when G was halved such that iteration number $I = 300$, the total execution time of the FD model reduced by 21.4% while the total operation cost reduced by 5.8% compared to its centralized counterpart model. Similarly, when X was halved such that $I = 300$, the total execution time reduced by 26.0% and the total operation cost reduced by 3.4% compared to its centralized counterpart model. In 150 iterations when X and G were both halved, the total execution time of the FD model reduced by 62.4% but with 1.8% increase in the total operation cost compared to its centralized counterpart model. The total operation and reserve costs of the FD model and the centralized counterpart model using the select MO algorithms for the worst-case (minimum and maximum) scenarios are presented in Table 4.5.

Table 4.5 – Operation cost (OC), reserve cost (RC) and %change of the total operation cost (TC) of the FD model and its centralized counterpart models for the worst-case (minimum and maximum) scenarios

Model	#Iteration	Scenario	RCEGA			PSO			DE		
			OC (\$)	RC (\$)	% Change in TC	OC (\$)	RC (\$)	% Change in TC	OC (\$)	RC (\$)	% Change in TC
Centralized	G, X	Min	1,101,886	421,819	-	1,122,682	441,831	-	1,075,232	449,509	-
		Max	1,296,344	7,077	-	1,340,564	8,754	-	1,336,920	7,280	-
FD	G, X	Min	1,039,426	432,484	-3.4	962,131	432,484	-10.9	955,295	441,713	-8.4
		Max	1,191,383	7584	-8.0	1,174,078	6,435	-12.5	1,151,982	4,791	-13.9
	0.5G, X	Min	1,029,980	433,355	-4.0	999,297	447,131	-7.5	1,020,567	431,714	-4.8
		Max	1,204,906	8,457	-6.9	1,161,365	6,511	-13.4	1,192,022	6,982	-10.8
	G, 0.5X	Min	1,094,241	415,430	-0.9	1,069,619	418,273	-4.9	1,043,921	442,381	-2.5
		Max	1,250,861	10,804	-3.2	1,242,180	9,130	-7.3	1,243,336	6,573	-7.0
	0.5G, 0.5X	Min	1,127,863	440,548	2.9	1,079,867	432,426	-3.3	1,095,717	427,601	-0.1
		Max	1,260,545	10,474	-2.5	1,264,652	10,038	-5.5	1,286,713	9,529	-3.6

*GA: G=20, X=40; PSO: G=30, X=20; DE: G=30, X=20.

Source: Authors.

As shown in Table 4.5, it turned out that the FD model showed capacity to better manage operational uncertainties compared to the centralized counterpart model using the select MO algorithms. For the minimum case, the FD model reduced the total operation cost by 3.4, 10.9, and 8.4% using the RCEGA, PSO and DE at their maximum iteration compared to their centralized counterpart models, respectively. A similar trend could also be observed with the FD model when X or G were reduced to half across border for the select MO algorithms, except for RCEGA where when X and G were both reduced to half, the FD model increased the total operation cost by 2.9%. On the other hand, for the maximum case, the FD model reduced the total operation costs by up to 8.0, 13.4 and 13.9% for the RCEGA, PSO, and DE for all cases compared to their centralized counterpart models, respectively.

4.3 CASE 3 - CONSIDERATION FOR BATTERY ENERGY STORAGE SYSTEMS

For the case 3, the inclusion of the BESS system is investigated on the performance of the FD and FC models considering the real-coded genetic algorithm only.

4.3.1 Parameter Settings – Case 3

For this study, the BESS of the independent agents in all areas are used for peak load leveling. All the BESS in the system have same operational ratings. The rating of the BESS in terms of the maximum power injection at time t and maximum capacity ratio is 80 MW/ 480 MWh across all areas. This means that the BESS can reach full rated capacity or be completely drained in 6 hours for a unity round-trip efficiency. However, considering operational losses, the charging and discharging efficiency of the BESS is assumed to be 0.85. The minimum permissible State of Charge of the BESS is 0.25 while the maximum Depth of Discharge is assumed to be 0.75. Because of the introduction of the new BESS in the system for all agents, the RCEGA parameters e.g., the number of generations and chromosomes are set to be 30 and 50, respectively, while cross-over and mutation probabilities are set to be 0.7 and 0.15, respectively, for the FD and FC models. The entire scheduling period is 1 day and is divided into 24-hour intervals. All cases (including the RCEGA coding) are entirely conducted in the PowerFactory 2022 environment using the DiGSILENT Programming Language (DPL) on a 2.50-GHz intel Core i7 CPU computer with 8 GB of RAM.

4.3.2 Simulation Results Considering Battery Energy Storage System (BESS)

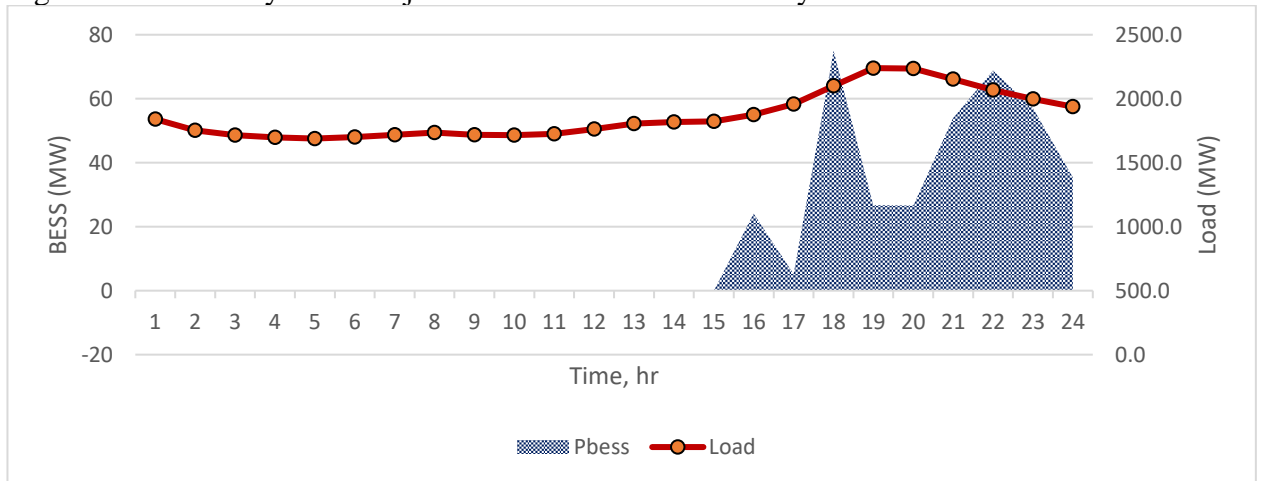
The simulation results considering battery energy storage for all agents in all areas are

presented in the following subsections.

4.3.2.1 Battery Depth of Discharge and Power Injection – FC Model

The battery power injection and hourly load of the TSO in Area 1 considering the FC model are presented in Figure 4.17.

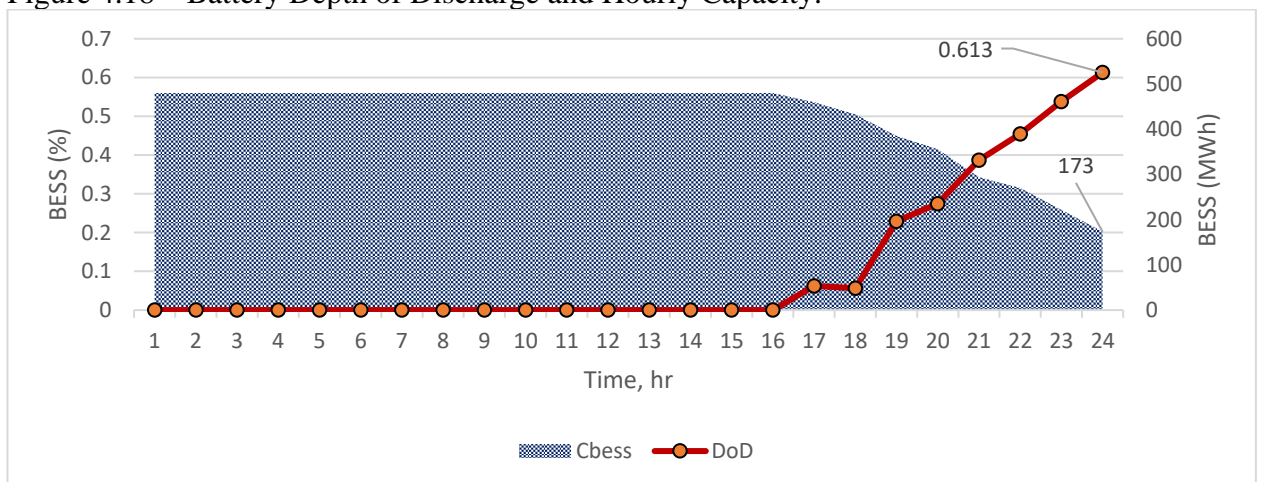
Figure 4.17 – Battery Power Injection and Total TSO’s Hourly Load



Source: Authors.

As shown in Figure 4.17, the BESS is discharged to level the peak load of the TSO. This occurred between the hour of 15 to 24. The battery depth of discharge and hourly capacity of the TSO BESS in Area 1 considering the FC model are presented in Figure 4.18.

Figure 4.18 – Battery Depth of Discharge and Hourly Capacity.



Source: Authors.

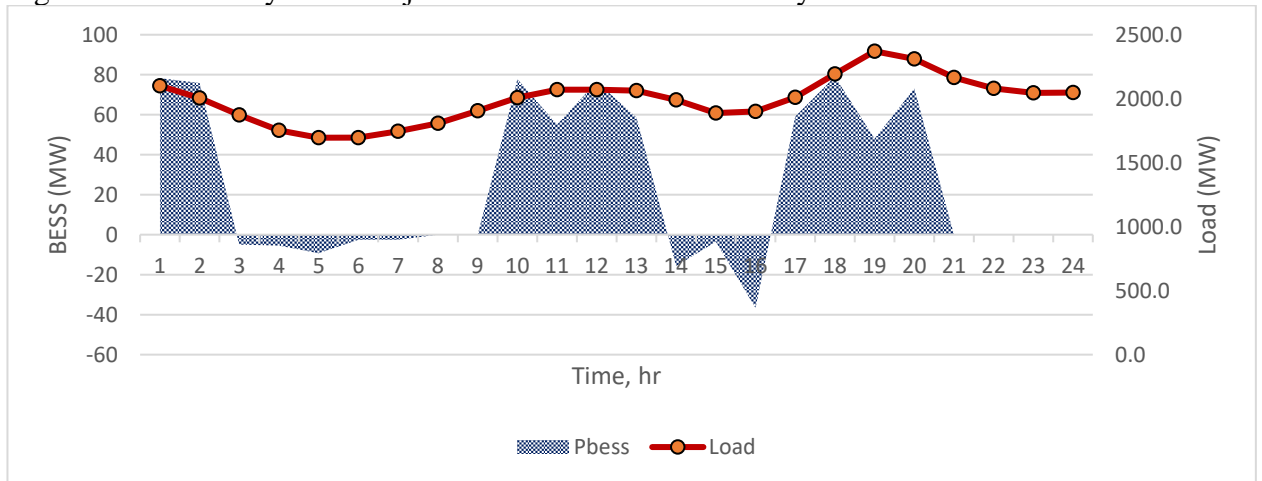
As shown in Figure 4.18, the discharging of the BESS occurred after the 15th hour until the 24th hour. The BESS depth of discharge and capacity at the end of the 24th hour are 61.3% and 173 MWh, respectively. The BESS operation for the local PAs and other TSOs in Area 2

and 3 are presented in Appendix C.

4.3.2.2 Battery Depth of Discharge and Power Injection – FD Model

The battery power injection and hourly load of the TSO in Area 3 considering the FD model are presented in Figure 4.19.

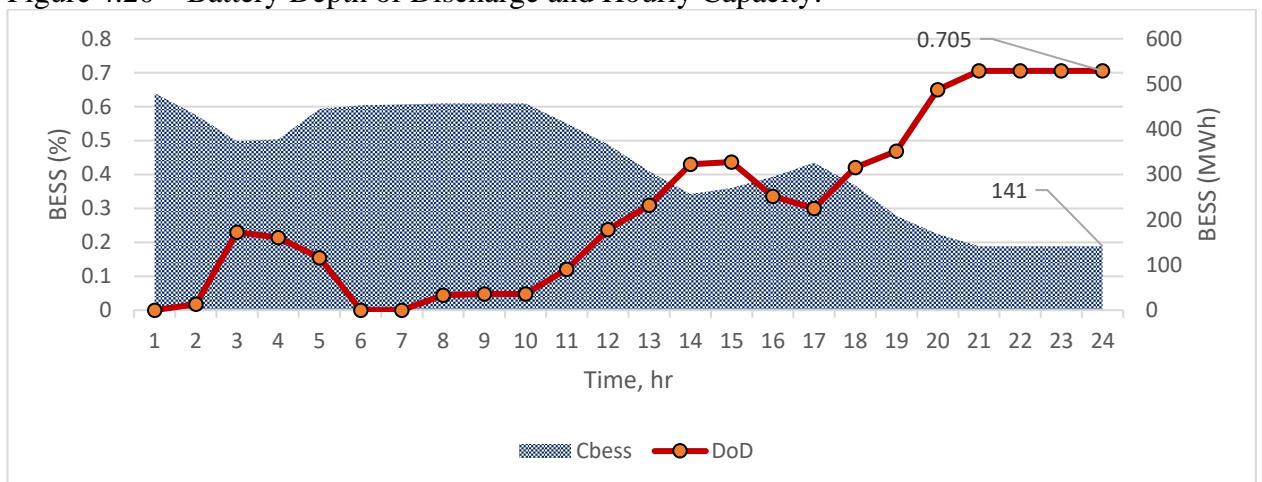
Figure 4.19 – Battery Power Injection and Total TSO’s Hourly Load



Source: Authors.

As shown in Figure 4.19, the BESS is discharged to level the peak load of the TSO. This occurred between the hour of 1-3, 9-14, and 17-21. On the other hand, the battery is charged during the hour of 3-8 and 14-16, respectively. Between the hour of 8-9 and 21-24, the BESS remained at resting state. The battery depth of discharge and hourly capacity of the TSO in Area 3 considering the FD model are presented in Figure 4.20.

Figure 4.20 – Battery Depth of Discharge and Hourly Capacity.



Source: Authors.

As shown in Figure 4.20, the BESS depth of discharge and capacity at the end of the

24th hour is 70.5% and 141 MWh, respectively. The BESS operation for the local PAs and other TSOs in Area 1 and 2 are presented in Appendix C.

4.3.2.3 Operation Cost with and without BESS – FD and FC Models

The total operation cost of the grid is for the FD and FC models are presented in Table 4.6.

Table 4.6 – total operation cost of the grid is for the FD and FC models

Model	With BESS				Without BESS			
	Area1	Area2	Area3	Total	Area1	Area2	Area3	Total
FD	332,888	414,209	369,929	1,117,026	384,476	356,350	401,595	1,142,421
FC	390,522	422,816	390,188	1,203,526	397,038	402,577	405,771	1,205,386
%Change	-14.8%	-2.0%	-5.2%	-7.2%	-3.2%	-11.5%	-1.0%	-5.2%

Source: Authors.

As shown in Table 4.6, the inclusion of BESS in the grid operation resulted in 7.2% decrease in the total operation cost for the FD model when compared with the centralized counterpart model, over the operation horizon of 24-hour. Similarly, when compared with the case without BESS, the grid achieved 2.2% reduction in total operation cost for the FD model and just 0.2% reduction in the total operation cost for the FC model. These simulation results still indicate that the FD model is effectiveness in coordinating the operation of multiple entities when compared with the centralized FC counterpart model.

4.4 SECTION SUMMARY IV

Case studies have been performed on a modified Nigerian 330 kV 39-bus transmission systems having three TSOs each with three PAs to demonstrate the effectiveness of the proposed models. For the case 1, it turned out that the PAs imported more power from the transmission system with the FC model in comparison with the SD and FD models. This contradicts the objective of the PAs to sell more power in the transmission system. Following the objective to enable incentive-based participation for the PAs, the PAs exported most power into the transmission system with the SD model by reducing the TSO's total power generated and total power purchased from the neighbouring areas by 8.9% and 86.4%, respectively. On the other hand, to preserve the existing participants and enable equal operation opportunity for all entities, the exported and imported power of the PAs with the FD model is more effectively coordinated with the TSOs compared to the FC model as the FD model reduced the PAs exported power by 69.1% and improved the overall area's selling capacity by 52.3%. Furthermore, in terms of operation costs, the SD and FD models reduced the total operation

cost of the grid by 3.0 and 5.1%, respectively when compared with their centralized counterpart model. Similarly, the operation cost considering the worst-case minimum and maximum uncertainties of the SD and FD models are 17.2 and 7.7% less compared with the FC model.

For the case 2, the performance of the FD model is further demonstrated using differential evolution and particle swarm algorithms. For the expected case when the number of iterations “I” is reduced by reducing the chromosome number “X” to half, the FD model reduced the total operation cost by 5.0, 5.7 and 5.8%, and the execution time by 15.3, 32.8 and 21.4% using the RCEGA, PSO and DE compared to their centralized models, respectively. Also, when the number of iterations “I” is reduced by reducing the generations number “G” to half, the FD model also reduced the total operation cost by 1.2, 4.6 and 3.4% and the total execution time by 30.4, 31.8 and 26.0% using the RCEGA, PSO and DE, compared to their centralized models, respectively. Similarly for the case 3, the effectiveness of the FD to handle more complex multicarrier energy systems is demonstrated through extending the grid operations to include battery energy storage systems. The inclusion of BESS in the grid operation resulted in 7.2% decrease in the total operation cost for the FD model when compared with the centralized counterpart model, over the operation horizon of 24-hour.

5 CONCLUSION

This paper presents a semi-decentralized and fully decentralized multiarea power system economic dispatch models considering local private aggregators based on meta-heuristic method. The developed methodology, which was validated through several case studies, showed that the inclusion of PAs can provide several benefits to a power system. In terms of the system total operation cost and net-operation cost, the effectiveness of the FD model to coordinate the TSOs and PAs operations and the tendency to preserve their operation baselines were demonstrated. The results showed that the FD model outperformed its counterpart FC model by reducing the system total operation cost by 4.2% and 5.1%, and net-operation costs by 0.4 and 1.2% with and without restrictions, respectively. The TSOs' net-operation cost also improved by 4.7 and 6.3% in comparison with the FC model with and without restrictions, respectively. It should be mentioned that the FD model is preferably suitable for the existing system operators as it indicates fair share of net-operation cost ratios between the TSOs and the newly included PAs.

On the other hand, the SD model proved to be particularly useful for incentivizing and attracting private investors and new participants into the system as it indicates capacity for quick investment recovery for the PAs, especially, while considering the immediate results to meet the increasing power system operational needs. In terms of the system total operation cost, the SD model is superior to its FC counterpart by 2.6 and 3.0% with and without restrictions, and in terms of total net-operation cost, it stands out by 3.6 and 4.7% with and without restrictions, respectively.

Considering the inclusion of multiple *LAs* into the transmission grid operation using select meta-heuristic optimization methods including RCEGA, PSO and DE algorithms, the FD model, showed that much better operation cost could be achieved at the expense of execution time, and where lower execution time is required, the FD model could still result in better solutions when compared to the centralized counterpart model. For the expected case when the number of iterations $I = X * 0.5G$, the FD model reduced the total operation cost by 5.0, 5.7 and 5.8%, and the execution time by 15.3, 32.8 and 21.4% using the RCEGA, PSO and DE compared to their centralized models, respectively. Also, when the number of iterations was reduced such that $I = 0.5X * G$, the FD model reduced the total operation cost by 1.2, 4.6 and 3.4% and the total execution time by 30.4, 31.8 and 26.0% using the RCEGA, PSO and DE, compared to their centralized models, respectively. A similar trend was also observed for

the worst-case (minimum and maximum) scenarios. The results showed that the FD model reduced the total operation costs by up to 8.0, 13.4 and 13.9% using the select MO algorithms compared to their centralized counterpart models, respectively.

Furthermore, the FD model at maximum iteration further reduced the total operation cost but with significant increase in the simulation time using the select MO algorithms. The results showed that the total operation cost of the FD model at maximum iteration reduced by 5.2, 7.8, and 10.8% but increased the total execution time by 43.4, 45.5, and 52.9% using the RCEGA, PSO and DE compared to their centralized models, respectively. Also, the number of iterations of both RCEGA and DE may not be kept below $I = 0.5X * 0.5G$ to obtain the desired results for the FD model. The results of the expected case showed that when $I = 0.5X * 0.5G$, the FD model reduced the total execution time by 63.9 and 62.4% but increased the total operation cost by 0.4 and 1.8% for the RCEGA and DE, respectively. Meanwhile, using the PSO, the FD model reduced the operation cost and execution time for all cases compared to the centralized counterpart model.

In addition, the FD model also promises to achieve better solutions for very complex systems having multiple energy matrix. When battery energy storages were added in to the grid operation, the FD model achieved 7.2% decrease in the total operation cost when compared with the centralized FC counterpart model over the operation horizon of 24-hour. This also indicates that the FD model could better reduce the overall operation cost for the grid as the grid operation and complexity increases. In conclusion, the results presented in this study proved the suitability of the select MO algorithms for coordinating the operations of multiple *TSOs* and *PAs* in a decentralized manner to minimize the total operation cost of the system.

5.1 FUTURE STUDIES

The developed SD and FD models have been presented as value-based trade-offs for power system planning including existing and new participants. Future studies can be conducted to integrate the SD and FD models into a single jointly operated model for power system planners. Also, determining optimal operation baselines for the *TSOs* and *PAs* as a multi-objective function on short- and long terms basis, and at same time investigating power system technical performance considering optimal allocation (i.e., size and location) of *PAs* in the power system areas could also be explored in a future work. A method for predictive data can also be developed as the proposed methodology needs a day-ahead forecast data which was obtained from the online database of some system operators.

5.2 PUBLICATIONS

5.2.1 Journal Publications

ADEYANJU, O. M., CANHA, L. N.; RANGEL, C. A. S., and CAMPOS DO PRADO, J., "Semi-Decentralized and Fully Decentralized Multiarea Economic Dispatch Considering Participation of Local Private Aggregators Using Meta-Heuristic Method," **International Journal of Electrical Power and Energy Systems**, vol. 128, p. 106656, 2021.

ADEYANJU, O. M., and CANHA, L. N., "Decentralized Multi-Area Multi-Agent Economic Dispatch Model Using Select Meta-Heuristic Optimization Algorithms," **Electric Power Systems Research**, vol. 175, p. 107128, 2021.

5.2.2 Conference Papers

5.2.2.1 Peer-Reviewed

ADEYANJU, O. M., CANHA, L. N., and CAMBAMBI, C. A. C., "Coordinated Microgrids Integration in Distribution System with Different Power Purchase Agreement Options," in **IEEE PES ISGT Europe**, Finland, 2021.

ADEYANJU, O. M., and CANHA, L. N., "Analysis of Microgrid Operation for Distribution System Support with Different Power Purchase Agreement Terms," in **IEEE PES/IAS PowerAfrica**, Online, 2021.

5.2.2.2 Accepted for Presentation

ADEYANJU, O. M., and CANHA, L. N., "Multiagent Power Transaction in Multiarea System with Decentralized Metaheuristic Frameworks," in **2022 IEEE PES Innovative Smart Grid Technologies (ISGT) North America**, Washington DC, 2022.

ADEYANJU, O. M., and CANHA, L. N., "Coordinated vs Uncoordinated Grid-Connected Microgrids with Short- and Long-Term PPAs: A Comparative Study," in **2022 IEEE/PES Transmission and Distribution Conference and Exposition (T&D)**, New Orleans, 2022.

REFERENCES

- ALI, M. A., DUBEY, H. M., and PANDIT, M., "Moth-Flame Optimization for Multi Area Economic Dispatch: A Novel Heuristic Paradigm," in **International Conference on Energy, Communication, Data Analytics and Soft Computing (ICECDS-2017)**, 2017.
- ALSHEHRI, K., NDRIO, M., BOSE, S., and BASAR, T., "Quantifying Market Efficiency Impacts of Aggregated Distributed Energy Resources," **IEEE Transaction on Power Systems**, p. 1-11, 2020.
- BASU, M., "Fast Convergence Evolutionary Programming for Multi-area Economic Dispatch," **Electric Power Components and Systems**, vol. 45, no. 15, p. 1629-1637, 2017.
- BASU, M., "Multi-area dynamic economic emission dispatch of hydro-wind-thermal power system," **Renewable Energy Focus**, vol. 28, p. 11-35, 2019a.
- BASU, M., "Multi-region dynamic economic dispatch of solar-wind-hydro-thermal power system incorporating pumped hydro energy storage," **Engineering Applications of Artificial Intelligence**, vol. 86, p. 182-196, 2019b.
- BASU, M., "Quasi-oppositional group search optimization for multi-area dynamic economic dispatch," **International Journal of Electrical Power and Energy Systems**, vol. 78, p. 356-367, 2016.
- BASU, M., "Squirrel search algorithm for multi-region combined heat and power economic dispatch incorporating renewable energy sources," **Energy**, vol. 182, p. 296-305, 2019c.
- BASU, M., "Teaching-learning-based optimization algorithm for multi-area economic dispatch," **Energy**, vol. 68, p. 21-28, 2014.
- DING, C., YAN, W., REN, Z., ZHAO, R., LEE, W.-J., and TANG, X., "Continuation Power Flow Model for Interconnected Systems Considering the Electricity Market Influence and Its Corresponding Distributed Algorithm," **IEEE Access**, vol. 7, p. 75910-75924, 2019.
- DIVÉNYI, D., POLGÁRI, B., SLEISZ, Á., SÓRÉS, P., and RAISZ, D., "Algorithm design for European electricity market clearing with joint allocation of energy and control reserves," **International Journal of Electrical Power and Energy Systems**, vol. 111, p. 269-285, 2019.
- DOOSTIZADEH, M., AMINIFAR, F., LESANI, H., and GHASEMI, H., "Multi-area market clearing in wind-integrated interconnected power systems: A fast parallel decentralized method," **Energy Conversion and Management**, vol. 113, p. 131-142, 2016.
- DUBEY, H. M., PANDIT, M., and PANIGRAHI, B. K., "Ant lion optimization for short-term wind integrated hydrothermal power generation scheduling," **International Journal of Electrical Power and Energy Systems**, vol. 83, p. 158-174, 2016.
- FARIA, P., SPÍNOLA, J., and VALE, Z., "Methods for Aggregation and Remuneration of Distributed Energy Resources," **Applied Science**, vol. 8, no. 8, p. 1-16, 2018.

FARROKHIFAR, M. "Optimal operation of energy storage devices with RESs to improve efficiency of distribution grids; Technical and economical assessment," **International Journal of Electrical Power and Energy Systems**, vol. 74, pp. 153-161, 2016.

FIRST, A., and JINBEI, L., "Improve Crisscross optimization algorithm for solving the multi-area economic/emission dispatch," in **2018 China International Conference on Electricity Distribution**, Tianjin, 2018.

FU, Y., WANG, C., TIAN, W., and SHAHIDEHPOUR, M., "Integration of largescale offshore wind energy via VSC-HVDC in day-ahead scheduling," **IEEE Transactions on Sustainable Energy**, vol. 7, no. 2, p. 535–545, 2016.

GHASEMI, M., AGHAEI, J., AKBARI, E., GHAVIDEL, S., and LI, L., "A differential evolution particle swarm optimizer for various types of multi-area economic dispatch problems," **Energy**, vol. 107, p. 182-195, 2016.

GUAN, Y., and WANG, J., "Uncertainty sets for robust unit commitment," **IEEE Transaction on Power Systems**, vol. 29, no. 3, p. 1439-1440, 2014.

GUO, Y., TONG, L., WU, W., ZHANG, B., and SUN, H., "Coordinated Multi-Area Economic Dispatch via Critical Region Projection," **IEEE Transactions on Power Systems**, vol. 32, no. 5, p. 3736-3746, 2017.

GUZMAN, C. P., ARIAS, N. B., FRANCO, J. F., RIDER, M. J., and ROMERO, R., "Enhanced Coordination Strategy for an Aggregator of Distributed Energy Resources Participating in the Day-Ahead Reserve Market," **Energies**, vol. 13, no. 8, p. 1-22, 2020.

HELLMERS, A., ZUGNO, M., SKAJAA, A., and MORALES, J. M., "Operational strategies for a portfolio of wind farms and chp plants in a two-price balancing market," **IEEE Transaction on Power System**, vol. 31, no. 3, p. 2182-2191, 2016.

HIRTH, L., and ZIEGENHAGEN, I., "Balancing power and variable renewables: Three links," **Renewable Sustainable Energy Review**, vol. 50, p. 1035-1051, 2015.

JADOUN, V. K., GUPTA, N., NIAZI, K. R., and SWARNKAR, A., "Multi-area economic dispatch with reserve sharing using dynamically controlled particle swarm optimization," **International Journal of Electrical Power and Energy Systems**, vol. 73, p. 743–756, 2015.

JEAN-MICHEL, C., and JAVIER RODRÍGUEZ-GARCÍA, C. Á.-B., "Assessment of Technical and Economic Impacts of EV User Behaviour on EV aggregator Smart Charging," **Journal of Modern Power Systems and Clean Energy**, vol. 8, no. 2, p. 356-366, 2020.

JEBARAJA, L., VENKATESANB, C., SOUBACHEC, I., CHRISTOBER, C., and RAJAND, A., "Application of differential evolution algorithm in static and dynamic economic or emission dispatch problem: A review," **Renewable and Sustainable Energy Reviews**, vol. 77, p. 1206-1220, 2017.

JI, Y., and TONG, L., "Multi-Area Interchange Scheduling Under Uncertainty," **IEEE**

Transactions on Power Systems, vol. 33, no. 2, p. 1659-1669, 2018.

JIANG, Y., HOU, J., LIN, Z., WEN, F., LI, J., HE, C., JI, C., LIN, Z., DING, Y., and YANG, L., "Optimal Bidding Strategy for a Power Producer Under Monthly Pre-Listing Balancing Mechanism in Actual Sequential Energy Dual-Market in China," **IEEE Access**, vol. 7, p. 70986-70998, 2019.

KABOURIS, J. and KANELLOS, F. D., "Impacts of large-scale wind penetration on designing and operation of electric power systems," **IEEE Transactions on Sustainable Energy**, vol. 1, no. 2, p. 107–114, 2010.

KARDAKOS, E. G., SIMOGLU, C. K., and BAKIRTZIS, A. G., "Optimal offering strategy of a virtual power plant: A stochastic bi-level approach," **IEEE Transactions on Smart Grid**, vol. 7, no. 2, p. 794-806, 2016.

KARGARIAN, A., FU, Y., and LI, Z., "Distributed security-constrained unit commitment for large-scale power systems," **IEEE Transactions on Power Systems**, vol. 30, no. 4, p. 1925–1936, 2014.

KHANABADI, M., FU, Y., and GONG, L., "A Fully Parallel Stochastic Multiarea Power System Operation Considering Large-Scale Wind Power Integration," **IEEE Transactions on Sustainable Energy**, vol. 9, no. 1, p. 138-147, January 2018.

KUMAR, S., and NARESH, R., "Efficient real coded genetic algorithm to solve the non-convex hydrothermal scheduling problem," **International Journal of Electrical Power and Energy Systems**, vol. 29, no. 10, p. 738-747, 2007.

KUMAR, V., PANDEY, A. S., and SINHA, S. K., "Grid Integration and Power Quality Issues of Wind and Solar Energy System: A Review," in **International Conference on Emerging Trends in Electrical, Electronics and Sustainable Energy Systems (ICETEESES-16)**, Sultanpur, 2016.

KUMAR, V., SHARMA, R. N., and SIKARWAR, S. K., "Multi-area Economic Dispatch Using Dynamically Controlled Particle Swarm Optimization," **Springer**, p. 151-161, 2018.

LI, Z., WU, W., ZHANG, B., and WANG, B., "Decentralized Multi-Area Dynamic Economic Dispatch Using Modified Generalized Benders Decomposition," **IEEE Transactions on Power Systems**, vol. 31, no. 1, p. 526-538, 2016.

LIAO, X., ZHOU, J., OUYANG, S., ZHANG, R., and ZHANG, Y., "An adaptive chaotic artificial bee colony algorithm for short-term hydrothermal generation scheduling," **International Journal of Electrical Power and Energy Systems**, vol. 53, p. 34-42, 2013.

LIN, J. and WANG, Z. J., "Multi-area economic dispatch using an improved stochastic fractal search algorithm," **Energy**, vol. 166, p. 47-58, 2019.

LU, W., LIU, M., LIN, S., and LI, L., "Fully Decentralized Optimal Power Flow of Multi-Area Interconnected Power Systems Based on Distributed Interior Point Method," **IEEE Transactions on Power Systems**, vol. 33, no. 1, p. 901-910, 2018.

LUCÍA, M. and JIM, H., "European power markets - A journey towards efficiency," **Energy**

Policy, vol. 116, p. 78-85, 2018.

LUO, X., WANG, J., DOONER, M., AND CLARKE, J., "Overview of current development in electrical energy storage technologies and the application potential in power system operation," **Applied Energy**, vol. 137, pp. 511-536, 2015.

MADADI, S., MOHAMMADI-IVATLOO, B., and TOHIDI, S., "Decentralized optimal multi-area generation scheduling considering renewable resources mix and dynamic tie line rating," **Journal of Cleaner Production**, vol. 223, p. 883-896, 2019.

MAKAROV, Y. V., ETINGOV, P. V., and DU, P., "Improve system performance with large-scale variable generation addition," in *Power Grid Operation in a Market Environment: Economic Efficiency and Risk Mitigation*, First Edition, **John Wiley and Sons, Inc.**, 2017, p. 91-114.

MAZZI, N., TRIVELLA, A., and MORALES, J. M., "Enabling Active/Passive Electricity Trading in Dual-Price Balancing Markets," **IEEE Transactions on Power Systems**, p. 1-11, 2018.

MELODI, A. O., MOMOH, J. A., and ADEYANJU, O. M., "Probabilistic Long-Term Load Forecast for Nigerian Bulk Power Transmission System Expansion Planning," in **2016 IEEE PES Power Africa Conference**, Zambia, 2016.

MHANNA, S., and VERBI, G., "Adaptive ADMM for Distributed AC Optimal Power Flow," **IEEE Transactions on Power Systems**, vol. 34, no. 3, p. 2025-2035, May 2019.

MOHITI, M., MONSEF, H., ANVARI-MOGHADDAM, A., GUERRERO, J., and LESANI, H., "A decentralized robust model for optimal operation of distribution companies with private microgrids," **International Journal of Electrical Power and Energy Systems**, vol. 106, p. 105-123, 2019.

MUELLER, F. L., SZABÓ, J., SUNDSTRÖM, O., and LYGEROS, J., "Aggregation and Disaggregation of Energetic Flexibility from Distributed Energy Resources," **IEEE Transactions on Smart Grid**, p. 1-10, 2017.

NARIMANI, H., RAZAVI, S.-E., AZIZIVAHED, A., NADERI, E., FATHI, M., ATAEI, M. H., and NARIMANI, M. R., "A multi-objective framework for multi-area economic emission dispatch," **Energy**, vol. 154, p. 126-142, 2018.

NGUYEN, P. K., DINH, D. N., and FUJITA, G., "Multi-area economic dispatch using hybrid cuckoo search algorithm," in **50th international universities power engineering conference (UPEC)**, UK: Stoke on Trent, 2015.

OLANG, S. A., MUSAU, P. M., and ODERO, N. A., "Multi Objective Multi Area Hydrothermal Environmental Economic Dispatch using Bat Algorithm," in **2018 International Conference on Power Systems Technology**, Guangzhou, 2018.

OLSEN, D., BYRON, J., DESHAZO, G., and SHIRMOHAMMADI, D., "Collaborative Transmission Planning: California's Renewable Energy Transmission Initiative," **IEEE Transactions on Sustainable Energy**, vol. 3, no. 4, October 2012.

- PANDIT, M., JAIN, K., DUBEY, H. M., and SINGH, R., "Large Scale Multi-Area Static/Dynamic Economic Dispatch using Nature Inspired Optimization," **Springer**, vol. 98, no. 2, p. 221-229, 2017.
- PÉTER, S., DÁVID, R., and DÁNIEL, D., "Day-ahead market design enabling co-optimized reserve procurement in Europe," in **11th International Conference on the European Energy Market (EEM)**, 2014.
- RAMTEEN SIOSHANSI, O. S., "Three-part auctions versus self-commitment in day-ahead electricity markets," **Utilities Policy**, vol. 18, p. 165-173, 2010.
- REZA, H., AMIR, A. L., and MEHDI, E., "A risk-constrained decision support tool for EV aggregators participating in energy and frequency regulation markets," **Electric Power Systems Research**, vol. 185, p. 106367, 2020.
- ROSTAMPOUR, V., HAAR, O. T., and KEVICZKY, T., "Distributed Stochastic Reserve Scheduling in AC Power Systems with Uncertain Generation," **IEEE Transactions on Power Systems**, vol. 34, no. 2, p. 1005-1020, 2019.
- SECUI, D. C., "Large-scale multi-area economic/emission dispatch based on a new symbiotic organisms search algorithm," **Energy Conversion and Management**, vol. 154, p. 203-223, 2017.
- SECUI, D. C., "The chaotic global best artificial bee colony algorithm for the multiarea economic/emission dispatch," **Energy**, vol. 93(Part 2), p. 2518-2545, 2015.
- SHAHIRINIA, A. H., SOOFI, E. S., and YU, D. C., "Probability distributions of outputs of stochastic economic dispatch," **International Journal of Electrical Power and Energy Systems**, vol. 81, p. 308–316, 2016.
- SHIWEI, X., ZHAOHAO, D., TING, D., ZHANG, D., SHAHIDEHPOUR, M., and DING, T., "Multi-time scale coordinated scheduling for the combined system of wind power, photovoltaic, thermal generator, hydro pumped storage and batteries," **IEEE Transactions on Industry Applications**, p. 1-9, 2020.
- TAVAKOLI, A., NEGNEVITSKY, M., SAHA, S., HAQUE, M. E., ARIF, M. T., CONTRERAS, J., and OO, A., "Self-Scheduling of a Generating Company with an EV Load Aggregator Under an Energy Exchange Strategy," **IEEE Transaction on Smart Grid**, vol. 10, no. 4, p. 4253-4263, 2019.
- THAKUR, M., and KUMAR, A., "Optimal coordination of directional over current relays using a modified real coded genetic algorithm: A comparative study," **International Journal of Electrical Power and Energy Systems**, vol. 82, p. 484-495, 2016.
- WANG, C and FU, F., "Fully parallel stochastic security-constrained unit commitment," **IEEE Transactions on Power Systems**, vol. 31, no. 5, p. 3561-3571, September 2016.
- WANG, XI-FAN; SONG, YONGHUA; IRVING, MALCOLM., *Modern Power Systems Analysis*, New York: **Springer**, 2010.

WU, L., "A Transformation-Based Multi-Area Dynamic Economic Dispatch Approach for Preserving Information Privacy of Individual Areas," **IEEE Transactions on Smart Grid**, vol. 10, no. 1, p. 722-731, 2019.

ZHANG, R., YAN, K., LI, G., JIANG, T., LI, X., and CHEN, H., "Privacy-preserving decentralized power system economic dispatch considering carbon capture power plants and carbon emission trading scheme via over-relaxed ADMM," **International Journal of Electrical Power and Energy Systems**, vol. 121, p. 106094, 2020.

ZOU, X. D., LI, S., WANG, G. G., LI, Y. Z., and OUYANG, B. H., "An improved differential evolution algorithm for the economic load dispatch problems with or without valve point effects," **Applied Energy**, vol. 181, p. 375-390, 2016.

APPENDICES

Appendix A – Parameters of TSOs And PAs

Table A.1 – Thermal unit name, output power limit, cost coefficients, and ramp rates limits for TSOs

AREA	Gen. Name	Gen. Limits (MW)		Gen. Costs Coefficients (\$/hr)			Gen. Valve-Point Effect Coefficients.		Ramp Limits (MW/hr.)	
		Min	Max	$a_{g,i}$	$b_{g,i}$	$c_{g,i}$	$e_{g,i}$	$f_{g,i}$	Down	Up
AREA 1	TG1	0	550	913.4	12.5	0.00421	300	0.035	300	300
	TG2	0	550	649.69	7.95	0.00313	300	0.035	300	300
	TG3	0	550	245	5.67	0.0032	180	0.025	300	300
	TG4	0	550	348	3.22	0.0032	120	0.025	300	300
AREA 2	TG1	0	550	148.89	5.35	0.0114	120	0.077	300	300
	TG2	0	550	647.83	7.97	0.00313	300	0.035	300	300
	TG3	0	550	280	6.34	0.00567	140	0.088	300	300
	TG4	0	550	647.83	7.97	0.00313	300	0.035	300	300
AREA 3	TG1	0	550	647.83	7.97	0.00313	300	0.035	300	300
	TG2	0	550	1055.1	8.33	0.05214	240	0.077	300	300
	TG3	0	550	555.1	3.33	0.02214	250	0.077	300	300
	TG4	0	550	345	2.26	0.0065	120	0.043	300	300

Table A.2 – Thermal unit name, output power limit, cost coefficients, and ramp rates limits for PAs

AREA	Gen. Name	Gen. Limits (MW)		Gen Costs Coefficients. (\$/hr)			Ramp Limits (MW/hr)	
		Min	Max	$a_{g,i}$	$b_{g,i}$	$c_{g,i}$	Down	Up
AREA 1	PA1	0	250	287.71	8.03	0.00357	100	100
	PA2	0	250	391.98	6.99	0.00492	100	100
	PA3	0	250	455.76	6.6	0.00573	100	100
AREA 2	PA1	0	250	326.9	4.4	0.0044	100	100
	PA2	0	250	354.1	7.6	0.0043	100	100
	PA3	0	250	365.9	7.7	0.0055	100	100
AREA 3	PA1	0	250	302.3	8.1	0.0019	100	100
	PA2	0	250	535.4	9.3	0.0052	100	100
	PA3	0	250	326.8	9.8	0.0082	100	100

Appendix B – Hydro Generator Parameters

Table B.1 – Reservoir storage capacity limits, plant discharge limits, reservoir end conditions and plant generation limits (MW) for TSO by area.

AREA	PLANT	Vmin (10^4m^3)	Vmax (10^4m^3)	Vini (10^4m^3)	Vend (10^4m^3)	Qmin (10^4m^3)	Qmax (10^4m^3)	Phmin (MW)	Phmax (MW)
AREA 1 - 3	Plant1	80	150	100	120	5	15	0	500
	Plant2	60	120	80	70	6	15	0	500
	Plant3	100	240	170	170	10	30	0	500
	Plant4	70	160	120	140	6	20	0	500

- The hydropower plants coefficients of the TSO by area in Table B.2.

Table B.2 – Hydropower plants coefficients

AREA 1 - 3				
	Plant 1	Plant 2	Plant 3	Plant 4
C1	-0.0042	-0.004	-0.0016	-0.003
C2	-0.42	-0.3	-0.3	-0.31
C3	0.03	0.02	0.01	0.03
C4	0.9	1.14	0.55	1.44
C5	10	9.5	5.5	14
C6	-50	-70	-40	-90

- The hydraulic system network for the TSO are provided by area in Table B.3.

Table B.3 – Hydraulic system network

AREA 1 - 3		
Plant	Ru (#)	Td (hr.)
Plant 1	0	2
Plant 2	0	3
Plant 3	2	4
Plant 4	1	0

*Ru = No. of upstream plants; *Td = Time delay to immediate downstream

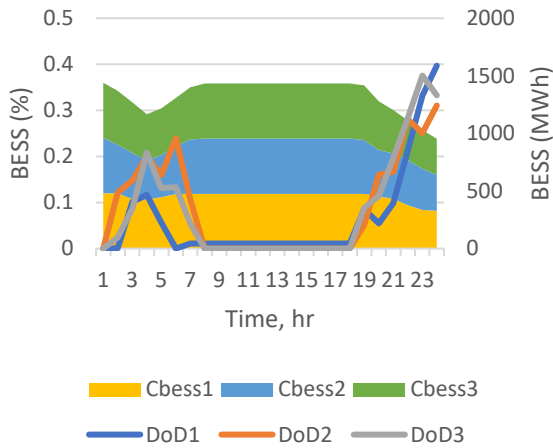
- The reservoir inflows rates for the TSO hydro power plant are provided by area in Table B.4.

Table B.4 – Reservoir inflows rates (10^4m^3).

Hour	AREA 1 - 3				Hour	AREA 1 - 3			
	Reservoir					Reservoir			
	Plant 1	Plant 2	Plant 3	Plant 4		Plant 1	Plant 2	Plant 3	Plant 4
1	10	8	8.1	2.8	13	11	8	4	0
2	9	8	8.2	2.8	14	12	9	3	0
3	8	9	4	1.6	15	11	9	3	0
4	7	9	2	0	16	10	8	2	0
5	6	8	3	0	17	9	7	2	0
6	7	7	4	0	18	8	6	2	0
7	8	6	3	0	19	7	7	1	0
8	9	7	2	0	20	6	8	1	0
9	10	8	1	0	21	7	9	2	0
10	11	9	1	0	22	8	9	2	0
11	12	9	1	0	23	9	8	1	0
12	10	8	2	0	24	10	8	0	0

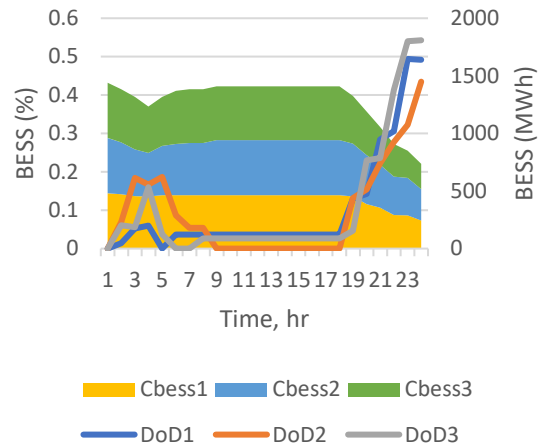
Appendix C – BESS Performance

Figure C.1 – Battery Depth of Discharge and Hourly Capacity of PAs in Area 1: FC Model



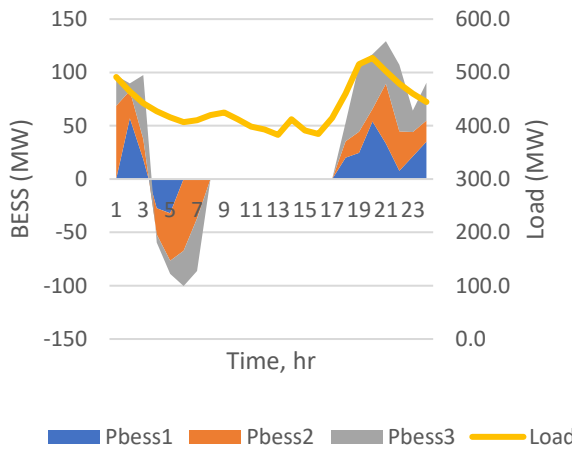
Source: Authors.

Figure C.3 – Battery Depth of Discharge and Hourly Capacity of PAs in Area 2: FC Model



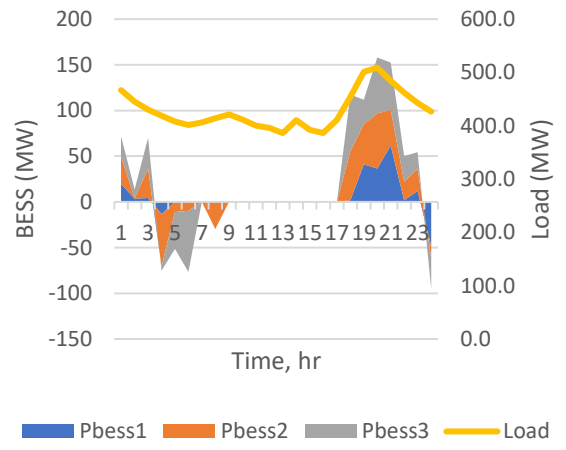
Source: Authors.

Figure C.2 – Battery Power Injection and Total PAs' Hourly Load in Area 1: FC Model



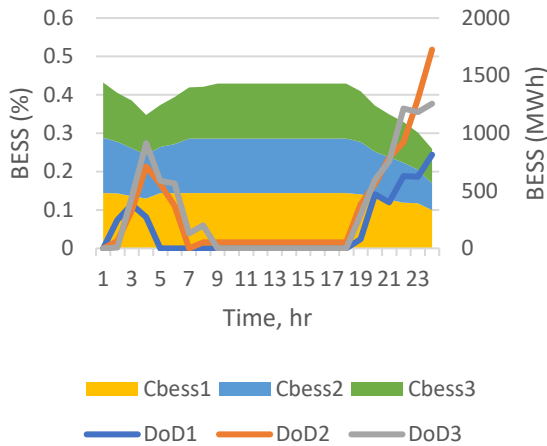
Source: Authors.

Figure C.4 – Battery Power Injection and Total PAs' Hourly Load in Area 2: FC Model



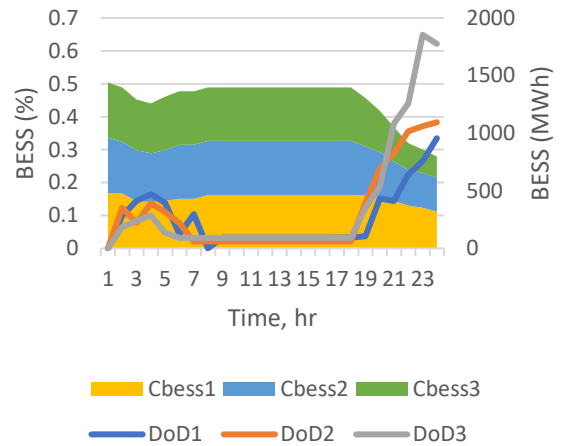
Source: Authors.

Figure C.5 – Battery Depth of Discharge and Hourly Capacity of PAs in Area 3: FC Model



Source: Authors.

Figure C.7 – Battery Depth of Discharge and Hourly Capacity of PAs in Area 1: FD Model:



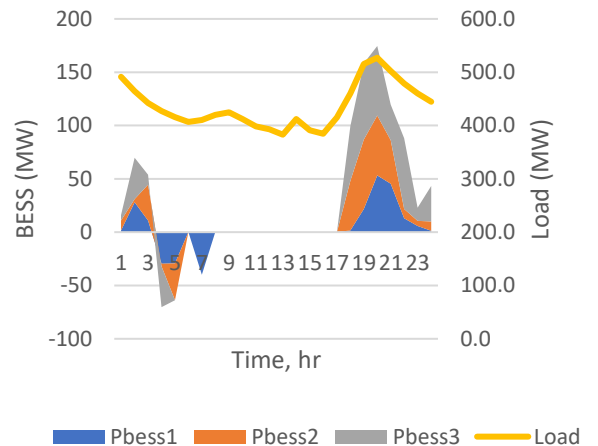
Source: Authors.

Figure C.6 – Battery Power Injection and Total PAs' Hourly Load in Area 3: FC Model



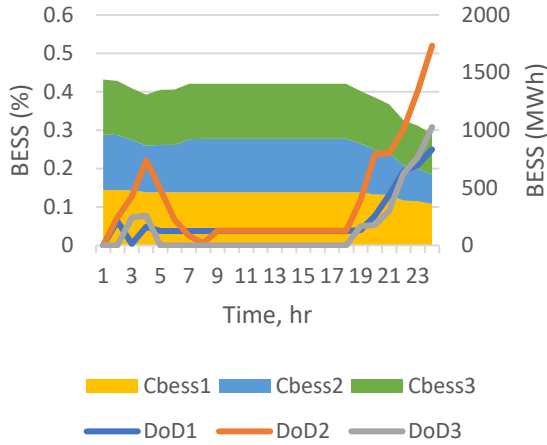
Source: Authors.

Figure C.8 – Battery Power Injection and Total PAs' Hourly Load in Area 1: FD Model:



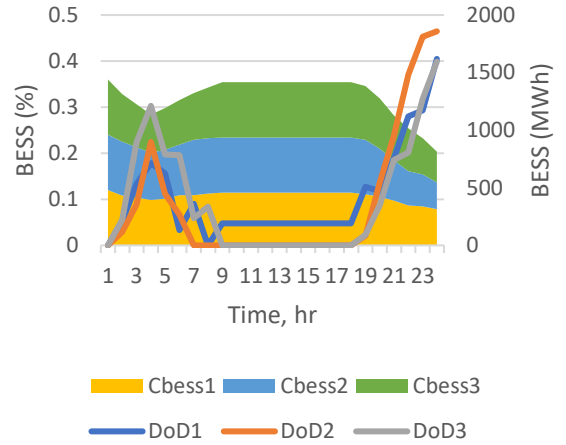
Source: Authors.

Figure C.9 – Battery Depth of Discharge and Hourly Capacity of PAs in Area 2: FD Model:



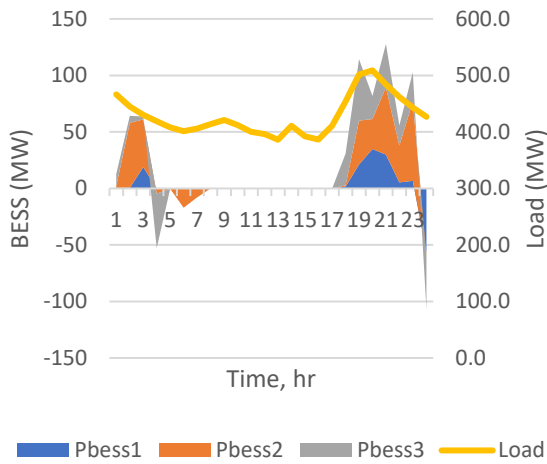
Source: Authors.

Figure C.11 – Battery Depth of Discharge and Hourly Capacity of PAs in Area 3: FD Model



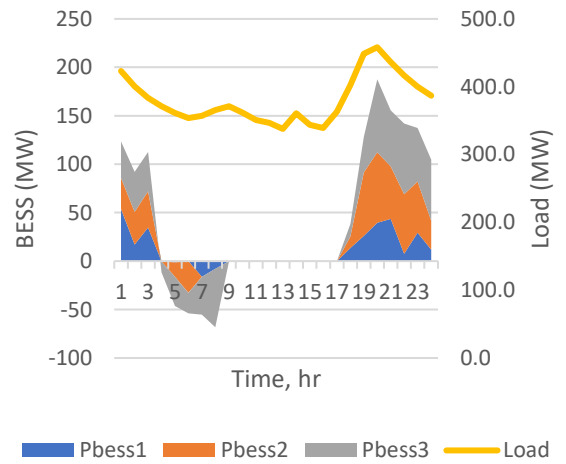
Source: Authors.

Figure C.10 – Battery Power Injection and Total PAs' Hourly Load in Area 2: FD Model



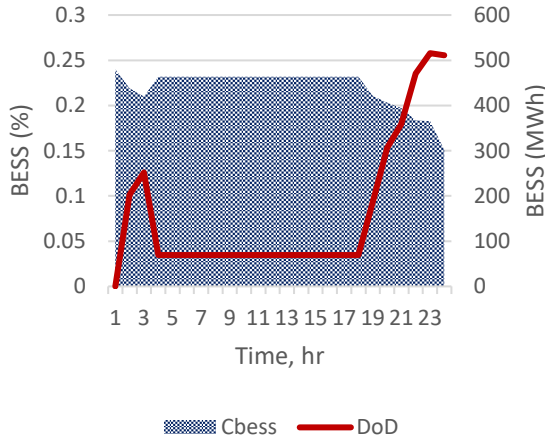
Source: Authors.

Figure C.12 – Battery Power Injection and Total PAs' Hourly Load in Area 3: FD Model



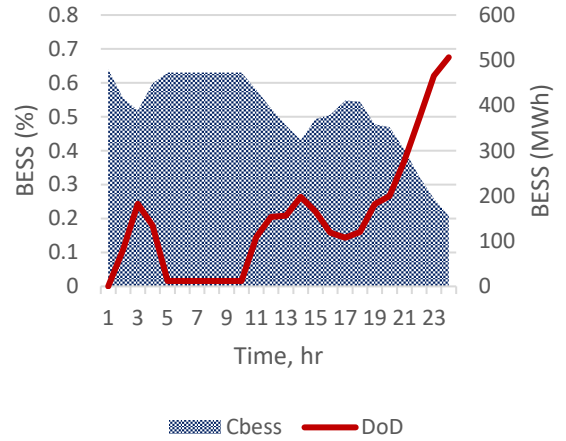
Source: Authors.

Figure C.13 – Battery Depth of Discharge and Hourly Capacity of TSO in Area 2: FC Model



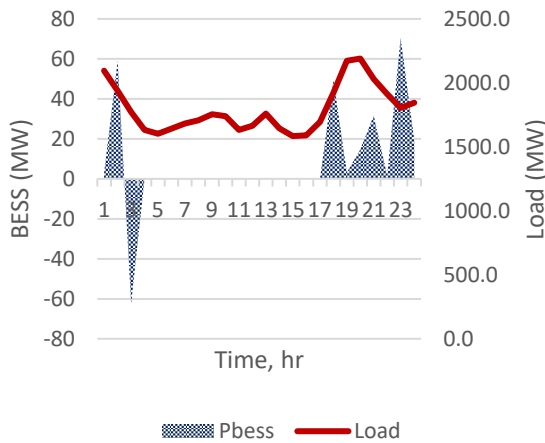
Source: Authors.

Figure C.15 – Battery Depth of Discharge and Hourly Capacity of TSO in Area 3: FC Model



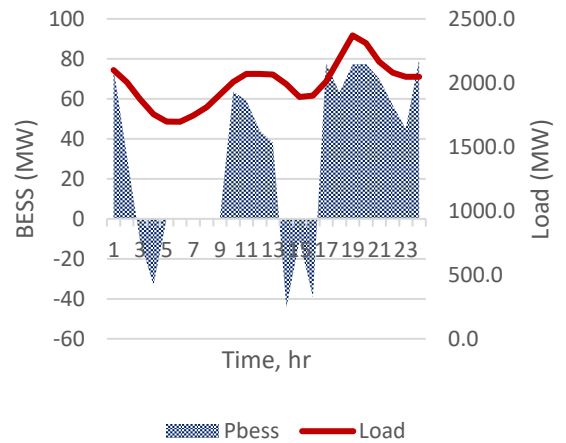
Source: Authors.

Figure C.14 – Battery Power Injection and Total TSO's Hourly Load in Area 2: FC Model



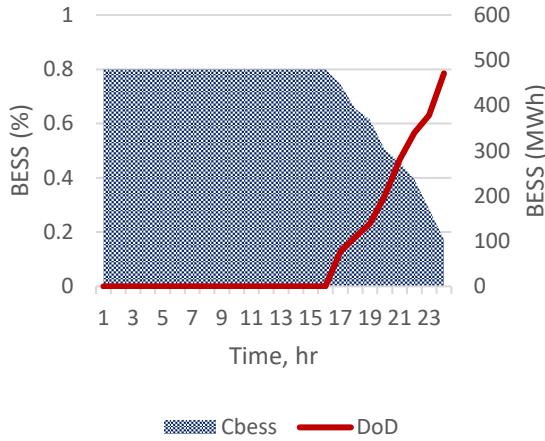
Source: Authors.

Figure C.16 – Battery Power Injection and Total TSO's Hourly Load in Area 3: FC Model



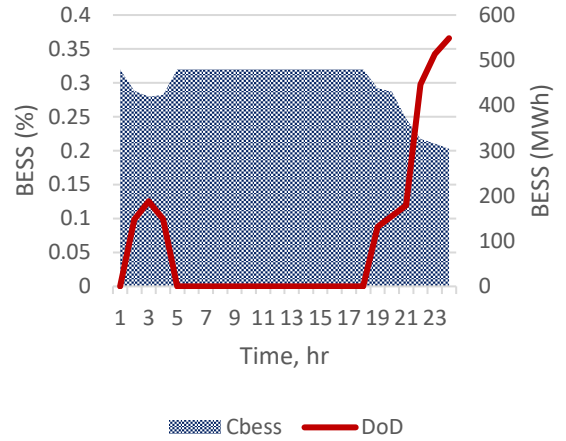
Source: Authors.

Figure C.17 – Battery Depth of Discharge and Hourly Capacity of TSO in Area 1: FD Model



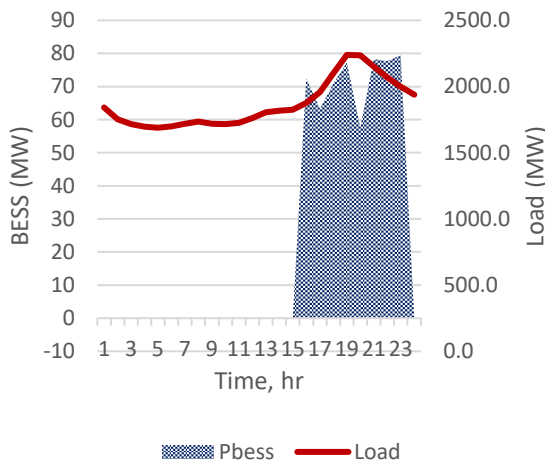
Source: Authors.

Figure C.19 – Battery Power Injection and Total TSO’s Hourly Load in Area 2: FD Model



Source: Authors.

Figure C.18 – Battery Power Injection and Total TSO’s Hourly Load in Area 1: FD Model



Source: Authors.

Figure C.20 – Battery Power Injection and Total TSO’s Hourly Load in Area 2: FD Model



Source: Authors.

